

Modeling and control of autonomous public transport vehicles

Thesis by:
Balázs Varga



Department of Control for Transportation and Vehicle Systems
Budapest University of Technology and Economics

Supervisors:
Dr. Tamás Tettamanti and Dr. Balázs Kulcsár

Submitted in Partial Fulfillment of the Requirements for the Degree of
Doctor of Philosophy

October 18, 2020

Declaration

Undersigned, Balázs Varga, hereby state that this Ph.D. Thesis is my own work wherein I have used only the sources listed in the Bibliography. All parts taken from other works, either in a word for word citation or rewritten keeping the original contents, have been unambiguously marked by a reference to the source.

The reviews of this Ph.D. Thesis and the record of defense will be available later in the Dean Office of the Faculty of Transportation Engineering and Vehicle Engineering of the Budapest University of Technology and Economics.

Nyilatkozat

Alulírott Varga Balázs kijelentem, hogy ezt a doktori értekezést magam készítettem és abban csak a megadott forrásokat használtam fel. Minden olyan részt, amelyet szó szerint vagy azonos tartalomban, de átfogalmazva más forrásból átvettem, egyértelműen, a forrás megadásával megjelöltem.

A doktori értekezésről készült bírálatok és a jegyzőkönyv a későbbiekben a Budapesti Műszaki és Gazdaságtudományi Egyetem Közlekedésmérnöki és Járműmérnöki Karának Dékáni Hivatalában lesznek elérhetőek.

Budapest, October 18, 2020

Balázs Varga

Contents

Contents	ii
List of Figures	v
List of Tables	viii
Nomenclature	ix
1 Introduction	1
1.1 Background	1
1.2 Purpose and scope	4
1.3 Methods	5
1.3.1 Modeling	5
1.3.2 Model predictive control	6
1.3.3 Scenario approach and the sampling and discarding technique	7
1.4 Overview and structure of the Thesis	8
1.5 Related Publications of the Author	8
2 Multi-objective public transport model	12
2.1 Bus dynamics model	12
2.2 Reference tracking	13
2.2.1 Timetable tracking	14
2.2.2 Headway tracking	14
2.3 Energy consumption model	14
2.4 Bus stop operations	17
2.4.1 Passenger arrival model	17
2.4.2 Bus stop model	18
2.4.3 Passenger wait model	19
2.5 Public transport network model	20
2.5.1 Merging bus lines	20
2.5.2 Centralized bus network model	23
2.6 Contribution	26
3 Stochastic shockwave profile model	27
3.1 Stochastic queuing model	28
3.2 Shockwaves at signalized intersections	30

3.3	CDF of shockwaves	33
3.4	Number of vehicles	35
3.5	Monte Carlo simulation example	35
3.6	Network stochastic SPM	37
3.7	Contribution	39
4	Model predictive bus velocity control	40
4.1	Shrinking horizon model predictive control	41
4.2	Multi-objective cost function	42
4.2.1	Headway and timetable tracking MPC	43
4.2.1.1	Deduction of the cost function	43
4.2.1.2	Proving the convexity of the control problem	47
4.2.2	Energy-aware MPC	47
4.2.3	Passenger wait costing	50
4.2.4	Multi-objective cost function	51
4.2.5	Weighting strategies	52
4.2.5.1	Adaptive control	53
4.2.5.2	Pareto Front	54
4.2.5.3	Trajectory shapes	55
4.3	Numerical simulations	56
4.3.1	Service homogeneity performance	56
4.3.2	Energy consumption	63
4.3.3	Average passenger waiting times	65
4.4	Contribution	66
5	Chance-constrained trajectory control	68
5.1	Chance-constraints	68
5.2	Numerical simulations	70
5.2.1	Feasibility study	70
5.2.2	Microscopic traffic simulation	75
5.3	Contribution	77
6	Centralized public transport network velocity control	78
6.1	Network MPC	78
6.2	Analysis	81
6.2.1	Experimental results	81
6.2.2	Feasibility study	85
6.2.2.1	Random simulations	85
6.2.2.2	Set theory	85
6.2.3	Comparison to the decentralized model	89
6.2.4	Computational demand	90
7	Conclusions and future work	95
7.1	Conclusions	95
7.2	Future work	96
7.3	Implementation related questions	96

A Example networks	98
A.1 Gothenburg network	98
A.2 Budapest network	99
B Benchmark control strategies	103
References	104
Publications of the Author (related to the theses)	114
Publications of the Author (unrelated to the theses)	116

List of Figures

1.1	Structural overview of the dissertation	9
2.1	Reference tracking	15
2.2	Sankey diagram of an electric powertrain with regenerative braking . .	16
2.3	Arrival rate of each passenger type: <i>a</i>) coincident or just in time (JIT) arrivals (λ_{JIT}), <i>b</i>) waiting time minimizers (λ_{min}), <i>c</i>) random arrivals (λ_{rand})	18
2.4	Merging bus lines at a two-legged junction	20
2.5	Pattern of three merging buses with $T_{hw,A} = 1$, $T_{hw,B} = 2$, and $T_{hw,C} = 3$.	21
2.6	Flowchart of the control algorithm for one bus (<i>this</i> denotes the controlled bus, <i>it</i> denotes the leading bus	22
2.7	Space-time diagram of the merging area	23
3.1	Traffic flow states in front of a signalized intersection	29
3.2	Triangular link fundamental diagram of traffic flow with shockwave speeds ($W_1 \dots W_4$). $Q_A(t, \omega)$ is represented with a probability density function, showing how it affects the slope of the queuing shockwave $W_1(t, \omega)$. . .	31
3.3	Traffic states at a single intersection assuming generic link fundamental diagram.	32
3.4	Monte Carlo simulation of queue lengths to validate the SSPM	36
3.5	Stochastic shockwave profile model based queues at on network level . .	37
3.6	Traffic flow states with probabilistic spillover	38
4.1	Overlapped, decentralized control strategy	41
4.2	MPC horizon length calculation	42
4.3	Relevant bus stops for the passenger waiting time model ($Stop_1 \dots Stop_Y$)	51
4.4	Proposed weighting strategies. <i>a</i>) Timetable tracking only, <i>b</i>) Headway tracking only, <i>c</i>) Balanced - timetable and headway tracking, <i>d</i>) Passenger demand driven - headway tracking and waiting time minimization, <i>e</i>) Cheap service driven - timetable tracking and energy consumption minimization, <i>f</i>) Balanced, advanced - timetable and headway tracking plus energy consumption and waiting time minimization. Abbreviations at each direction match the subscript of the respective cost function element	54
4.5	Pareto Front	59

4.6	Trajectory predictions from a fixed initial state with different weighting strategies compared to the reference trajectories (vertical axis: Position (m), horizontal axis: Time (s))	60
4.7	Trajectory of a single bus and its velocity profile	61
4.8	Trajectories of consecutive buses with different control strategies	61
4.9	Trajectories of consecutive buses with different control strategies - 10 minute service perturbation. Dashed lines denote the speed of congestion dissipation	62
4.10	Energy consumption profile of one vehicle	64
4.11	Average energy consumption and regeneration	64
4.12	Total energy consumption on the bus line. The relative energy consumptions are normalized with the holding control strategy	64
5.1	Trajectory prediction distribution. Red areas indicate jam regions $R_J(t, \omega)$, yellow areas indicate queue discharge regions $R_C(t, \omega)$. Dashed lines at the shockwave profiles indicate the queue length distribution with $\pm 3\sigma_{queue}$	72
5.2	Standard deviations of the queue length σ_{queue} and the predicted trajectories σ_{traj}	73
5.3	Correlation coefficient between the queue lengths and the predicted trajectories over the prediction horizon	73
5.4	Scatter plot of the queue length vs the instantaneous position samples at prediction time 35 s	73
5.5	Predicted trajectories for -2σ (dotted line) - 700 (solid line) - $+2\sigma$ (dashed line) veh/h compared to the SPM at 647 ($mean - 2\sigma$) (top left) - 700 (top right) - 753 ($mean + 2\sigma$) (bottom) veh/h	74
5.6	Bus trajectories. A detailed section of this figure can be seen in Figure 5.7	76
5.7	Bus trajectories - zoomed	76
6.1	System states upon a bus approaching a bus stop	82
6.2	Experimental network	83
6.3	Trajectory of one bus in the experimental network with its reference trajectories. The bus makes three laps. The shaded area denotes the common line section.	83
6.4	Trajectory of every bus in the network. Different line styles are used to distinguish individual buses. Trajectories of Line 1 are shifted so positions match in the common line section.	84
6.5	Passenger numbers at Stop II	84
6.6	Sum of accumulated passengers at every stop for every scenario	85
6.7	EMPC projection to the state plane of the 1 st bus with 12 passengers limit at stops	87
6.8	EMPC projection to the state plane of the 1 st bus with 2 passengers limit at stops	88
6.9	Trajectories of consecutive buses with centralized and decentralized control	89
6.10	Trajectories of consecutive buses with centralized and decentralized control with service perturbation	90

6.11	Optimization time - convex, balanced control	92
6.12	Optimization time - non-convex, timetable, headway, passenger wait and energy aware control	92
6.13	Optimization time - non-convex, traffic aware control	93
6.14	Optimization time - centralized control	93
A.1	Modeled route section: Gothenburg, Line 16. Dots mark stops and semaphore pictograms indicate traffic lights. The route in darker shade of blue represents mixed traffic (i.e. lack of dedicated bus lane). (GPS coordinates: 57.711 N, 11.944 E; source: Google maps)	100
A.2	Modeled real-world section (GPS coordinates: 47.465 N, 19.034 E; source: OpenStreetMap)	101
A.3	Detailed route section of Figure A.2 with traffic lights; source: OpenStreetMap)	101

List of Tables

3.1	Boundaries of traffic states	33
4.1	Cost function values with different weighting strategies	56
4.2	Congestion dissipation speed (m/s)	58
4.3	Statistics of the trajectories for headway reliability (target headway: 180 s)	59
4.4	Average total waiting time (in seconds) of passengers at each stop	65
5.1	Signal program and vehicle flow upstream each traffic light	71
5.2	Constraint violation metric V . Horizontal: actual arrival rate, vertical: presumed arrival rate.	74
6.1	Bus stops on the experimental network	82
A.1	Number of boarding and alighting passengers at each stop (passengers/hour), scheduled departure time (seconds)	100
A.2	Bus arrival times (with entry to the network being 0, in seconds) and passenger demand at each stop (passengers/hour)	102
A.3	Signal program and mean traffic flow upstream each traffic light.	102

Nomenclature

Acronyms

<i>APC</i>	Automatic Passenger Count
<i>AVL</i>	Automatic Vehicle Location
<i>CDF</i>	Cumulative Distribution Function
<i>EMPC</i>	Explicit Model Predictive Control
<i>GNSS</i>	Global Navigation Satellite System
<i>GPS</i>	Global Positioning System
<i>ITS</i>	Intelligent Transportation Systems
<i>JIT</i>	Just in Time
<i>LMI</i>	Linear Matrix Inequality
<i>LTI</i>	Linear Time Invariant
<i>MIQP</i>	Mixed Integer Quadratic Program
<i>MPC</i>	Model Predictive Control
<i>PCE</i>	Passenger Car Unity
<i>PDF</i>	Probability Density Function
<i>QP</i>	Quadratic Program
<i>SPM</i>	Shockwave Profile Model
<i>SQP</i>	Sequential Quadratic Program
<i>SSPM</i>	Stochastic Shockwave Profile Model
<i>V2G</i>	Vehicle to Grid
<i>V2I</i>	Vehicle to Infrastructure

Notations

x	position of the controlled bus
v	velocity of the controlled bus
a	acceleration of the controlled bus
Δt	discrete time step interval
k	time step index
τ	relaxation parameter
v_{des}	desired velocity of the controlled bus (control input)
v_{dist}	velocity disturbance
β	relaxation parameter
v_{mac}	link macroscopic average velocity
x_{tt}	timetable reference signal
z_{tt}	timetable reference tracking error
x_{hw}	headway reference signal
z_{hw}	headway reference tracking error
t_0	current time instant, time instant of the prediction
P_{roll}	power required to overcome the rolling resistance
μ	road friction coefficient
m	vehicle weight (vehicle and passengers)
g	gravitational acceleration
θ	road inclination angle
m_{veh}	curb vehicle weight
m_p	average weight of a passenger
p_o	number of on-board passengers
P_g	extra power required for driving uphill (or downhill)
P_{drag}	power to overcome air drag
c_w	drag coefficient
ρ_{air}	density of air
A_f	face area of the bus
P_{acc}	power to accelerate the bus
P_{regen}	power recuperated during braking
η_{regen}	efficiency of regenerative braking
P_w	power at the wheels
η_{batt}	battery efficiency
η_{pe}	efficiency of the power electronics
η_{mot}	efficiency of the electric motor
η_{pt}	powertrain efficiency - efficiency of the mechanical parts
E_{cons}	energy consumed during a time interval
λ	passenger arrival rate at a bus stop
t_{dep}	departure time of a bus from a stop
λ_{rand}	arrival rate of randomly arriving passengers
λ_{min}	arrival rate of wait time minimizing passengers
λ_{JIT}	passengers arriving just in time
t_d	bus dwell time at a stop

p	number of boarding passengers
t_b	average boarding time per passenger
t_a	average alighting time per passenger
t_{oc}	door opening and closing time
p_a	number of alighting passengers
ξ	integer value denoting passenger exchange at a bus stop
x_{stop}	location of the bus stop along the route
t_w	cumulated wait time of passengers
T_{hw}	time headway of a bus
pat	merging pattern - the order buses from different lines follow each other
MP	merging point
Z_ϱ	start of the merging zone on bus line ϱ .
t_{Z,ϱ_i}	time when bus i from line ϱ enters the merging zone
t_{MP,ϱ_i}	time when bus i from line ϱ enters the common line
$\Delta t_{\rho_{i-1},\rho_i}$	available time window for headway equalization
M_B	number of buses in the network
M_S	number of stops in the network
M_L	number of bus lines making up the network
i	subscript for individual buses
j	subscript for individual bus stops
ϱ	subscript for bus lines, the next bus in the merging order
κ	running index for the prediction
v_A	average velocity on the link upstream a signalized intersection outside the queue
ω	symbol of an elementary event
ρ_J	jam density
ρ_C	critical density
ρ_A	actual density
Q_C	peak capacity
Q_A	arrival rate of vehicles, macroscopic vehicle flow
$F_{Q_A}(t, \varphi)$	CDF of the arrival rate $Q_A(t, \omega)$
φ	probability level
v_J	jam velocity
v_C	critical velocity
l_q	tail of the queue
l_l	location of the traffic light
c	traffic light cycle counter
t_{cyc}	traffic light cycle time
t_1	start of the red traffic light phase
t_2	end of the red traffic light phase
t_{green}	green time interval
$W_1(t, \omega)$	queuing shockwave velocity
W_2	queue discharge wave velocity
$W_3(t, \omega)$	departure shockwave velocity

W_4	pressure wave
$R_J(t, \omega)$	queue traffic state
$R_C(t, \omega)$	queue discharge traffic state
$n(c, \omega)$	number of vehicles crossing the intersection at cycle c
t_{arr}	desired arrival time of the bus at the next stop
t_{sch}	scheduled departure time from a bus stop
N	MPC horizon length
X	bus dynamic states
A	state matrix of a bus
B_u	control input matrix in the bus dynamics model
B_w	disturbance matrix in the bus dynamics model
C_{tt}	output matrix for the timetable tracking error
D_{tt}	direct feedthrough matrix for the timetable reference trajectory
C_{hw}	output matrix for the headway tracking error
D_{hw}	direct feedthrough matrix for the headway reference trajectory
$\hat{\mathbf{x}}$	vector of predicted system states
$\underline{\underline{A}}$	stacked (hyper-)matrix of the state matrix
$\underline{\underline{B}}_u$	stacked matrix of the control input coefficients
\mathbf{u}	predicted control input sequence
$\underline{\underline{B}}_w$	stacked matrix of the disturbance coefficients
\mathbf{w}	disturbance along the prediction horizon
$\hat{\mathbf{z}}_{tt}$	predicted timetable tracking error
$\underline{\underline{C}}_{tt}$	stacked output matrix
$\underline{\underline{D}}_{tt}$	stacked direct feedthrough matrix for the timetable reference trajectory
ζ_{tt}	timetable reference along the prediction horizon
$\hat{\mathbf{z}}_{hw}$	predicted headway tracking error
$\underline{\underline{C}}_{hw}$	stacked output matrix
$\underline{\underline{D}}_{hw}$	stacked direct feedthrough matrix for the headway reference trajectory
ζ_{hw}	headway reference along the prediction horizon
q_{tt}	weighting coefficient for timetable tracking
Q_{tt}	weighting matrix for timetable tracking
$\underline{\underline{Q}}_{tt}$	stacked weighting matrix for timetable tracking
q_{hw}	weighting coefficient for headway tracking
Q_{hw}	weighting matrix for headway tracking
$\underline{\underline{Q}}_{hw}$	stacked weighting matrix for headway tracking
R_{tt}	control input cost for timetable tracking
$\underline{\underline{R}}_{tt}$	stacked control input cost for timetable tracking
R_{hw}	control input cost for timetable headway
$\underline{\underline{R}}_{hw}$	stacked control input cost for headway tracking
J_{tt}	cost term for timetable tracking
J_{hw}	cost term for headway tracking

Φ_{tt}	quadratic coefficient of the timetable tracking cost function
Ω_{tt}^T	linear coefficient of the timetable tracking cost function
Φ_{hw}	quadratic coefficient of the headway tracking cost function
Ω_{hw}^T	linear coefficient of the headway tracking cost function
η_{acc}	efficiency of acceleration
η_{reg}	efficiency of regeneration
v_{min}	lower bound for the desired velocity
v_{max}	upper bound for the desired velocity
a_{min}	lower bound for the vehicle acceleration
a_{max}	upper bound for the vehicle acceleration
J_e	cost term for penalizing energy consumption
J_p	cost term for penalizing passenger wait time
$\underline{\underline{S}}$	row selector matrix for the velocity states over the prediction horizon.
$\underline{\underline{K}}_{acc}$	symbol for the constant terms in the energy costing (acceleration)
$\underline{\underline{K}}_{reg}$	symbol for the constant terms in the energy costing (braking)
$\underline{\underline{W}}_{acc}$	weighting matrix for the quadratic part of the acceleration cost
$\underline{\underline{W}}_{reg}$	weighting matrix for the quadratic part of the regeneration cost
$\underline{\mathcal{V}}_{acc}$	weights for the linear part of the acceleration cost
$\underline{\mathcal{V}}_{reg}$	weights for the linear part of the regeneration cost
χ	state vector for a bus stop
Λ	state matrix for a bus stop
\mathcal{E}	coefficient matrix for the passenger arrivals
Υ	coefficient matrix for passenger exchange
$\hat{\chi}$	vector of predicted system states
$\underline{\underline{\Lambda}}$	stacked (hyper-)matrix of the state matrix
$\underline{\lambda}$	predicted passenger arrival rate
$\underline{\underline{\mathcal{E}}}$	stacked matrix for the passenger arrivals
$\underline{\underline{\Upsilon}}$	stacked matrix for passenger exchange
$\underline{\xi}$	predicted passenger exchange status
$\underline{\mathcal{P}}$	tuning parameter for passenger wait costing
$X_N(k)$	vector of network states (bus positions $x_{i=1\dots M_B}$, velocities $v_{i=1\dots M_B}$, and passenger numbers at stops $p_{j=1\dots M_S}$)
A_N	state matrix combining the bus and stop dynamics
$B_{N,u}$	coefficient matrix for the control inputs (bus desired velocities)
$u_N(k)$	collects the control input for each bus
$B_{N,h}$	boarding status coefficient matrix
$\xi_N(k)$	vector of boarding states
$B_{N,w}$	coefficient matrix for external signals (velocity disturbance for buses and passenger arrival rates for stops)

$\bar{w}_N(k)$	external signals for the bus network (velocity disturbance and passenger arrival rates)
$Z_N(k)$	vector of tracking errors
C_N	output matrix
D_N	direct feedthrough matrix of the reference trajectories
$\zeta_N(k)$	reference trajectories for the buses $x_{tt,i=1\dots M_B}$, $x_{hw,i=1\dots M_B}$
$\hat{\mathbf{x}}_N$	vector of predicted system states
$\underline{\underline{A}}_N$	stacked (hyper-)matrix of the state matrix
$\underline{\underline{B}}_{N,u}$	stacked matrix of the control input coefficients
$\underline{\mathbf{u}}_N$	predicted control input sequence
$\underline{\underline{B}}_{N,\xi}$	stacked matrix of the boarding rate
$\underline{\xi}_N$	predicted boarding states
$\underline{\underline{B}}_{N,w}$	stacked matrix of the external signals
$\underline{\mathbf{w}}_N$	disturbance along the prediction horizon
$\hat{\mathbf{z}}_N$	predicted tracking errors
$\underline{\underline{C}}_N$	stacked output matrix
$\underline{\underline{D}}_N$	stacked direct feedthrough matrix
$\underline{\zeta}_N$	references along the prediction horizon
J_N	network level cost function
$\underline{\underline{Q}}_{N,x}$	stacked weighting matrix for the system states (passenger numbers)
$\underline{\underline{Q}}_{N,z}$	stacked weighting matrix for the tracking errors
$\underline{\underline{R}}_N$	stacked control input cost
Φ_N	quadratic coefficient of the network cost function
Ω_N^T	linear coefficient of the network cost function
ϕ	scaling parameter for the adaptive control

Mathematical Symbols

\mathbb{R}	Set of real numbers
\mathbb{R}^n	Set of n dimensional real vectors
$\mathbb{R}^{n \times m}$	Set of real matrices with n rows and m columns
$\text{floor}\left(\frac{x}{y}\right)$	The largest integer value less than or equal to $\frac{x}{y}$ ($x, y \in \mathbb{R}$)
A^T	Transpose of matrix A
A^{-1}	Inverse of matrix A
$A \succ 0$	Positive definite matrix, i.e. $x^T A x > 0, \forall x \neq 0, x \in \mathbb{R}^n$
$A \succeq 0$	Positive semidefinite matrix, i.e. $x^T A x \geq 0, \forall x \neq 0, x \in \mathbb{R}^n$
$\text{diag}(x)$	Diagonal matrix which diagonal consists of the elements of vector x , i.e. x_i for $i = 1, 2, \dots, n$
$\text{dim}(A)$	Dimension of quadratic matrix A
$x(\omega)$	It means a random process, where the symbol ω denotes one realization of a random process
$E\{x(\omega)\}$	Expected value of random variable $x(\omega)$
$\mathbb{P}(\omega : x(\omega))$	Probability of a random event $x(\omega)$
$F_x(\xi)$	Cumulative distribution function of a random variable $x(\omega)$. ξ denotes a given probability level, i.e. $F_x(\xi) = \mathbb{P}(\omega : x(\omega) < \xi)$
$\min(\star)$	Minimum function. Returns the smallest argument.
$\max(\star)$	Maximum function. Returns the largest argument.

Chapter 1

Introduction

1.1 Background

In the 1910s the first public transport buses were introduced to major cities of that time. Since then, the population and congestion of urbanized areas exploded. This rapid growth poses new challenges to transport planners, service providers and passengers alike. In busy urban arterials, particularly during peak hours delay of public transport is critical. Due to the stochastic nature of traffic networks, adherence to a bus schedule is not guaranteed. Fluctuation of passenger demand, intersection delays, changing traffic conditions and different driving styles of bus drivers bring several uncertainties into the system. Achieving timetable reliability in an environment where “traffic flow dynamics are dominated by external events (red traffic lights) rather than by the inherent traffic flow dynamics” (Papageorgiou [1998]) is especially difficult. Although, traffic lights are a way of traffic control, they often neglect public transport priority.

For this reason, the throughput of a road link or the quality of public transport deteriorate and travel times increase. With the emergence of ITS technologies and improvements in sensor technology (GNSS, AVL, APC) new doors opened for road traffic control (Mandelzys and Hellinga [2010]). By actuating different components of a traffic network, its efficiency (reduced delays, increased throughput, better energy efficiency etc.) can be improved. The control of road traffic can be realized on different levels. Automakers tend to focus on component or vehicle level control (Varga and Németh [2012]; Varga et al. [2013, 2014]; Németh et al. [2014b,a, 2015]; Varga et al. [2015, 2017]). On the other hand, traffic planners think on intersection or transportation network level (Lin et al. [2010]; Tettamanti et al. [2014]; Chow et al. [2017]; Varga and Kulcsár [2016]; Kulcsár and Varga [2017]). Through technological advancement systems become more and more connected. Automakers are considering the influence of surrounding traffic and exploit the opportunities of communicating with the traffic infrastructure (Tettamanti et al. [2016]; Horváth et al. [2019] Horváth et al. [2019]; Varga et al. [2020]). This connectedness enable novel, efficient transportation systems.

Without efficient supervisory control public transport service providers are unable to ensure a temporally and spatially homogeneous service. Increased passenger demand and interactions with dense traffic are contributing factors to bus bunching. At

frequent lines, if the schedule cannot be held and a bus arrives at the stop late, number of passengers is winding up. Increased dwell times further delay the bus. The headway between the current and the successor bus will eventually decrease so much that buses stick together. This instability in public transport is called bus bunching and was first described in [Newell and Potts \[1964\]](#). Due to bunching the periodicity of arrivals fail and homogeneous service cannot be maintained ([Ap. Sorratini et al. \[2008\]](#)). It leads to poor utilization of buses and therefore degradation of level of service. [Fonzone et al. \[2015\]](#) studied the effect of passenger arrival patterns on bunching, concluding that unexpected passenger demands are the root cause of bunching. Furthermore, passengers tend to board the first bus to reduce their own travel delay. Bus bunching has a well-established literature and several authors proposed different methods to overcome its adverse effect. The three main approaches to bunching reduction are bus holding, bus priority at signalized intersections and velocity control.

Bus holding: buses are held at designated stops to sync with the schedule. Bus bunching was mitigated with bus holding control in [Wu et al. \[2017\]](#). Public transport reliability is addressed in [Nesheli et al. \[2015\]](#) with bus holding, stop skipping to minimize passenger waiting time. [Jiang et al. \[2017\]](#) proposed a heuristic algorithm with stop skipping or inclusion for congested high-speed train lines. In densely populated urban areas where city space is scarce, including slack times might not be possible due to bus stop configurations ([Cats et al. \[2012\]](#)). Furthermore, slacks are an unproductive allocation of time of time in the cycle time of buses and results in queuing at stops ([Daganzo \[2009\]](#)). Slack times can be dynamically addressed via changing the speed of the vehicle rather than holding it. In that sense, a smoothed and pro-active way of slack time reduction foreseeing the trajectories (headway, timetable) seem more appealing.

Bus priority: a common method in improving timetable reliability provides priority to buses at signalized intersections ([Estrada et al. \[2016\]](#)). In [Estrada et al. \[2016\]](#) a velocity control method considering bus-to-bus communication and green time extension is formulated.

Velocity control: in [Daganzo \[2009\]](#) and [Daganzo and Pilachowski \[2011\]](#) algorithms are developed to control the headway of consecutive buses by adjusting their desired velocity. [Ampountolas and Kring \[2015\]](#) proposed a cooperative control algorithm for buses to balance headways. [Bartholdi and Eisenstein \[2012\]](#) provided a self-controlling algorithm to improve headway reliability without timetable. In [Xuan et al. \[2011\]](#) optimal control algorithms are considered, taking into account both headway and timetable keeping. [Andres and Nair \[2017\]](#) used predictive algorithms to improve public transport reliability. In [Xuan et al. \[2011\]](#), optimal control algorithms were considered taking into account both headway and timetable keeping. In [Varga et al. \[2018c\]](#), both bus bunching and timetable adherence are dealt with model predictive control (MPC). Velocity control received criticism in comparison to holding (e.g. [Daganzo and Pilachowski \[2011\]](#)), due to drivers adherence to the predefined velocity or propagating delays to other participants of traffic. Moreover, there is only a small field for velocity control action possible: (i) in front of signalized intersections vehicle speed is entirely determined by the current phase of traffic (i.e. queuing, discharge) and (ii) delaying (slowing down) a vehicle in the course of the journey would only propagate the delay

to other participants in traffic. Therefore, velocity control is only desirable when the controlled vehicle is further away from the intersection and traffic is not too dense or there is space for overtaking (e.g. multiple lanes, [Gu et al. \[2013\]](#)). From the perspective of other participants of traffic a slowed down bus acts as a moving bottleneck. This suggests that the velocity control is efficient when it does not perturb the trajectories of other participants of traffic significantly. One of the main arguments for velocity control is that with the emergence of highly automated and autonomous vehicles accurate control can be achieved. In addition, the uncertain nature of traffic (intersection delays, congestion or slower vehicles ahead) can be ruled out with high penetration of connected vehicles communicating with each other and the infrastructure ([Tettamanti et al. \[2016\]](#)). In a highly automated environment, the sole remaining uncertainty is the behavior of humans, i.e. the passenger demand. The velocity control can be combined with holding strategies and can be adapted to the instantaneous state of the traffic network (i.e. quick change in control inputs) too.

On top of level of service, an emerging trend in public transport is the reduction of its environmental footprint, dependency on fossil fuels and carbon emissions. Several cities where pollution is a strong concern are shifting public transportation towards electrified vehicles ([Gallet et al. \[2018\]](#)). Electric vehicles have no tailpipe emissions, are quieter, more energy efficient and simpler, requiring less maintenance too. The need for increasing energy efficiency and the advances in driver assistance systems brought eco-cruise control strategies to life ([Németh and Gáspár \[2011\]](#), [Saerens et al. \[2013\]](#), [Akhegaonkar et al. \[2018\]](#), [Mihály et al. \[2018\]](#)). In urban areas interaction with traffic control devices dictate energy savings [Kural et al. \[2014a\]](#). Speed advisory systems incorporating V2I communication with traffic lights can result in significant energy reduction [Vreeswijk et al. \[2010\]](#). [Lv et al. \[2019\]](#) gave different control strategies for different driving styles for automated electric vehicles, bearing energy efficiency in mind. In addition to energy management between stops, charging station allocation and charging strategies are in the spotlight [Bi et al. \[2015\]](#), [Rogge et al. \[2018\]](#), [Rupp et al. \[2019\]](#). Instead of focusing on individual vehicles, urban transportation can be viewed as an independent component of a smart city power network [Amini \[2018\]](#). In a comprehensive literature survey, [Amini \[2018\]](#) examined different distributed electrified transport networks and suggested cooperative energy management strategies. [Rogge et al. \[2015\]](#) studied the feasibility of an electric bus network focusing on battery capacity, charging and impact on the grid. They concluded, it is necessary to consider an electric bus network as a whole, rather than looking at individual bus trips. The state of the art and potential challenges for vehicle to grid (V2G) technology were summarized in [Su et al. \[2012\]](#). Sustainable V2G technology requires energy management [Su et al. \[2012\]](#), [Mohamed et al. \[2017\]](#).

In rural areas the focus of eco-cruise control is on road topology ([Hellström et al. \[2010\]](#), [Németh and Gáspár \[2011\]](#)). On the other hand, in urban areas interaction with traffic control devices dictate energy efficiency ([Saerens et al. \[2013\]](#), [Akhegaonkar et al. \[2018\]](#)). The eCoMove project ([Vreeswijk et al. \[2010\]](#)) proposed a speed advisory system incorporating V2I communication with traffic lights. Simulation results suggested significant emission reduction. [Kural et al. \[2014b\]](#) implemented a predictive traffic light assistant that considers traffic light cycles during trajectory planning. However,

they only considered traffic light cycles without queue lengths. [Park et al. \[2011\]](#) and [Yang et al. \[2017a\]](#) constructed a dynamic programming based strategy to minimize fuel consumption in urban areas with traffic lights. The model estimates queue lengths with the help of shockwaves. In [Li et al. \[2018\]](#) a trajectory smoothing algorithm was formulated considering platoons of connected automated vehicles and traffic lights. According to [Kivekas et al. \[2019\]](#) predictive velocity control is capable of reducing energy consumption of battery electric urban buses. The model of [Pariota et al. \[2019\]](#) suggest fuel consumption and emissions reduction in the region of 5 to 12%. In addition, energy efficiency suggests smaller batteries or sparser charging stations further reducing investment costs ([Desreveaux et al. \[2019\]](#)).

Recently, authors turned towards modeling and control of the public transport bus network as a whole. A coordinated multiline bus holding strategy was formulated and network sensitivity analysis was carried out by [Laskaris et al. \[2018\]](#). The network layout, link lengths and passenger demand have significant effect on the network performance. In [Schmöcker et al. \[2016\]](#) the effect of overtaking on a corridor served by two lines was studied in comparison to bus holding. The paper concludes that the holding strategy is an additional source of delay to the system.

The literature review suggests that operating a bus network efficiently has several aspects. Previous works focus on one or two objectives: either bus bunching or energy efficiency, but not in a combined way. Multi-objective, passenger demand-driven public transport receives increasing interest recently. [Yang et al. \[2017b\]](#) developed a bi-objective optimization model with the consideration of energy consumption and passenger waiting time in metro systems for energy efficiency. In [Xuan et al. \[2011\]](#), optimal control algorithms were considered, taking into account both headway and timetable keeping. [Andres and Nair \[2017\]](#) used predictive algorithms to improve public transport reliability. In conclusion, optimizing electrified bus networks can be approached from different directions based on the authors' intention (e.g. energy minimization, ensuring service homogeneity).

1.2 Purpose and scope

Finding a compromise solution between energy consumption and level of service leads to a multi-objective optimization problem. The goal is merging four conflicting, public bus service related objectives:

- adherence to a predefined schedule,
- vehicles shall keep equidistant headways from each other,
- minimal passenger delay: both at stops and in vehicle and,
- energy efficiency.

The objectives are to be achieved solely based on velocity control. Buses operate on fixed routes based on a timetable. Headway of consecutive buses are the result of the timetable in conjunction with the network layout. The location of the buses is assumed to be known at every time instant (i.e. AVL) and traffic information and

external inputs can be communicated to them (i.e. V2I). The vehicles shall be equipped with computing devices that can realize the speed advisory system in a decentralized fashion in real-time. The control input is a desired velocity. It can be either displayed to the driver or in case of autonomous driving it can be a strict reference speed. The velocity control shall work with dedicated bus lanes and in mixed traffic too. In case of mixed traffic environment, the knowledge of traffic states (or the link fundamental diagram) is necessary. The algorithms can synergize with dynamic signal controlling and bus priority strategies too. Due to the vast variety of such signal control strategies, combining velocity control and traffic signal control is not considered in this work.

The main idea is to use short time horizon predictions (1-2 minutes) and optimize the trajectory of every bus in real-time. The suggested rolling horizon policy is an adequate control solution to predict future obstacles along the route and incorporate reference trajectories from various sources. The control method focuses on network bunching, but in a distributed, overlapped way: every vehicle runs its own velocity controller and then they communicate their predicted trajectories among each other. The proposed control algorithms consider uncertainties such as varying dwell times and delays due to interaction with traffic and traffic lights too. Moreover, the decentralized control can be recast into a centralized network-level velocity control. In that case the speed advisory algorithm attempts to calculate public-transport network optimum for every vehicle in the network concurrently.

The goals set in this section are achieved using the following scientific methods.

1.3 Methods

1.3.1 Modeling

Most control design methods require a priori description of the controlled system. The behavior of a real system is translated into mathematical concepts and language. As physical systems are very diverse, different modeling concepts shall be employed bearing in mind the purpose of controller design. The MPC design is generally based on discrete-time state space models. Discrete-time state space systems are mathematical models of physical systems described as a set of input, output and state variables related by difference equations. The solvability of these difference equations depend on their form as they boil down to optimization problems. In this thesis convex and piecewise convex models are employed for which fast solvers are available: Nocedal and Wright [2006]; Gurobi [2014]. The modeling approach tries to follow a first principle one. Systems are described with the governing physical equations of the system and linearized when needed. When it is not possible, due to the nature of the system empirical formulas are borrowed from the literature. In addition, stochastic models are used too where state variables (or inputs) are not described by unique values, but rather by probability distributions.

1.3.2 Model predictive control

The proposed control strategies are MPC based. The MPC is a very popular control framework in the state-of-the-art engineering practice. Accordingly, the application of the MPC based control appears both in traffic control (e.g. [Tettamanti and Varga \[2010\]](#), [de Oliveira and Camponogara \[2010\]](#)) and vehicle-level control too (e.g. [Yi et al. \[2016\]](#), [Andres and Nair \[2017\]](#)). Due to the look-ahead nature of the MPC it can be computationally demanding in large-scale systems. Therefore, a decentralized approach is chosen.

The MPC is a model based control procedure which can be efficiently applied for optimal control problems restricted by physical constraints ([Maciejowski \[2002\]](#)). The controller comprises an optimization part and a system model. The control calculation is carried out as an iteration process between the controller and the model by the minimization of an appropriate cost function. During the iteration, the optimization calculates the control inputs for the system model. Then, the model provides a state prediction giving back to the optimization. The iteration is repeated until the solution converges. The optimal control signals are then forwarded to the controlled system.

Basically, the MPC realizes a rolling-horizon optimization. The control inputs of the MPC are computed by minimizing a cost function $J(k)$ over the prediction horizon N obeying various constraints. System state $X(k)$ is measured at time step k . Then, for a finite horizon length (N) predicted states $x(k+i|k)$ are calculated along with the corresponding control inputs $u(k+i-1|k)$. At the end of the optimization process, from the control input sequence only the first one ($u(k|k)$) is applied to the system. The rest is discarded. At the subsequent time step ($k+1$), the prediction horizon rolls on until $N+1$. The controller proceeds the calculation concerning time step $k+1$ according to the updated measurements and estimations. The process is then continued similarly by repeating the measurement, estimation, and optimization. When a disturbance or an external signal is handled in the MPC, its future states are often unknown. A common remedy to this issue is fixing these signals along the prediction horizon (e.g. [Papamichail et al. \[2010\]](#)).

The method of a basic MPC controller is summarized in [Algorithm 1.1](#).

Algorithm 1.1 MPC based control

1. Measure state $x(k|k)$.
 2. Solve the finite horizon optimal control problem minimizing $J(k)$ to obtain $u(k+i-1|k)$ for $i = 1, 2, \dots, N$.
 3. Apply $u(k|k)$ to the system.
 4. At the end of the current control time step increment k by one: $k = k + 1$.
 5. Go to step 1.
-

1.3.3 Scenario approach and the sampling and discarding technique

A transportation system is inherently uncertain. In spite of uncertainty, a public transport system shall provide adequate service in all cases. Therefore, robust performance is desired instead of nominal performance or optimality. The system shall have good performance and be stable even if there are disturbances. Varying demand (passenger demand or traffic flow volume) and uncertain behavior of drivers make analysis and control of public transport challenging. Instead of closed mathematical formulations, analysis and control can be carried out more conveniently via numerical methods.

The scenario approach is a theoretically sound and practically effective technique for solving robust convex optimization problems in a probabilistic setting. These problems in systems and control design are generally hard to tackle via standard, deterministic techniques. Solvability of the robust problem is obtained through random sampling of the constraints. The scenario approach presumes a probabilistic description of uncertainty that is uncertainty is characterized through a set Δ describing the set of admissible situations, and a probability distribution over Δ . Solvability can be obtained through random sampling of constraints provided that a probabilistic relaxation of the worst-case robust paradigm is accepted. With this probabilistic approach robustness can only be guaranteed in a probabilistic sense, against the majority of the scenarios rather than all of them. On the other hand, the developer can decide which level of robustness is satisfactory if retained. The following theorem shows that randomly sampling N_t scenarios satisfies all chance constraints except a user-chosen fraction that tends rapidly to zero as N_t increases:

Theorem 1. *Select a ‘violation parameter’ $\epsilon_t \in (0, 1)$ and a ‘confidence parameter’ $\beta_t \in (0, 1)$. If*

$$N_t \geq \frac{2}{\epsilon} \left(\ln \frac{1}{\beta} + d_t \right) \quad (1.1)$$

where d_t is the number of optimization variables. Then, with probability no smaller than $1 - \beta_t$ the solution satisfies all constraints in Δ but at most an ϵ -fraction.

The scenario approach consists of the following steps:

- reformulation of the problem as a robust (with infinite constraints) convex optimization problem;
- randomization over constraints and resolution (by means of standard numerical methods) of the so-obtained finite optimization problem;
- evaluation of the constraint satisfaction level of the obtained solution through Theorem 1.

(Campi et al. [2009], Campi and Calafiore [2009])

The sampling and discarding method is the relaxation of chance-constrained optimization problems through constraint removal. Constraints removal allows one to improve the cost function at the price of a decreased feasibility. A continuous stochastic

event can be replaced with a finite sample of independent instances $\omega^{(1)}, \omega^{(2)}, \dots, \omega^{(M_t)} \in \Omega$, distributed according to \mathbb{P} where Ω is the sample-space. The optimization is then solved for M_t chance-constraints and the additional non-chance-constraints. When all the M_t constraints are enforced, one cannot expect that good approximations of chance-constrained solutions are obtained. Thus, constraint violation is allowed of the sampled constraints to improve the optimization value. If M_t constraints are sampled and k_t them are eliminated according to any arbitrary rule, then the solution that satisfies the remaining $M_t - k_t$ constraints is, with high confidence, feasible for the chance-constrained optimization program (Campi and Garatti [2011]).

1.4 Overview and structure of the Thesis

The body of the dissertation consists of two modeling and three control chapters. See the structural overview in Figure 1.1.

Chapter 2 provides control oriented models to condense the characteristics of public transport buses and stops into mathematical formulas. The proposed models can serve as a basis of a decentralized, reference tracking velocity control and can be extended to a whole public transport network. This contribution manifests in *Thesis 1*.

Next, the surroundings of the public transport line is modeled: in a busy urban setting traffic light cycles constrain the flow of traffic. Chapter 3 aims at grasping this phenomenon in a stochastic way. The contribution of *Thesis 2* extends the urban shockwave profile model with the randomness of traffic flow at signalized intersections.

Chapter 4 presents the contributions of *Thesis 3*. It builds upon the models formulated in Chapter 2 as they are extended for a finite horizon, realizing a rolling horizon control. The aim of the velocity control is calculating an optimal velocity profile towards the next bus stop. The chapter proposes various control strategies based on different weighting of four conflicting control objectives (punctuality, equidistant headways, minimal passenger waiting time and energy consumption). The control strategies are analyzed in various traffic simulator based scenarios.

Chapter 5 builds upon Chapter 3 and Chapter 4. The stochastic shockwave profile model (SPM) is incorporated into the model predictive trajectory planning through chance-constraints. Stochasticity is relaxed with the help of the sampling and discarding method and probability levels are sought where the predicted trajectories remain feasible. The findings of this chapter are summarized in *Thesis 4*.

Finally, Chapter 6 discusses the contributions of *Thesis 5*. The public transport network model from Chapter 2 is used for a centralized MPC. The centralized controller is analyzed from different aspects and compared to the decentralized approach in Chapter 4.

Finally, Chapter 7 concludes the thesis results and sets future research directions.

1.5 Related Publications of the Author

The contributions of the thesis are based on previously published journal and conference papers with the participation of the thesis author. These papers are collected below.

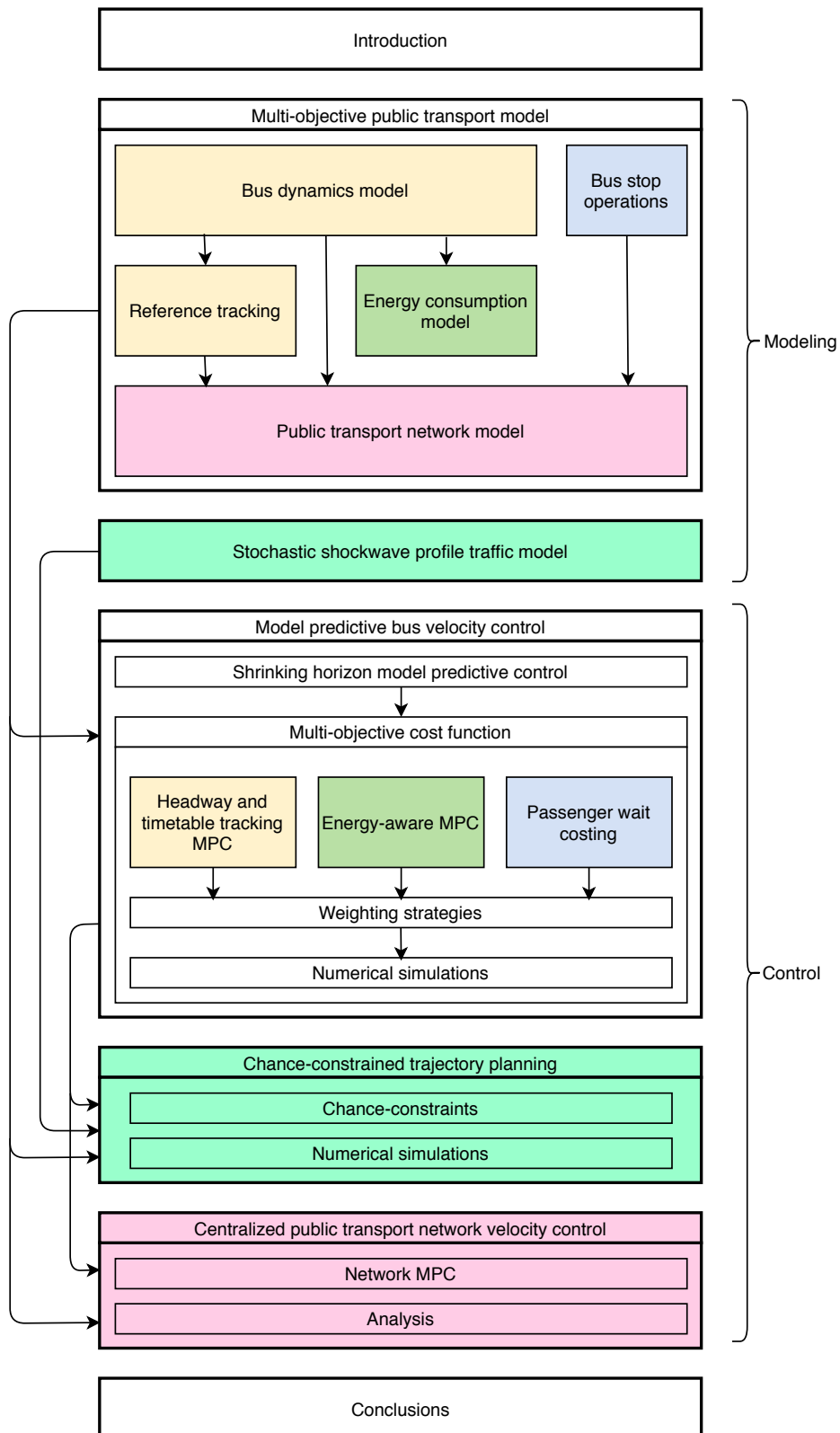


Figure 1.1: Structural overview of the dissertation

The system modeling chapter (Chapter 2) builds upon:

Kulcsár, B.; Varga, B. Drive us - into sustainable automatized bus trains. *Research report*, Chalmers University of Technology, 2016.

Varga, B.; Tettamanti, T.; Kulcsár, B. Multiobjective control to mitigate bus bunching and improve schedule reliability of public transport. In *Swedish Transportation Research Conference*, 17-18 October 2017, Stockholm, Sweden

Varga, B.; Tettamanti, T.; Kulcsár, B. Optimally combined headway and timetable reliable public transport system. In *Transportation Research Part C: Emerging Technologies*, Elsevier, 2018, 92, pp 1-26

Varga, B. Energy Aware Cruise Control For Urban Public Transport Buses. In *16th Mini Conference on Vehicle System Dynamics, Identification and Anomalies (VSDIA 2018)*, 5-7. November 2018, Budapest, Hungary

Varga, B.; Tettamanti, T.; Kulcsár, B. Optimal headway merging for balanced public transport service in urban networks. In *15th IFAC Symposium on Control in Transportation Systems (CTS 2018)*, pp 416-421, June 6-8 2018, Savona, Italy

Varga, B.; Tettamanti, T.; Kulcsár, B. Energy-aware predictive control for electrified bus networks. In *Applied Energy*, Elsevier, 2019, 252, pp 1-27

Varga, B.; Péni, T.; Kulcsár, B.; Tettamanti, T. Network-level optimal control for public bus operation. In *21st IFAC World Congress*, 12-17 July 2020, Berlin, Germany, 2020

The stochastic shockwave profile model detailed in Chapter 3 is also described in the following publications:

Varga, B.; Tettamanti, T.; Kulcsár, B. Urban cruise control based on stochastic shockwaves. In *Swedish Transportation Research Conference*, 15-17 October 2018, Gothenburg, Sweden

Varga, B.; Tettamanti, T.; Kulcsár, B. Chance-constrained trajectory planning. In *Swedish Transportation Research Conference*, 22-23 October 2019, Linköping, Sweden

Varga, B.; Tettamanti, T. Sztochasztikus lökeshullámmódel levezetése és alkalmazási lehetőségei (Deduction and possible applications of the stochastic shockwave profile model) *Közlekedéstudományi Szemle*, 2019, 69, pp 45-52. In *Hungarian*

Varga, B.; Tettamanti, T.; Kulcsár, B.; Qu, X. Public transport trajectory planning with probabilistic guarantees In *Transportation Research Part B: Methodological*, Elsevier, 2020 (submitted)

Chapter 4 builds upon the following publications:

Varga, B.; Tettamanti, T.; Kulcsár, B. Multiobjective control to mitigate bus bunching and improve schedule reliability of public transport. In *Swedish Transportation Research Conference*, 17-18 October 2017, Stockholm, Sweden

Varga, B.; Tettamanti, T.; Kulcsár, B. Optimally combined headway and timetable reliable public transport system. In *Transportation Research Part C: Emerging Technologies*, Elsevier, 2018, 92, pp 1-26

Varga, B. Energy Aware Cruise Control For Urban Public Transport Buses. In *16th Mini Conference on Vehicle System Dynamics, Identification and Anomalies (VSDIA 2018)*, 5-7. November 2018, Budapest, Hungary

Varga, B.; Tettamanti, T.; Kulcsár, B. Energy-aware predictive control for electrified bus networks. In *Applied Energy*, Elsevier, 2019, 252, pp 1-27

Chapter 5 is based upon:

Varga, B.; Tettamanti, T.; Kulcsár, B. Optimally combined headway and timetable reliable public transport system. In *Transportation Research Part C: Emerging Technologies*, Elsevier, 2018, 92, pp 1-26

Varga, B.; Tettamanti, T.; Kulcsár, B. Urban cruise control based on stochastic shockwaves. In *Swedish Transportation Research Conference*, 15-17 October 2018, Gothenburg, Sweden

Varga, B.; Tettamanti, T.; Kulcsár, B. Chance-constrained trajectory planning. In *Swedish Transportation Research Conference*, 22-23 October 2019, Linköping, Sweden

Varga, B.; Tettamanti, T. Sztochasztikus lökeshullámmodell levezetése és alkalmazási lehetőségei (Deduction and possible applications of the stochastic shock-wave profile model) *Közlekedéstudományi Szemle*, 2019, 69, pp 45-52. In *Hungarian*

Varga, B.; Tettamanti, T.; Kulcsár, B.; Qu, X. Public transport trajectory planning with probabilistic guarantees In *Transportation Research Part B: Methodological*, Elsevier, 2020 (submitted)

The centralized network control in Chapter 6 is summarizing the results of the following publications:

Varga, B.; Tettamanti, T.; Kulcsár, B. Optimal headway merging for balanced public transport service in urban networks. In *15th IFAC Symposium on Control in Transportation Systems (CTS 2018)*, pp 416-421, June 6-8 2018, Savona, Italy

Varga, B.; Péni, T.; Kulcsár, B.; Tettamanti, T. Network-level optimal control for public bus operation. In *21st IFAC World Congress*, 12-17 July 2020, Berlin, Germany

Chapter 2

Multi-objective public transport model

This chapter describes the mathematical model of public transport bus operation. Modeling is divided into five parts:

- First, the dynamical model of a single bus traveling on an urban arterial is described.
- Buses shall follow a fixed timetable and attempt to keep a predefined headway from the preceding bus. To this end, reference trajectories are prescribed.
- Energy efficiency is an essential factor in public transport. Energy consumption of buses are taken into account via a first principle model.
- An integral part of public transport networks are bus stops. The accumulation of passengers and the passenger exchange (boarding and alighting) at stops are modeled too.
- Finally, the bus network operation problem can be grasped in a centralized way too. Accordingly, bus dynamics and bus stop operations can be fused into a single public transport network model.

2.1 Bus dynamics model

Movement along an urban corridor is characterized by a longitudinal car following model based on [Bando et al. \[1995\]](#). The discrete-time model for the bus dynamics (position $x(k)$, velocity $v(k)$ and acceleration $a(k)$) can be given as follows:

$$x(k+1) = x(k) + v(k)\Delta t, \quad (2.1)$$

$$v(k+1) = v(k) + a(k)\Delta t, \quad (2.2)$$

$$a(k) = \frac{1}{\tau}(v_{des}(k) - v(k) - v_{dist}(k)), \quad (2.3)$$

where position $x(k+1)$ and velocity $v(k+1)$ denote the states over the time period of $[\cdot k\Delta t, (k+1) \cdot \Delta t]$ with Δt being the discrete time-step length, and $k = 1, 2, 3, \dots$

the discrete time-step index. The acceleration is modeled with a linear relaxation term where $v_{des}(k)$ denotes the desired velocity (i.e. velocity setpoint) of the vehicle. τ is a model parameter capturing the sensitivity of drivers to the change of their desired velocity. According to Helbing and Tilch [1998] it shall be calibrated between (1.25 s) s and (2.5 s). Considering buses are heavier than passenger cars and bus drivers shall drive more carefully due to standing passengers, the relaxation term shall be closer to the upper limit (2, 5 s) Too small values would result in rapid acceleration or deceleration towards the desired velocity. With autonomous vehicles these parameters could change, but still it is preferred to mimic the behavior of human drivers so their presence does not perturb traffic significantly and does not disturb other drivers participating in traffic (Kesting et al. [2008]).

In addition, an additive error structure is proposed to include the adverse effect of other vehicles participating in traffic: $v_{dist}(k) = \beta(v_{des}(k) - v_{mac}(k))$, with $v_{mac}(k)$ being the macroscopic average velocity on the link the bus travels on. $\beta \in [0, 1]$ describes relaxation of bus speed towards a traffic dependent equilibrium speed. With this term, road link specific obstacles such as traffic lights or bottlenecks can be considered. The smaller β is, the slower vehicles adjust their velocity to the macroscopic average velocity (Hoogendoorn and Bovy [2001], Van den Berg et al. [2003]). $v_{mac}(k)$ denotes the macroscopic equilibrium speed (Daganzo and Geroliminis [2008]). Note that if the desired velocity falls below the equilibrium speed ($v_{des}(k) < v_{mac}(k)$) the sign of the disturbance term changes. It forces the vehicle to increase its speed, in order to flow with the traffic. Nevertheless, this simplistic approach only considers the average velocity of other vehicles interacting with the controlled bus and cannot capture more complex situations such as signalized intersections, shockwaves etc. Via dynamically varying the relaxation parameter ($\beta \rightarrow \beta(t)$), the surrounding traffic could be more accurately considered at the cost of losing the LTI nature of the model. A more sophisticated model for the surrounding traffic and signalized intersections will be given in Chapter 3.

The above equations can be written into state space form with $v_{des}(k)$ being the controlled variable of the system: it serves as a display to the driver or a strict reference in case of autonomous driving. $X(k) = [v(k), x(k)]^T$ is the vector of system states at time step k . Finally, $v_{mac}(k)$ is the traffic disturbance. The state space representation of the system is therefore:

$$\begin{bmatrix} v(k+1) \\ x(k+1) \end{bmatrix} = \begin{bmatrix} 1 - \frac{\Delta t}{\tau} & 0 \\ \Delta t & 1 \end{bmatrix} \begin{bmatrix} v(k) \\ x(k) \end{bmatrix} + \begin{bmatrix} \frac{\Delta t}{\tau}(1 - \beta) \\ 0 \end{bmatrix} v_{des}(k) + \begin{bmatrix} \beta \\ 0 \end{bmatrix} v_{mac}(k). \quad (2.4)$$

2.2 Reference tracking

The buses on a line shall aim at achieving two conflicting objectives characterized via two error terms. Setpoints are designed to increase public transport reliability both in time (adhering to the schedule) and space (equidistant headways to reduce bus bunching).

2.2.1 Timetable tracking

Define an idealized “optimal” trajectory based on the bus schedule $x_{tt}(k)$. The timetable reference trajectory is calculated offline considering the average travel time between stops and idealized dwell times. Based on the timetable reference and the actual position of the bus an error term can be formulated:

$$z_{tt}(k) = x(k) - x_{tt}(k). \quad (2.5)$$

If this error term is zero, the bus follows the timetable accurately. Each bus has an ideal timetable consisting of ideal dwell and average velocities between them (i.e. a broken line in the space-time diagram). Bus stop locations are calculated from the starting point of the bus line.

2.2.2 Headway tracking

The purpose of the second reference trajectory is headway tracking (i.e. eliminating the bus bunching effect). The headway reference trajectory is the past trajectory of the leading bus shifted by one ideal headway time T_{hw} ahead: $x_{hw}(k) = x_{i-1}(k - T_{hw}\Delta t)$. Subscript $i - 1$ denotes the bus ahead. If the bus follows this trajectory, one headway distance is guaranteed in an insensitive way to the actual velocity of the leading bus.

If this error term is to be used in a predictive scheme, its future values shall be known. It can be assumed, that the preceding bus already traveled on that route so its historical trajectory can be used as long as the prediction horizon is smaller than the actual time headway between the two buses. The headway tracking error term is

$$z_{hw}(k) = x(k) - x_{hw}(k). \quad (2.6)$$

Other authors (e.g. [Daganzo and Pilachowski \[2011\]](#)) considered two-way-looking (forward and backward) strategies for headway control. They concluded that effect of the backward looking part (following bus) is only significant in case of considerable headway disturbance. Due to the chosen model predictive approach in this thesis, only forward looking control is considered. That is, because the backward looking reference trajectory cannot be easily constructed. The position of the following bus is known for the current time instant k , however unknown for any future $k + \kappa$, $\kappa = 1, 2, \dots$ time steps.

The two reference trajectories are depicted in [Figure 2.1](#).

2.3 Energy consumption model

In this section, an energy consumption model is proposed for electric public transport vehicles, based on their velocity profile. Further in this section, the proposed model is simplified and reformulated into a piecewise cost function. The model discusses the share of resistances and the effect of recuperation. The energy consumption model is based on the longitudinal motion of the vehicle ([Section 2.1](#)) and the losses occurring during operation. Energy consumption is obtained by summing the power required to

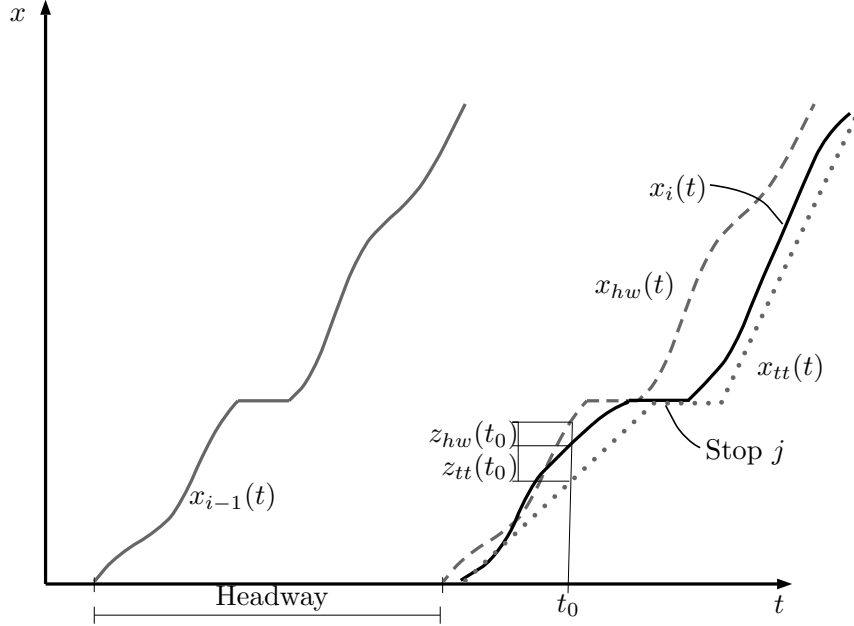


Figure 2.1: Reference tracking

move the vehicle in every time instant k . The modeling framework is based on the model used by [Guzzella et al. \[2013\]](#) and [Barth and Boriboonsomsin \[2009\]](#).

The tractive power at the wheels P_w consists of five terms:

$$P_{roll}(k) = \mu \cdot m \cdot g \cdot \cos\theta \cdot v(k) \quad (2.7)$$

is the rolling resistance with m the total vehicle mass and inertia, $g = 9.81m/s^2$ the gravitational constant, $v(k)$ the velocity and μ the rolling resistance factor. Rolling resistance for buses on dry asphalt is approximately 0.01. θ is the road inclination. In civil engineering practice, road grade is given in percentage: how much the road ascends or descends (*asc*) over 100 meters. Thus, road inclination can be written as: $\theta = \tan^{-1} \frac{asc}{100}$. Weight consists of the curb weight of the vehicle m_{veh} and the weight of passengers m_p : $m = m_{veh} + p_o m_p$. The average weight of a passenger m_p is assumed to be $80kg$ and p_o is the number of passengers on board the bus. The total vehicle mass is passenger number dependent, its value changes after each bus stop. Fortunately, passenger load is measurable, so it can be considered as a varying parameter in the model.

The extra power required when driving uphill (or downhill) is

$$P_g(k) = m \cdot g \cdot \sin\theta \cdot v(k). \quad (2.8)$$

Next the air drag is analyzed.

$$P_{drag}(k) = \frac{1}{2} \cdot c_w \cdot \rho_{air} \cdot A_f \cdot v(k)^3, \quad (2.9)$$

where c_w is the drag coefficient, $\rho_{air} = 1.293kg/m^3$ the air density and A_f the frontal area of the vehicle.

The last two terms are related to acceleration and deceleration $a(k)$ of the vehicle. For convenience, denote acceleration with $a^+(k)$ and deceleration with $a^-(k)$. The power required to accelerate is:

$$P_{acc}(k) = m \cdot v(k) \cdot a^+(k). \quad (2.10)$$

This term is zero when decelerating, regeneration is taken into account in the following term:

$$P_{regen}(k) = m \cdot v(k) \cdot a^-(k) \cdot \eta_{regen}, \quad (2.11)$$

where this term is negative, because it is not a loss, but a power gain. η_{regen} stands for the efficiency of regeneration.

The power required to move the vehicle is the summation of the five terms in Equations (2.7)-(2.11):

$$P_w(k) = P_{roll}(k) + P_g(k) + P_{drag}(k) + P_{acc}(k) + P_{regen}(k). \quad (2.12)$$

Next, drivetrain of electric buses is examined from efficiency point of view. Figure 2.2 depicts the losses of an electric powertrain. The efficiency of batteries of electric

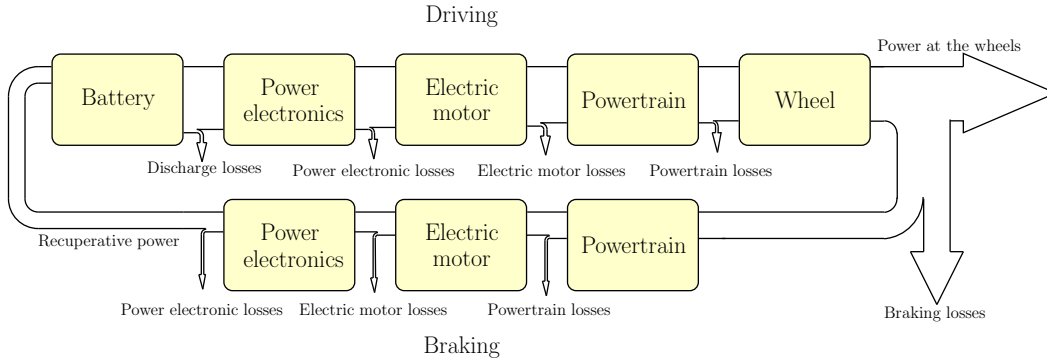


Figure 2.2: Sankey diagram of an electric powertrain with regenerative braking

vehicles varies in a wide range. For Lithium-ion batteries it is around $\eta_{batt} = 90 - 95\%$. The efficiency of the electric machine varies based on its operation point, but the aim is to keep it as high as possible. The power electronics (e.g. inverter, cabling, etc.) loss is between 1 - 4%, thus $\eta_{pe} = 96 - 99\%$. The electric motor efficiency is assumed to be between $\eta_{mot} = 90 - 97\%$. Finally, the mechanical efficiency of the powertrain is $\eta_{pt} = 98\%$. The regeneration efficiency of electric vehicles is considered. It depends on several factors such as the intensity of braking (i.e. using friction brakes too) the state of charge etc. (Olsson et al., Lv et al. [2018]). Feeding back means the direction of the energy flow is reversed, the losses in the drivetrain will apply again. For the sake of simplicity, regeneration efficiency is assumed to be $\eta_{regen} = 50\%$.

The losses arising during operation are summarized in the Sankey diagram in Figure 2.2.

The energy consumption of a vehicle during one discrete time step:

$$E_{cons}(k) = \left(\frac{P_{roll}(k) + P_g(k) + P_{drag}(k) + P_{acc}(k)}{\eta_{batt} \cdot \eta_{pe} \cdot \eta_{mot} \cdot \eta_{pt}} + P_{regen}(k) \cdot \eta_{batt} \cdot \eta_{pe} \cdot \eta_{mot} \cdot \eta_{pt} \right) \Delta t. \quad (2.13)$$

2.4 Bus stop operations

This section presents the models used to describe the pattern of passenger arrivals at stops and the dynamics of boarding and alighting. The passenger arrival model in conjunction with the dwell time model describe the operations taking place at a bus stop. The proposed models give a deterministic (mean-valued) characterization of the status of a bus stop. First, assumptions are made on the arrival patterns of passengers to a bus stop based on the literature. Then, a passenger wait model is given that can be employed for control purposes.

2.4.1 Passenger arrival model

The average passenger waiting time at a stop can simply be described as half of the arrival rate of the public transport vehicle. This assumption holds if the following conditions are fulfilled: passengers arrive randomly and independently; passengers can get on the first arriving vehicle and vehicles have equal headways (Holroyd and Scraggs [1966]). In routes with frequent service (headways with 10 minutes or less) passengers typically do not consult schedules before arriving at their stops, their arrival rate can be thought random (Dessouky et al. [2003]). If a stop is shared by multiple lines, arrival rates are harder to estimate, since they shall be split between the lines. A passenger may wait for a particular line or board the next bus.

In Jolliffe and Hutchinson [1975] three types of passengers are categorized.

- a) There are passengers whose arrival time is coincident with the bus. These are the passengers who run to the stop because they see the bus coming, and thus wait zero time.
- b) There are some passengers who plan their arrival at the bus stop so as to be there just before the bus comes, minimizing their expected waiting time. This decreases the average waiting time (O'Flaherty and Mangan [1970]).
- c) Finally, there are independent, uniformly distributed random passenger arrivals.

The arrival rate of group *b*) and *c*) is described by Poisson distribution and their ratio depends on the length of bus headways.

The time between successive arrivals is modeled with parameter $\lambda(k)$ (arrival rate) and independent of the past. This demand can be split into the three aforementioned categories. Figure 2.3 depicts the arrival rate of each passenger type between successive bus departures ($t_{dep,i}$ and $t_{dep,i+1}$). The area under the graph equals the number of passengers waiting at the stop. This is the number of boarding passengers p which is used in the dwell time model.

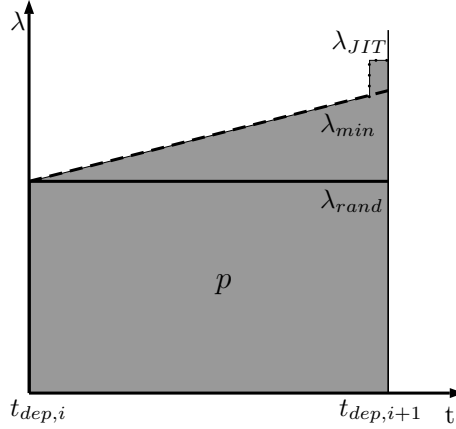


Figure 2.3: Arrival rate of each passenger type: *a*) coincident or just in time (JIT) arrivals (λ_{JIT}), *b*) waiting time minimizers (λ_{min}), *c*) random arrivals (λ_{rand})

2.4.2 Bus stop model

Dwell time is the average amount of time a public transport bus is stopped at the curb to serve passenger movements, including the time required to open and close the doors (Kittelson et al. [2003]). Uncertainty in dwell times is a major factor for bus bunching and it directly affects travel time and level of service. The total time spent at stops can consume up to 26% of the total travel time Rajbhandari et al. [2003]. It is influenced by several factors: the configuration and occupancy of the bus, the number of boarding and alighting passengers, the configuration of stops, and the method of fare collection (e.g. on board or pre-ticketing) (Sun et al. [2014]).

According to Kittelson et al. [2003] time spent at a bus stop can be estimated knowing the number of boarding and alighting passengers, door configuration and other factors such as low floor, fare paying method etc. The average dwell time t_d at a bus stop can be calculated as:

$$t_d = \max(p \cdot t_b, p_a \cdot t_a) + t_{oc}, \quad (2.14)$$

where

- t_b is the average boarding time per passenger,
- t_a is the average alighting time per passenger,
- t_{oc} is the door opening and closing time,
- p is the number of boarding passengers and
- p_a is the number of alighting passengers.

Transportation Research Board [2016] gives rule of thumb values for the above parameters depending on bus and bus stop configuration: $t_{oc} = 3.5$ s, $t_a = 1.2$ s and $t_b = 1.5$ s. It is also assumed, that the boarding time takes longer than the alighting

and the two are done parallel (Sun et al. [2014]). Therefore, the dwell time is proportional to the number of boarding passengers Kittelson et al. [2003]. For simplicity, the number of passengers waiting at the stop is assumed to be known (via measurement Garcia-Bunster and Torres-Torriti [2009] or estimation Luethi et al. [2007]).

2.4.3 Passenger wait model

With the above assumptions, the passenger numbers at a stop can be modeled. The purpose of the model is short-term prediction of the occupancy of the bus stop as well as the dwell time and cumulated waiting times. The number of passengers $p(k)$ waiting at a stop can be written as:

$$p(k+1) = p(k) + \lambda(k)\Delta t - \frac{\Delta t}{t_b}\xi(k). \quad (2.15)$$

where λ denotes the number of passengers arrived at time step k and may be computed from the passenger arrival model, described in Section 2.4.1. In addition, the boarding rate (passenger / time-step) is $\frac{\Delta t}{t_b}$ (Transportation Research Board [2016]). The integer variable $\xi(k)$ denotes ongoing passenger exchange. This variable will play a key role in formulating the network model as a hybrid dynamical system. $\xi(k)$ equals to the number of buses performing passenger exchange at the stop. This means passenger boarding rate is multiplied when multiple buses are present. A bus is performing passenger exchange if it is at the stop, its velocity is zero and there are passengers at the stop. In mathematical form:

$$\begin{aligned} \xi(k) &= \sum_{i=1}^{M_B} \exists i : (|x_i(k) - x_{stop}|) < \epsilon \\ &\& v_i(k) \leq \epsilon. \& p(k) \geq \epsilon, \end{aligned} \quad (2.16)$$

where M_B is the number of buses in the network and ϵ are numerical tolerances. It shall be further assumed that the boarding rate is greater than the passenger arrival rate: $\frac{1}{t_b} > \lambda(k)$.

The cumulated passenger waiting time can be expressed as

$$t_w(k+1) = t_w(k) + p(k)\Delta t. \quad (2.17)$$

Finally, the algebraic equation for the dwell time is

$$t_d(k) = p(k)t_b + t_{oc}. \quad (2.18)$$

Since the control algorithms outlined in this dissertation are time-based (i.e. the independent variable is time), dwell time (Eq. (2.18)) cannot be directly considered. On the other hand, the cumulated passenger waiting time can be used as a performance output. The two discrete-time differential equations (Eq. (2.15) and Eq. (2.17)) can be organized into a state space representation of a single bus stop.

$$\begin{bmatrix} t_w(k+1) \\ p(k+1) \end{bmatrix} = \begin{bmatrix} 1 & \Delta t \\ 0 & 1 \end{bmatrix} \begin{bmatrix} t_w(k) \\ p(k) \end{bmatrix} + \begin{bmatrix} 0 \\ \Delta t \end{bmatrix} \lambda(k) + \begin{bmatrix} 0 \\ -\frac{\Delta t}{t_b} \end{bmatrix} \xi(k). \quad (2.19)$$

A further logical condition shall be made: if a bus arrived at a stop and finished boarding, the passenger wait time state $t_w(k)$ shall be reset. That is, to prevent the wait time to wind up and result in arbitrarily large wait times distorting the optimization cost. When multiple bus lines serve the stop, virtual stops are proposed at the same location with different passenger arrival rates for different bus lines. E.g. a bus stop shared by two lines A and B it will consist of three virtual stops with the state-space model in (2.19) but with independent states and arrival rates λ_A , λ_B , and $\lambda_{A \vee B}$. Subscript $A \vee B$ denotes passengers that board the bus that arrives first.

2.5 Public transport network model

2.5.1 Merging bus lines

The models described in the previous sections focus on individual buses or bus stops. A public transport network is the interaction of these elements. In a complex network bus lines merge or split up. This means different bus headways at different parts of a bus's route. When bus lines merge, buses enter the common line according to their own schedule and the headway with the other line is not synchronized. It is desirable to introduce buses to the common route with equal headways to avoid bunching. The purpose of the bus merging model is providing a framework to order buses and adjust their headways prior entering a common road link. Figure 2.4 depicts the merging problem for two bus lines. Buses operate on their dedicated lines with a desired period-

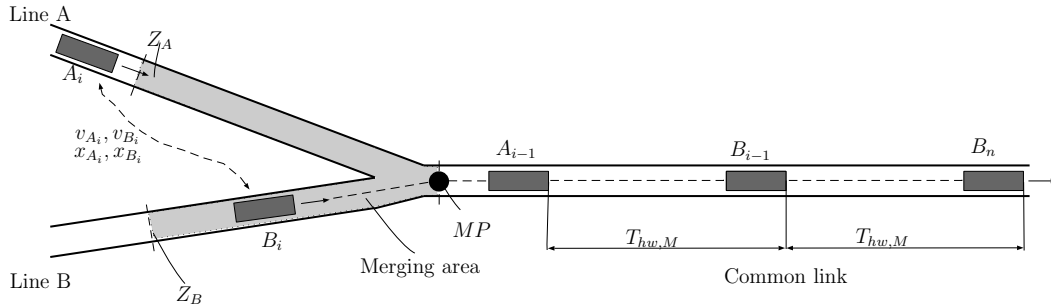


Figure 2.4: Merging bus lines at a two-legged junction

icity. When these lines merge, they have to adhere to a different periodicity. Without control action, time headways are offset from the ideal. Moreover, arrival patterns shall be prescribed in order to remedy irregular service.

Through an example of finite K merging bus lines the time headway on the common is determined. Assume bus line A, B, \dots, K have headways $T_{hw,A}, T_{hw,B}, \dots, T_{hw,K}$ on their own routes, respectively. Then the headway on the common corridor M can be calculated similar to the resistance of parallel resistors in electronics.

$$T_{hw,M} = \frac{\prod_{\ell=A}^K T_{hw,\ell}}{\sum_{\ell=A}^K T_{hw,\ell}}. \quad (2.20)$$

Next, based on the timetable of individual bus lines, define a merging pattern pat . It determines the order in which the buses shall travel on the common line. The

simplest way to obtain such pattern is by taking the uncontrolled, periodic arrivals of each line at the merging point or at the first common stop. This inherently results in an arrival pattern but it can also be adjusted by the transport service provider. An example of three merging lines is presented in Figure 2.5. Timetable periodicity on individual lines results in a circular pattern, in Figure 2.5 two periods of pat are shown. This pattern does not define the timetable exactly, only the order in which they shall operate on the common line. The pointer ϱ shows the desired line to enter the common line. The control action is able to adjust the velocity of the buses such that they reach the merging point MP according to the desired pattern. The point on the bus network where two (or more) lines join shall be called merging point MP . The common timetable is the combination of pat (order of buses) and $T_{hw,M}$ (headway).

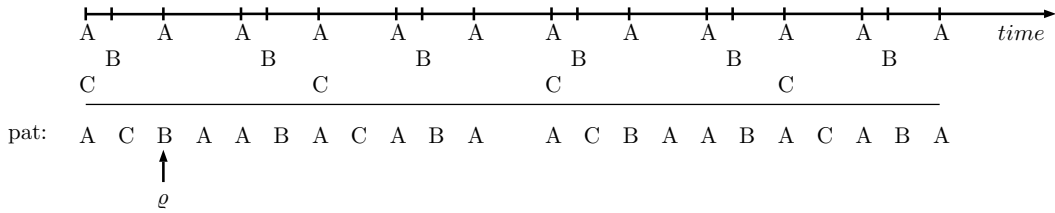


Figure 2.5: Pattern of three merging buses with $T_{hw,A} = 1$, $T_{hw,B} = 2$, and $T_{hw,C} = 3$.

In addition, define merging areas. The merging area spans from the merging point upstream each leg of the intersection. Denote the start of each merging zone with Z_A, Z_B, \dots, Z_K for lines A, B, \dots, K respectively. Once buses enter the merging zone the headway balancing velocity control can start. The flowchart of the velocity control is outlined in Figure 2.6.

If a bus reaches the proximity (e.g. 500 m) of the start of the merging area Z_ϱ it is checked whether it can enter the common line. The line number of the bus (A, B, \dots, K) is compared to the desired one, defined by the ϱ^{th} element of the pattern (pat). If it matches, the velocity control starts and ϱ is incremented by one. In case a bus arrives at the merging area but its line number does not match $pat(\varrho)$, its velocity is reduced until another bus enters the merging area. It is then checked if this newly arrived bus can be the leader of the slowed down bus. This strategy makes it possible to reorganize buses in the merging area.

If buses are arriving at a common corridor from separate lines, prior to merging their headway cannot be defined. The problem is demonstrated in Figure 2.4 in the case of buses A_i and B_i too. In order to formulate this virtual headway, extrapolation is needed. It shall be predicted, when the leading bus from another line will reach the merging point $t_{MP,\varrho_{i-1}}$ for arbitrary line index ϱ . From this time instant and an assumed average velocity the time when the controlled bus shall arrive at the merging point can be determined. The position and moving average velocity of the leading vehicle $x_{\varrho_{i-1}}$ and $\bar{v}_{\varrho_{i-1}}$, respectively.

$$t_{MP,\varrho_{i-1}} = t_0 - \frac{MP - x_{\varrho_{i-1}}}{\bar{v}_{\varrho_{i-1}}}, \quad (2.21)$$

where t_0 is the actual time instant. For the sake of simplicity, the extrapolation does not consider obstacles in the merging area, such as traffic lights, intersections etc., it

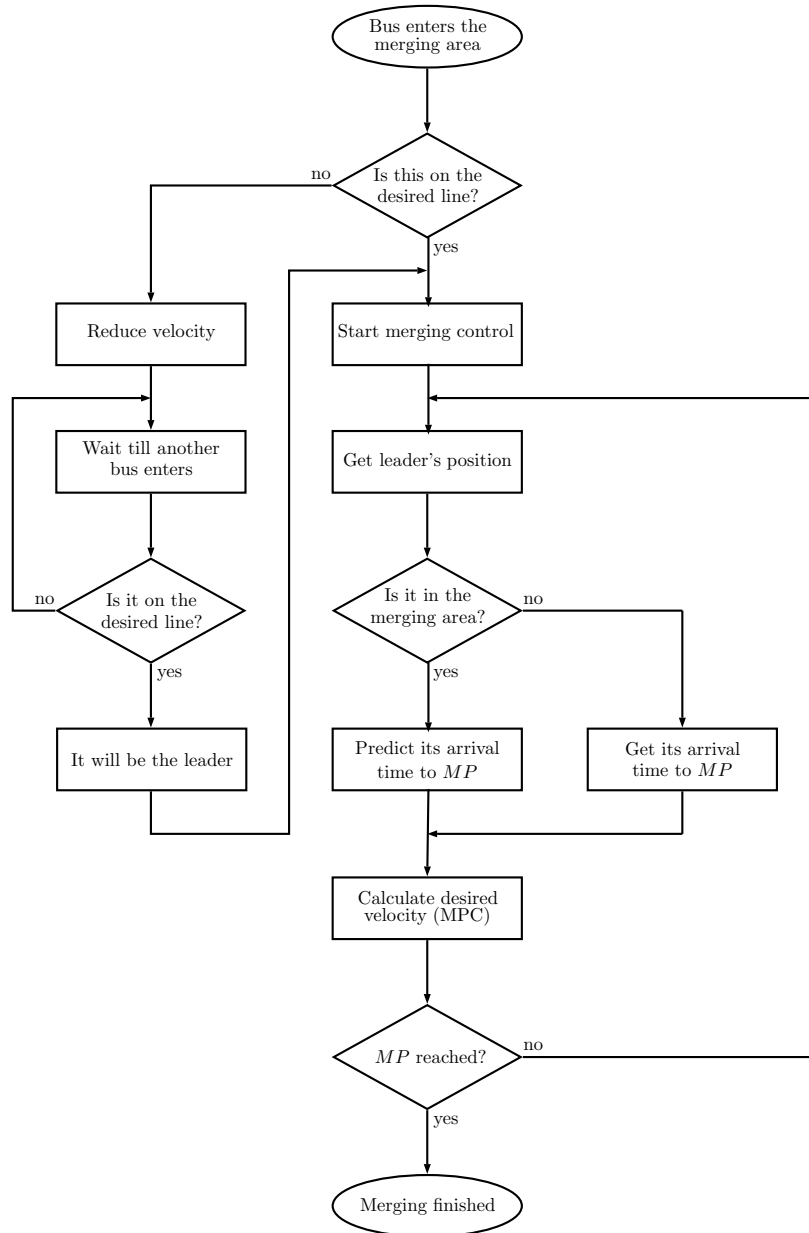


Figure 2.6: Flowchart of the control algorithm for one bus (*this* denotes the controlled bus, *it* denotes the leading bus)

is encompassed the moving average velocity of the bus. If the leading bus already left the merging area, extrapolation is not needed, $t_{MP, \rho_{i-1}}$ can be directly forwarded to the controlled bus.

Figure 2.7 depicts the merging strategy in space-time diagram with three buses as example. The second bus B_i arrives at the merging area at t_{Z_B, B_i} after the leader bus A_{i-1} which has already passed it. The departure time of A_{i-1} from MP , $t_{MP, A_{i-1}}$ is transmitted to B_i and time interval $\Delta t_{A_{i-1}, B_i}$ and the desired merging velocity are calculated. After B_i leaves the merging area its desired velocity is set back to normal or determined by another control law. In Figure 2.7, when bus A_i arrives the bus ahead

of it B_i is still in the merging area so t_{MP,B_i} is extrapolated.

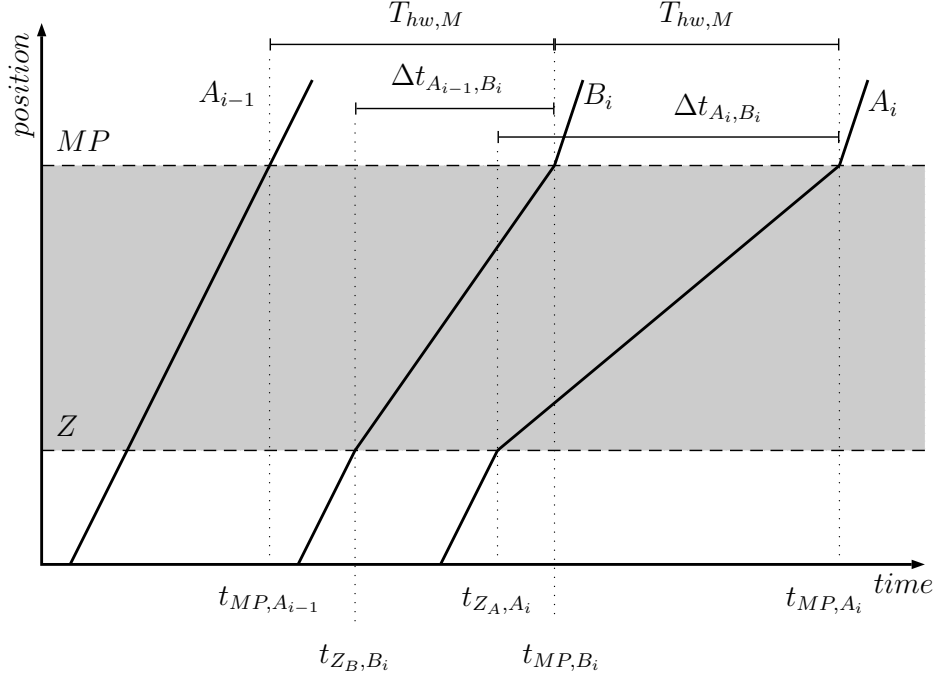


Figure 2.7: Space-time diagram of the merging area

This section showcased a simple rule-based control for the bus merging problem in complex public transport networks. The merging strategy with the merging areas and the merging pattern can be used for more sophisticated, adaptive velocity control too. The reference headways x_{hw} can be computed based on the location of the leading bus. Entering the merging area can be used to switch the reference headway. Then, the control algorithm can adjust the headway of the controlled bus to enter the common line with equalized following distance while considering other control objectives.

2.5.2 Centralized bus network model

The models presented in Section 2.1 and 2.4 can be combined into a bus network model. The network model can be used for centralized public transport bus control, i.e. the control algorithm considers the state of the whole system when calculating control inputs for each bus. This can lead to a network optimal solution at the cost of computational difficulties. Lets denote the buses in the network with index $i = 1, 2, \dots, M_B$ and stops with index $j = 1, 2, \dots, M_J$. For brevity, different bus lines are not indicated in the network model. It is assumed they can be combined based on the results in Section 2.5.1.

The network model is achieved by stacking individual buses with dynamics in Eq. (2.4) and stops described in Eq. (2.15). The model assumes identical buses and stops (i.e. bus dynamics and boarding rates are same among the vehicles). In addition, the two reference trajectories from Section 2.2 (timetable and headway) are added to the network model for each bus. The timetable reference is left unchanged as it is static

and calculated externally. The headway reference, however, is the is the past trajectory of the leading bus shifted by one headway time ahead: $x_{hw,i}(k) = x_{i-1}(k - T_{hw,i}(x_i)\Delta t)$. Since both buses (leader $x_{i-1}(k)$ and follower $x_i(k)$) are present in the network model this relation indirectly couples vehicles in the bus network. The headway $T_{hw,i}(x_i)$ shall be adjusted depending on which link the bus travels on. In addition the index of the leading vehicle can change too, see Section 2.5.1. In addition, the product $T_{hw,i}(x_i)\Delta t$ shall be an integer number as it is subtracted from the discrete time step index k . The public transport system state-space model are presented in Eq. (2.22) and Eq. (2.23).

2.6 Contribution

Thesis 1

Discrete-time state-space based control oriented models were constructed for urban public transport trajectory planning. The models consider the vehicle dynamics of individual buses and passenger dynamics at bus stops. Using a first principle model, the energy consumption model of electrified buses was developed. The proposed models can serve as a basis of a decentralized, reference tracking velocity control. The modular nature of the models enables formulating different control strategies. The models can be extended to a whole public transport network and can be adapted to other modes of city public transport.

This chapter introduced control oriented models describing the operations of a public transport network. Modeling was done in a modular fashion: bus dynamics, energy consumption and passenger waiting times were formulated as independent models.

First, the longitudinal dynamics of a public transport bus was formulated. The model is a simple double integrator (in discrete-time) with a relaxation term towards a desired velocity. Then, two reference trajectories were introduced: a timetable reference trajectory based on a fixed timetable and a headway reference trajectory based on the historical trajectory of the leading bus. The longitudinal motion model with the desired input and the two reference trajectories can be used for a linear trajectory planning control algorithm.

Next, two nonlinear models are annexed. A physical based energy consumption model of a bus was formulated. The model takes into account the different resistances, drivetrain efficiencies and regenerative braking. Then, public transport stops were modeled. The accumulation of passengers and passenger exchange were handled with a piecewise affine model.

Finally, the problem of merging and splitting public transport lines were presented. Then, the proposed models were combined into a single public transport network model.

The goal with this modeling step was obtaining discrete-time state-space based models that can be used as basis a multi-objective model predictive control. Discrete-time enables convenient extension of the models for a finite horizon in the model predictive scheme. The modular structure of the models allows handling them separately, facilitating the introduction of multi-objective control strategies.

Related publications:

The problem formulation of merging and splitting bus lines and a simplistic energy consumption model is presented in [Kulcsár and Varga \[2016\]](#). In addition, the motivation for bus bunching control was based on this pre-study. The longitudinal bus following model and bus stop dynamics are formulated based on [Varga et al. \[2017\]](#) and [Varga et al. \[2018c\]](#). The energy consumption was fit into the optimization framework based on [Varga \[2018\]](#) and [Varga et al. \[2019a\]](#). A model to handle merging and splitting bus lines is discussed in [Varga et al. \[2018a\]](#), then a network level model is formulated based on [Varga et al. \[2020a\]](#).

Chapter 3

Stochastic shockwave profile model

Public transport coexists with other modes of traffic, especially passenger cars. For urban public transport buses cars act as moving bottlenecks and vice versa. The bottleneck effect strongly depends on the road configuration (e.g. multilane network, dedicated bus lanes). Contemporary urban transport design revolves around car-free and public transport oriented cities [Kenworthy \[2019\]](#). This urban planning approach leads (intentionally or unintentionally) to the increase of delay of people who chose to travel by car. Accordingly, this work focuses on the efficiency of public transport while considering cars as disturbance.

Before proceeding, this assumption shall be further disseminated. Applying velocity control on a bus might turn it into a moving bottleneck depending on the road layout and the magnitude of velocity difference. If the link where the controlled bus is traveling on is uncongested and it can be freely overtaken, this bottleneck effect is minor. When there is heavy congestion, the bus is most likely late, so its desired velocity is higher than the that the surrounding traffic permits. Thus other vehicles act as bottlenecks for the controlled buses. Significant delay propagation from a slowed down bus to other participants of traffic only arises if the traffic on the link is close to its peak capacity.

In busy urban arterials, particularly during peak hours delay of public transport is critical. Due to the stochastic nature of traffic networks, adherence to a bus schedule is not guaranteed. Fluctuation of passenger demand, intersection delays, changing traffic conditions and different driving styles of bus drivers bring several uncertainties into the system. Achieving timetable reliability in an environment where “traffic flow dynamics are dominated by external events (red traffic lights) rather than by the inherent traffic flow dynamics” ([Papageorgiou \[1998\]](#)) is especially difficult.

Determining real-time queue length accurately at an intersection is difficult. Queue length is usually estimated from traffic flow data from loop detectors ([Sharma et al. \[2007\]](#)), video cameras ([Fathy and Siyal \[1998\]](#)) or various vehicle to infrastructure applications such as probe vehicles ([Comert and Cetin \[2009\]](#)). Several model based queue length and traffic state approximation methods exist. [Liu et al. \[2009\]](#) estimated intersection queue length by using shockwave theory. The approach could estimate time-dependent queue length even when the signal links are congested with long queues.

Previous authors tried to grasp the stochastic nature of traffic at signalized intersections. [Darroch \[1964\]](#) modeled queues at traffic lights as ergodic Markov chains.

Heidemann [1994] dealt with statistical distribution of queue length at traffic signals and derived the probability generating functions of queue length and vehicle delays considering vehicle arrivals as Poisson process. In Mung et al. [1996] formulas are developed for the probability distributions of queue lengths at fixed time traffic signals. In Zheng et al. [2018] traffic flow states in an urban network with signalized intersections are estimated via stochastic Gaussian approximation.

This chapter presents the shockwave profile model (SPM) used to describe traffic conditions in urban areas with signalized intersections. The shockwave profile model estimates traffic states on a link with traffic signal entirely based on the inflow to the link and the link fundamental diagram. The model assumes discrete traffic states (free flow, stationary queue and queue discharge). The transition between these states are determined by the shockwave profiles. A common critique of the shockwave profile model is that it is very sensitive to input flow error so it cannot robustly model the tail of the queue Liu et al. [2009]. To tackle this problem, the SPM is handled in a probabilistic way. The advantage of the stochastic approach is that it extends the simple shockwave model in a mathematically sound way.

As a contribution, this model is extended with stochasticity through the randomness of traffic flow. The model is discretized using passenger car equivalents (PCE) and a simulation example is given to demonstrate the effectiveness of the model. The possible extension of the model to a whole network and its limitations are studied too.

3.1 Stochastic queuing model

The deterministic SPM model, described in Wu and Liu [2011] is efficient in modeling traffic links with signalized intersections, where signal cycles and shockwaves shape traffic flow. The model distinguishes three different traffic states.

- i) Traffic flows freely towards the queue at the intersection, vehicles travel at their desired speed $v_A(t)$ [$\frac{m}{s}$] and slow down when they approach the queue.
- ii) Traffic is jammed inside the queue, assuming jam density ρ_J and zero velocity $v_J = 0$. This traffic state is denoted by $R_J(t, \omega)$.
- iii) When the queue starts dissipating, the traffic flow state goes from jammed to its critical capacity. The model calls this state queue discharge region $R_C(t, \omega)$. Here, the traffic flow is assumed to be saturated, the average velocity of vehicles is the critical velocity v_C . Stochasticity is introduced to this traffic state by the randomness of vehicle arrivals feeding the moving queue. The queue discharge is assumed to be deterministic.

The symbol $\omega \in \Omega$, appearing in $R_J(t, \omega)$ and $R_C(t, \omega)$ denotes one realization of the stochastic process. The probability space is defined as $[\Omega, \mathcal{A}, \mathbb{P}]$, where Ω is the sample space, \mathcal{A} is a σ -algebra and \mathbb{P} is the probability measure (Arnold [2013]). The three regions of the model are depicted in Figure 3.1. The tail of the queue $l_q(t, \omega)$ is marked by shockwave profiles. The SPM (Wu and Liu [2011]) is extended with the probabilistic nature of vehicle arrivals. Stochasticity is injected into the model through the following assumptions.

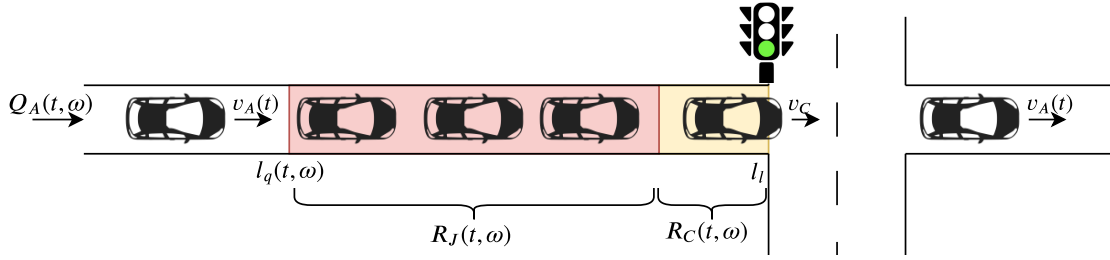


Figure 3.1: Traffic flow states in front of a signalized intersection

Assumption 1. Arrival rate distribution function The mean traffic inflow to the intersection, which is feeding the queue is assumed to be known (from real-time measurement or historical data (Daganzo and Lehe [2016])): $Q_A(t) = E\{Q_A(t, \omega)\}$ with known cumulative distribution function (CDF) $F_{Q_A}(t, \varphi) = \mathbb{P}(\omega : Q_A(t, \omega) \leq \varphi)$. In addition, the distribution function is truncated at zero flow and at peak capacity flow. When vehicles arrive from a link without traffic light or any obstacle that would perturb their distribution of arrivals, Poisson or Binomial process can be assumed (Heidemann [1994], Mung et al. [1996]), with arrival rate $Q_A(t)$. Otherwise, arrivals have generic truncated or discontinuous distributions. In addition, arrival rates may not be independent from traffic flow on the preceding links. Although, the model can give a probabilistic measure for queue spillover, it is assumed it does not occur. In related works (e.g. in Chow et al. [2017]) it is handled with the help of a minimum function (i.e. truncating the queue length distribution function), where the queue length cannot be longer than the link length. The SPM model itself could not handle spillover without a limit function. In the trajectory planning control, where this model will be employed handles spillover in an indirect (but physically not realistic) way. In case of multiple traffic lights, spillover would mean overlapping jammed regions. This implies pessimistic preconditions and therefore cautious speed commands. Furthermore, if a network is blocked, no speed advisory or holding system work, the top priority is decongesting the network.

Assumption 2. Scalability This assumption is the continuation of Assumption 1. In traffic engineering practice, traffic flow $Q_A(t)$ is usually given in vehicles per hour, i.e. traffic signal program is planned based on hourly average traffic demand, usually determined from historical traffic data. However, a traffic light cycle time is only a fraction of an hour, i.e. more frequent sampling is needed. The hourly averaged traffic flow $Q_A(t)$ and the cycle averaged traffic flow are not necessarily proportional, ergodicity of the traffic flow cannot be assumed. For example, 600 *veh/h* inflow and 60 s traffic light cycle does not mean that exactly 10 *veh* arrives in each cycle). This uncertainty is grasped through the distribution function of $Q_A(t, \omega)$ ($F_{Q_A}(t, \varphi)$).

Assumption 3. Fundamental diagram It is further assumed, that the link fundamental diagram (FD) is known in mean value (e.g. from measurement (Chiabaut et al. [2009], Daganzo and Lehe [2016], Qu et al. [2017], Seo et al. [2019])). The link fundamental diagram describes the relation between the traffic flow states in a mixed traffic environment where the controlled buses operate. The purpose of the link FD

in this work is to describe the traffic environment where the bus velocity control takes place. It is assumed that the network layout is such (e.g. multiple lanes, pull-in bus stops) and the frequency of the buses is so low that the repercussion of buses to the link FD is minor. For the sake of simplicity, triangular link fundamental diagram is chosen (Laval and Castrillón [2015]). With the help of the specific points of the fundamental diagram (i.e. actual flow $[\rho_A(t, \omega), Q_A(t, \omega)]$, peak capacity $[\rho_C, Q_C]$ and jam density $[\rho_J, 0]$) the shockwave velocities $W_i(t, \omega) [\frac{m}{s}]$ $i = 1...4$ can be computed analytically, see Figure 3.2. It is further assumed, that the traffic flow is constant for short time intervals. The time-independent $Q_A(\omega)$ implies linear shockwave profiles.

Assumption 4. Signal program It is assumed, that the location of the traffic light l_l [m] and the signal program are known. The signal program is represented by three variables: t_{cyc} [s] is the cycle time which is constant, $t_{1,c}$ [s] is the start of red phase, and $t_{2,c}$ [s] is the end of red phase in the cycle. Subscript c denotes the c^{th} traffic light cycle. The model is capable of handling traffic-responsive signal control too. In case of traffic responsive signal program, there are some limitations however. According to the relevant literature, traffic signal control can follow various logics. In a model predictive framework, between two prediction steps the external signals (such as the signal program) are frozen. Therefore, if the traffic light program changes significantly between two prediction steps it bias the result of the prediction. For brevity, the deductions and simulations employ static timing.

3.2 Shockwaves at signalized intersections

With the assumptions made in Section 3.1, herewith, the effect of randomness in the SPM is described. The model distinguishes four shockwaves, depicted both in the link fundamental diagram (Figure 3.2) and time-space diagram (Figure 3.3).

Queuing shockwave velocity, $W_1(t, \omega)$ is formed by vehicles accumulating at the red light. Vehicles stopping at the tail of the queue from their actual velocity to zero form a shockwave. This process is also stochastic due to the randomness of vehicle arrivals affecting the queue length.

$$W_1(t, \omega) = -\frac{Q_A(t, \omega)}{\rho_J - \rho_A(t, \omega)}. \quad (3.1)$$

Discharge shockwave velocity, W_2 is assumed to be deterministic, as it is not affected by vehicle arrivals. In the fundamental diagram the discharge shockwave velocity is the slope of the line connecting the jam density and the critical density:

$$W_2 = -\frac{Q_C}{\rho_J - \rho_C}. \quad (3.2)$$

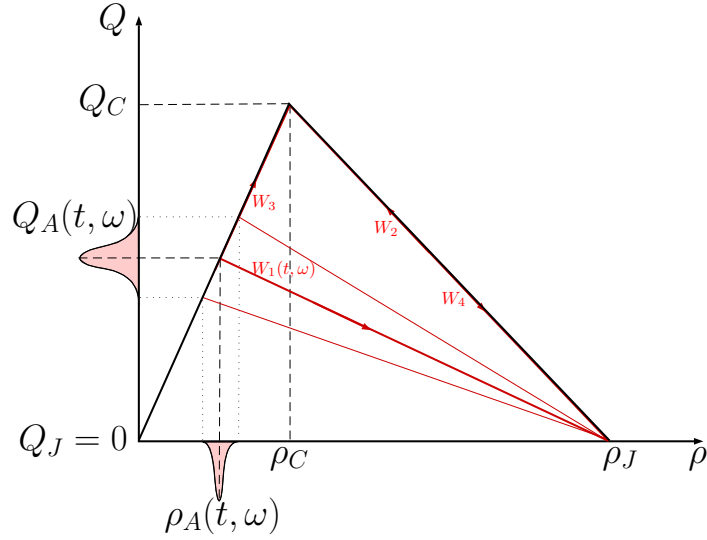


Figure 3.2: Triangular link fundamental diagram of traffic flow with shockwave speeds ($W_1 \dots W_4$). $Q_A(t, \omega)$ is represented with a probability density function, showing how it affects the slope of the queuing shockwave $W_1(t, \omega)$.

Departure wave velocity $W_3(t, \omega)$ is generated as the queue dissipates as vehicles leave the intersection at green. It starts at the intersection of the queuing and discharge shockwaves. In addition, newly arrived vehicles feed the queue, hence

$$W_3(t, \omega) = \frac{Q_C - Q_A(t, \omega)}{\rho_C - \rho_A(t, \omega)}. \quad (3.3)$$

Assuming a triangular link FD, the departure wave velocity becomes deterministic, and equal to the free flow velocity v_f see Figure 3.2.

Pressure wave velocity W_4 separates a critical density and a jam density region, and it has the same speed as the discharge wave W_2 . The pressure wave is only present if there is a residual queue, i.e. the traffic from the queue cannot fully cross the stop line during a green interval:

$$W_4 = -\frac{Q_C}{\rho_J - \rho_C}. \quad (3.4)$$

Shockwave velocities can be represented in time-space diagram too, see Figure 3.3. Shockwave profiles represent the evolution and dissipation of queues upstream a signalized intersection. The geometrical intersection point of the queuing and discharge shockwaves is the point $[t_{s,c}(t, \omega), l_{s,c}(t, \omega)]$. In addition, $t_{r,c}(t, \omega)$ is the time instant when the queue starts growing again in the next red phase. The residual queue length is $l_{r,c}(t, \omega)$. The shockwave intersection points $[t_{s,c}(t, \omega), l_{s,c}(t, \omega)]$ and $[t_{r,c}(t, \omega), l_{r,c}(t, \omega)]$ can be given analytically for c traffic light cycles ahead as:

$$t_{s,c}(t, \omega) = \frac{-W_1(t, \omega)t_{r,c-1}(t, \omega) + W_2(t_{2,c} + ct_{cyc}) + l_{r,c-1}(t, \omega) - l_l}{W_2 - W_1(t, \omega)}, \quad (3.5)$$

$$l_{s,c}(t, \omega) = W_1(t, \omega)(t_{s,c}(t, \omega) - t_{r,c-1}(t, \omega)) + l_{r,c-1}(t, \omega), \quad (3.6)$$

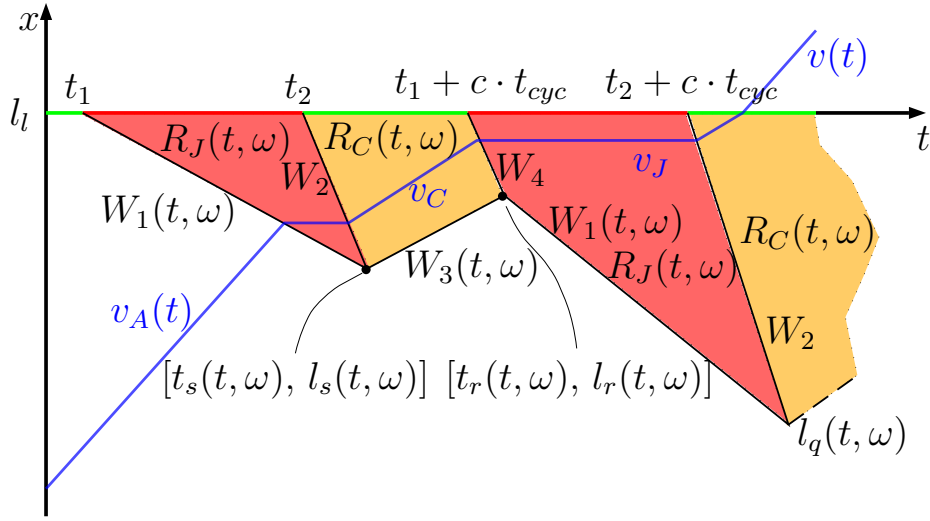


Figure 3.3: Traffic states at a single intersection assuming generic link fundamental diagram.

$$t_{r,c}(t, \omega) = \min \left(t_{1,c} + ct_{cyc}, \frac{-W_3(t, \omega)t_{s,c}(t, \omega) + W_4(t_{1,c} + ct_{cyc}) + l_{s,c}(t, \omega) - l_l}{W_4 - W_3(t, \omega)} \right), \quad (3.7)$$

$$l_{r,c}(t, \omega) = \min (l_l, W_3(t, \omega)(t_{r,c}(t, \omega) - t_{s,c}(t, \omega)) + l_{s,c}(t, \omega)). \quad (3.8)$$

The discontinuities with $\min(\cdot)$ are introduced to limit shockwaves upstream the intersection l_l . For brevity, ct_{cyc} is used to denote the time elapsed since an arbitrary initial time instant. In case of varying cycle lengths the notation modifies to $\sum_c t_{cyc,c}$.

In Figure 3.3, the blue line depicts a vehicle trajectory with its velocity at each traffic phase, based on the SPM model. Upstream the intersection the vehicle travels freely at its desired velocity $v_A(t)$. When it enters the queue it stops, the jam velocity $v_J = 0$. In queue discharge vehicles assumed to travel with the equilibrium velocity at the critical density v_C .

To summarize, the space-time evolution of traffic phases in the SPM model can be given using the shockwave equations presented above for c traffic cycles ahead, where the number of elapsed cycles is

$$c = \text{floor} \left(\frac{t}{t_{cyc}} \right). \quad (3.9)$$

The regions in Figure 3.3 can be described with the help of polygons made up of lines (assuming time independent vehicle inflow). The boundaries of $R_J(t, \omega)$ and $R_C(t, \omega)$ are summarized (for the c^{th} cycle) in Table 3.1. These boundaries will be used for introducing chance-constraints into the trajectory planning later, in Chapter 5.

Outside these regions, vehicles travel at their desired speeds $v_A(t)$. The stochastic

Table 3.1: Boundaries of traffic states

Jam region ($R_J(t, \omega)$)	
Stop line during red (between $t_{1,c} + ct_{cyc}$ and $t_{2,c} + ct_{cyc}$)	l_l
Pressure wave (if exists)	$l_l + W_4(t - (t_{1,c} + ct_{cyc}))$
Queuing wave	$l_{r,c-1}(t, \omega) + W_1(t, \omega)(t - t_{r,c-1}(t, \omega))$
Discharge wave	$l_l + W_2(t - (t_{2,c} + ct_{cyc}))$
Discharge region ($R_C(t, \omega)$)	
Stop line during green (between $t_{2,c} + ct_{cyc}$ and $\min(t_1 + ct_{cyc}, t_{r,c}(t, \omega))$)	l_l
Discharge wave	$l_l + W_2(t - (t_2 + ct_{cyc}))$
Departure wave	$l_{s,c}(t, \omega) + W_3(t, \omega)(t - t_{s,c}(t, \omega))$
Pressure wave (if exists)	$l_l + W_4(t - (t_1 + ct_{cyc}))$

process for the queue length is:

$$l_q(t, \omega) = \begin{cases} W_1(t, \omega)(t - t_{r,c-1}(t, \omega)) + l_{r,c-1}(t, \omega), \\ \text{if } t_{r,c-1}(t, \omega) \leq t < t_{s,c}(t, \omega) \text{ (queuing)}, \\ \max(l_l, W_3(t, \omega)(t - t_{s,c}(t, \omega)) + l_{s,c}(t, \omega)), \\ \text{if } t_{s,c}(t, \omega) \leq t < t_{r,c}(t, \omega) \text{ (departure)}. \end{cases} \quad (3.10)$$

3.3 CDF of shockwaves

Next, the stochastic shockwave profiles and their respective cumulative density functions (CDFs) are derived analytically. First, the relationship of the CDFs of traffic flow $F_{Q_A}(t, \varphi)$ and traffic density $F_{\rho_A}(t, \varphi)$ are derived, using Theorem 2.

Theorem 2. Let $\xi(\omega)$ be a random variable with CDF $F_\xi(\varphi)$. Let $\eta(\omega) = g(\xi(\omega))$. The CDF of $\eta(\omega)$ can be given as:

$$F_\eta(\varphi) = \begin{cases} F_\xi(g^{-1}(\varphi)), & \text{if } g(\varphi) \text{ is monotonically increasing,} \\ 1 - F_\xi(g^{-1}(\varphi)), & \text{if } g(\varphi) \text{ is monotonically decreasing,} \end{cases} \quad (3.11)$$

and if $g(x)$ has a unique inverse ([Arnold \[2013\]](#)).

Proof. By definition, the CDF of $\eta(\omega)$ is

$$F_\eta(x) = \mathbb{P}\{\omega : \eta(\omega) < x\}. \quad (3.12)$$

Substituting $\eta(\omega) = g(\xi(\omega))$ into Eq. (3.12) and multiplying both sides by g^{-1} , the solution is obtained:

$$\begin{aligned} F_\eta(x) &= \mathbb{P}\{\omega : \eta(\omega) \leq \varphi\} = \mathbb{P}\{\omega : g(\xi(\omega)) \leq \varphi\} \\ &= \mathbb{P}\{\omega : g^{-1}(g(\xi(\omega))) \leq g^{-1}(\varphi)\} = \mathbb{P}\{\omega : \xi(\omega) \leq g^{-1}(\varphi)\}. \end{aligned} \quad (3.13)$$

On the left hand side, the CDF of ξ has appeared. When $g(\varphi)$ is negative the direction of the inequality changes and the complementary CDF appears. Finally,

$$F_\eta(\varphi) = \begin{cases} F_\xi(g^{-1}(\varphi)), & \text{if } g(\varphi) \text{ is monotonically increasing,} \\ 1 - F_\xi(g^{-1}(\varphi)), & \text{if } g(\varphi) \text{ is monotonically decreasing.} \end{cases} \quad (3.14)$$

QED

In addition, the above Theorem 2 holds for stochastic processes too (Arnold [2013]). Now, let's analyze the relationship of the CDFs of traffic flow and traffic density.

Given the vehicle arrivals $Q_A(t, \omega)$ and assuming mean-valued triangular link fundamental diagram (Eq. (3.15)), the traffic density $\rho_A(t, \omega)$ in the uncongested region can be determined:

$$\rho_A(t, \omega) = \frac{1}{v_f} \cdot Q_A(t, \omega), \quad (3.15)$$

assuming free flow at the beginning of the link with v_f being the velocity at free flow. In addition, the distribution of $Q_A(t, \omega)$ has to be truncated from both sides: it has to be greater than zero and smaller than Q_C . $F_{\rho_A}(t, \varphi)$ in the free flow region is given as:

$$F_{\rho_A}(t, \varphi) = F_{Q_A}(t, g^{-1}(\varphi)), \quad (3.16)$$

with $g(x)$ being the relation in Eq. (3.15). Therefore:

$$F_{\rho_A}(t, \varphi) = F_{Q_A}(t, v_f \cdot \varphi). \quad (3.17)$$

The next step in formulating the stochastic traffic flow model to describe the CDFs of the shockwaves. In the model, only $W_1(t, \omega)$ and $W_3(t, \omega)$ depend on the random arrivals $Q_A(t, \omega)$ as:

$$W_1(t, \omega) = \frac{Q_J - Q_A(t, \omega)}{\rho_J - \rho_A(t, \omega)} = -\frac{Q_A(t, \omega)}{\rho_J - \frac{1}{v_f} Q_A(t, \omega)}. \quad (3.18)$$

$$W_3(t, \omega) = \frac{Q_C - Q_A(t, \omega)}{\rho_C - \rho_A(t, \omega)} = \frac{Q_C - Q_A(t, \omega)}{\rho_C - \frac{1}{v_f} Q_A(t, \omega)}. \quad (3.19)$$

Since $F_{Q_A}(t, \varphi)$ is known, $F_{W_1}(t, \varphi)$ and $F_{W_3}(t, \varphi)$ can be formulated for the arrival and the departure wave velocities, respectively, with the help of Theorem 2 again. The $g^{-1}(\varphi)$ functions are the inverses of Eq. (3.18) and Eq. (3.19), with $Q_A(t, \omega)$ replaced by level φ . Note that in Eq.(3.18) $W_1(t, \omega)$ is a decreasing function of $Q_A(t, \omega)$. Likewise, $W_3(t, \omega)$ is increasing function of $Q_A(t, \omega)$. With this in mind, the resulting CDFs become:

$$F_{W_1}(t, \varphi) = 1 - F_{Q_A} \left(t, -\frac{\rho_J - \frac{1}{v_f} \varphi}{\varphi} \right), \quad (3.20)$$

$$F_{W_3}(t, \varphi) = F_{Q_A} \left(t, \frac{\rho_C - \frac{1}{v_f} \varphi}{\rho_C - \varphi} \right), \quad (3.21)$$

if $Q_A(t, \omega)$ is nonzero. Similarly, the CDF of the queue length $F_{l_q}(t, \varphi)$ as a stochastic process can be computed. When the expressions for the shockwave velocities and recursively calculated intersection points are substituted, the stochastic process of the queue length becomes only $Q_A(t, \omega)$ dependent. The relation between $Q_A(t, \omega)$ and $l_q(t, \omega)$ is a piecewise, truncated, first order rational function. With Theorem 2, $F_{l_q}(t, \varphi)$ can be computed even though the expression becomes very long and is omitted for brevity.

3.4 Number of vehicles

To be able to compare the SPM to other urban traffic flow models, the number of vehicles (in passenger car equivalents, PCE) crossing the intersection in every cycle $n(c, \omega)$ shall be determined. The number of arriving vehicles per cycle is proportional to the slope of the arrival shockwave:

$$n_a(c, \omega) = \frac{W_1(t, \omega)t_{cyc}}{l_{PCE} + l_{jam}}. \quad (3.22)$$

The number of outflowing vehicles in cycle c is proportional to the decrement of queue length in the green phase $l_{s,c}(\omega)$. In mathematical form:

$$n_d(\omega) = \min \left(\frac{W_2 t_{green}}{l_{PCE} + l_{crit}}, n(c, \omega) + \frac{W_1(t, \omega)t_{cyc}}{l_{PCE} + l_{jam}} \right), \quad (3.23)$$

where l_{PCE} is the PCE length, l_{crit} is the average headway distance at the critical density (which is assumed to prevail in the queue discharge region). l_{jam} is the headway distance in jam. The green time interval is $t_{green} = t_{cyc} - t_2$. $n(c, \omega)$ denotes the number of vehicles in traffic light cycle c . In the same vein, the queue length evolution (in PCE) over one cycle c can be given as:

$$n(c + 1, \omega) = n(c, \omega) + n_a(c, \omega) - n_d(c, \omega), \quad (3.24)$$

within discrete time period $[ct_{cyc}, (c + 1)t_{cyc}]$. This result in Eq. (3.24) is a discrete-time traffic model, similar to the store-and-forward model (Aboudolas et al. [2009]), however the shockwave profile model is capable of handling undersaturated networks too. Furthermore, this formula is needed to extend the SPM to multiple links, see 3.6.

3.5 Monte Carlo simulation example

This section demonstrates how the proposed traffic model is capable of capturing the stochastic nature of queue lengths at a traffic light. For simplicity, the arrival rate of vehicles is characterized by a homogeneous Poisson distribution with constant $\lambda = Q_A = E\{Q_A(\omega)\}$ arrival rate.

Exploiting the linear property of the Poisson process, the arrival rate can be scaled down (e.g. $360 \text{ veh/h} \rightarrow 0.1 \text{ veh/s}$) and still being a Poisson process. Note: the resulting stochastic process is also a homogeneous Markov chain (Karlin [1957]). The

shockwave model, however, is different from an $M/M/1$ service model. It also considers the temporal piecewise nature of traffic signal phases (i.e. red and green phases) and distinguishes queuing and discharge sequences.

Next, a numerical simulation example is given, in order to validate the proposed traffic model. A Monte Carlo simulation was run in a microscopic traffic simulator VISSIM (PTV [2011]). The simulation consisted of one link, ending with a traffic light at 300 m. The link fundamental diagram was assumed to be known. The fixed-time traffic light cycle time is 60 s and the green time was set to 30 s. Vehicles arrived at the traffic light with Poisson distribution with hourly rate $\lambda = 500 \text{ veh/h}$. The simulation was 15000 s long, resulting 250 traffic light cycles. Queue lengths were logged and compared against the stochastic shockwave profile model. In VISSIM, a vehicle is assumed to be in a queue if its velocity drops below a certain threshold and leaves the queue if its velocity exceeds another threshold. In the comparative analysis the queue entry velocity was set to 5 km/h and the queue end velocity was set to 30 km/h. The

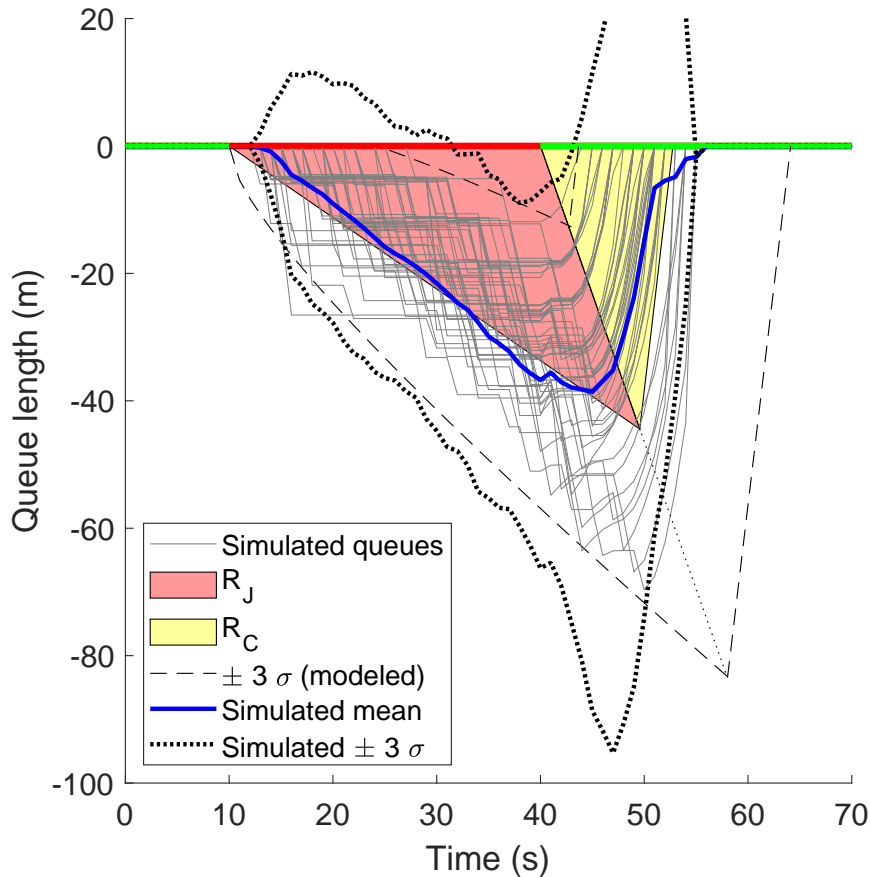


Figure 3.4: Monte Carlo simulation of queue lengths to validate the SSPM

method of comparison is the following. The mean values and standard deviation of the simulated queue lengths were computed and compared to the modeled queue length moments of the SSPM. According to Figure 3.4, the average queue length and standard deviations in the queuing phase were accurately estimated. The estimation error in the

queuing phase was 5.6%. Standard deviations are overestimated when two traffic states co-exist in the queue. The slope of the dissipation wave was well estimated too with 7.1% error but the start of the dissipation phase was incorrectly modeled. The error stems from the randomness of vehicle arrivals and the modeling error of the assumed link fundamental diagram.

3.6 Network stochastic SPM

The stochastic SPM can be further extended to handle more than a single link for queue length estimation, by taking into consideration the adjacent links, i.e. a traffic network can be modeled by SPM. Throughout this chapter, unconditional distribution for traffic inflow $Q_A(t, \omega)$ was assumed. The SPM model can recursively applied for upstream links. This assumes that the inflows (and their respective CDF) in the perimeter of the network are known. First, determine the stochastic process for the

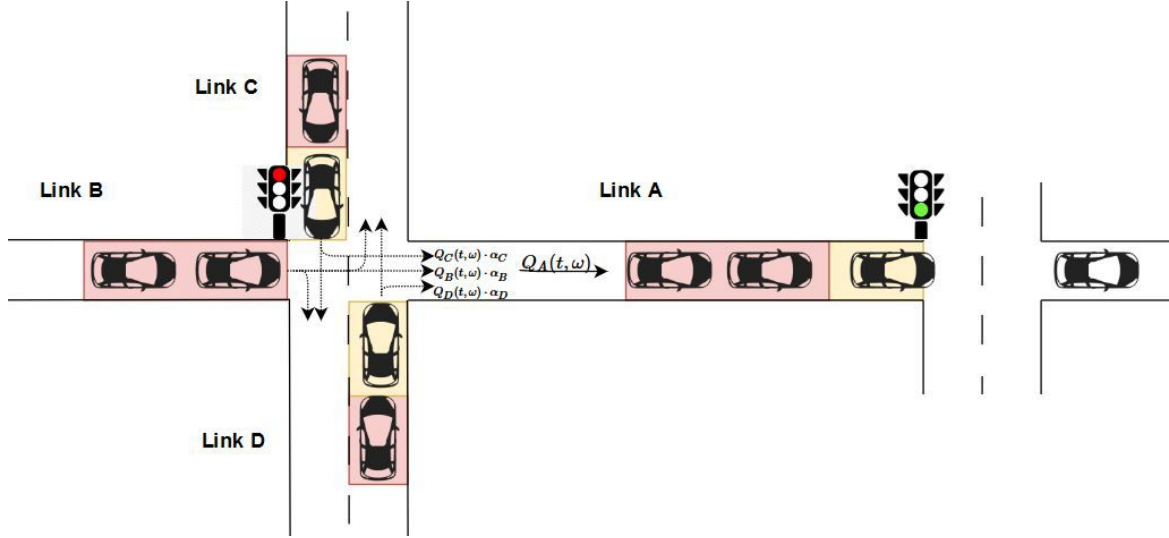


Figure 3.5: Stochastic shockwave profile model based queues at on network level

inflow $Q_A(t, \omega)$ to *Link A* for the network in Figure 3.5. The number of outflowing vehicles from a link per traffic light cycle can be computed with the help of Eq. (3.24) in Section 3.4. The computed outflow $n(c, \omega)$ can be scaled up with the help of cycle times t_{cyc} to compute the total outflow $Q_B(t, \omega)$ for link B and so on. Next, assume the turning rates α_B , α_C , α_D at every intersection are known. This is a common, practical assumption for network-level traffic models (e.g. Aboudolas et al. [2009], Lin et al. [2010]). Then, the stochastic process for $Q_A(t, \omega)$ can be given as:

$$Q_A(t, \omega) = Q_B(t, \omega)\alpha_B + Q_C(t, \omega)\alpha_C + Q_D(t, \omega)\alpha_D. \quad (3.25)$$

Next, the method for obtaining the CDF of the inflow $F_{Q_A}(t, \varphi)$ is given. If the inflows $Q_B(t, \omega)$, $Q_C(t, \omega)$, $Q_D(t, \omega)$ are independent,

$$F_{Q_A}(t, \varphi) = F_{Q_B}(t, \varphi_B) * F_{Q_C}(t, \varphi_C) * F_{Q_D}(t, \varphi_D) \quad (3.26)$$

as convolution is an associative operation. If the flows are not independent, their joint probability shall be known (Arnold [2013]). After obtaining $Q_A(t, \omega)$ and $F_{Q_A}(t, \omega)$ from the aforementioned steps, the computation of traffic states and queue lengths in a probabilistic sense can be performed as described in Section 3.3.

The SPM model can estimate queue lengths which can be used to detect spillover in a stochastic manner, see Figure 3.6. If this queue length is larger than the length of the link l_s , there is spillover. Moreover, if spillover occurs the queue length becomes deterministic, as it becomes equal to the link length. When handling oversaturated links in a network, this effect shall be taken into account as a conditional probability.

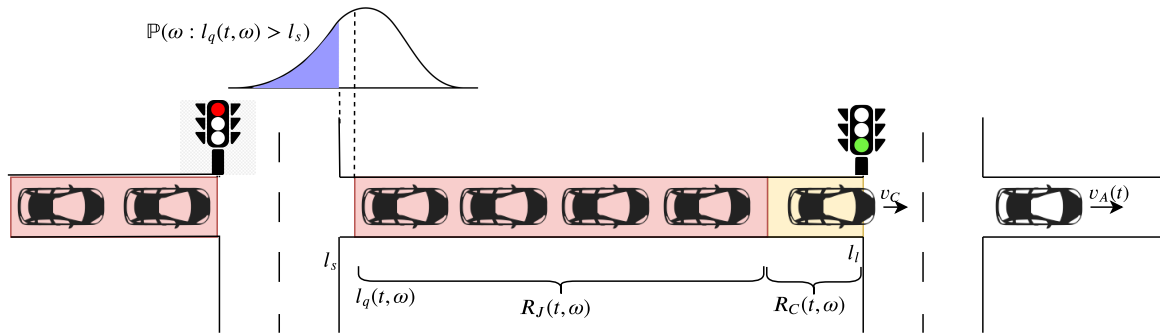


Figure 3.6: Traffic flow states with probabilistic spillover

3.7 Contribution

Thesis 2

The classic shockwave theory was extended with stochastic description of traffic flow. Vehicle arrivals to a link is modeled with its distribution function instead of its average value (hourly flow). Analytical description was given for the distribution functions of shockwave profiles and the queue length evolution. The proposed stochastic model was validated in microscopic traffic simulation. The stochastic model is suitable for predicting traffic flow states and queue length in signalized intersections. The model was extended to multiple intersections, thus it is capable of modeling urban networks with signalized intersections in a stochastic way.

The shockwave profile model is efficient in modeling traffic links with signalized intersections, where signal cycles and shockwaves shape traffic flow. The model, however, cannot handle the uncertain nature of traffic flow. Queue lengths at signalized intersections depend on the signal program and the rate of arrival of vehicles. In the stochastic extension of the model it was assumed that the signal program is known (either static or traffic-responsive) and the vehicle inflow is only known in distributional sense. The motivation behind this assumption is that in traffic engineering practice traffic flow is given in vehicles per hour. However, traffic light cycles are only a fraction of an hour. Therefore, the number of vehicles arriving at the traffic light within a given cycle is uncertain.

The shockwave profile model gives an explicit relation between vehicle flow and the shockwave velocities. If the signal program is known, the evolution of the queue length distribution can be deduced too. In this chapter this thought of train was performed with stochasticity in mind. Thus, the CDFs of the shockwave profiles were deduced. As an additional contribution, the possible extension of the model to multiple intersections was studied. Through microscopic traffic simulation the accuracy of the queue length prediction of the stochastic model was validated. The model can be used to describe the effect of surrounding traffic in an urban public transport line. Moreover, it can be incorporated into an eco-cruise control strategy.

Related publications:

The shockwave profile model with its stochastic extension for control purposes was presented in [Varga et al. \[2018b\]](#) and [Varga et al. \[2020b\]](#). Its validation via traffic simulation was carried out in [Varga et al. \[2019b\]](#). The results are presented in Hungarian as well in [Varga and Tettamanti \[2019\]](#).

Chapter 4

Model predictive bus velocity control

This chapter presents the model predictive control (MPC) for public transport buses. The goal with the proposed rolling horizon control scheme is to choose a proper velocity profile for public transport buses. Moreover, they shall satisfy conflicting objectives while obeying constraints imposed by vehicle dynamics, public transport characteristics and external traffic. The four (often) conflicting goals addressed in this thesis are as follows.

- A static timetable given by the service provider shall be kept. Timetable tracking is considered as an objective for the control.
- Without control the periodicity of headways fail (bunching). To keep equidistant headways, trajectory of the leading bus is also taken into account.
- Public transport shall be energy efficient, thus the optimal control shall also consider the energy required to move the vehicle from one point to another.
- Finally, an important level of service measure is the waiting time of passengers. The total amount of time passengers spend waiting for the bus to arrive shall be minimized.

On top of these four objectives the control shall also consider the surrounding traffic and traffic lights. Ignoring their effect would result in delays and poor energy efficiency and the public transport service would ultimately fail.

Based on the linear bus dynamics model presented in Section 2.1 and the two reference trajectories proposed in Section 2.2 the first two objectives (timetable- and headway tracking) can be addressed. By adding energy consumption into the optimization (Section 2.3) the third objective can be taken care of. The energy consumption model is not linear however. The separation of acceleration and braking turns it into a piecewise linear system. Thus, the optimization inevitably turns into a nonlinear problem, complicating the solution. The passenger waiting time model (Section 2.4) is also a piecewise affine system (because of the integer boarding state). A cost can be associated to passenger wait time and plugged into the optimization as an additional cost term.

The control method focuses on network bunching, but in a distributed, overlapped way: every vehicle runs its own velocity controller and then they communicate their predicted trajectories among each other. The control algorithm is generic, it can be applied to different routes, fleet configurations, schedules, etc. The controlled bus only requires the historical position of the preceding bus, the schedule (stop locations and desired departure times) and some measurable network parameters such as the number of passengers waiting at stops and hourly traffic flow at road links (measured or historical data), Figure 4.1. In case any of them are missing, either predictions can be made or fallback control strategies can be employed. Fallback strategies mean selection of objectives. If any of the objectives making up the cost function cannot be determined (e.g. data is missing), the optimization can be reconfigured taking into account only the available cost terms with different set of tuning weights. Different weighting strategies can be proposed not only for fallback but to emphasize on the preferences of the service provider. E.g. there might be situations where keeping the timetable is not so important while serving a large passenger demand is priority. This chapter will further discuss possible control strategies through optimization weight selection.

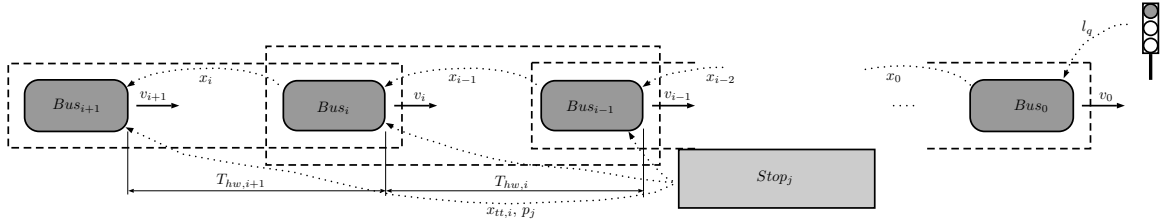


Figure 4.1: Overlapped, decentralized control strategy

4.1 Shrinking horizon model predictive control

The strategy used in this thesis is a shrinking horizon MPC design (Maciejowski [2002]). The goal of the controller is calculating an optimal velocity profile between the actual position of the vehicle and the next stop, while taking into account several uncertainties. Setting the next bus stop as a target to reach within the prediction horizon is a natural way of creating a terminal set for the optimization. The advantage of the shrinking horizon strategy over a fixed prediction window length is that buses are only controlled between bus stops and the optimization does not have to deal with the discrete event whether the bus is at a stop or not. Therefore, the optimization remains convex. The bus shall be at the next stop by a desired arrival time t_{arr} , obtained from the schedule. The desired arrival time is the scheduled departure time t_{sch} minus the estimated dwell time t_d (from Section 2.4.2). In addition, it shall come to a full stop when reaching its destination, thus its velocity shall be zero. The existence of a terminal set guarantees the stability of the MPC controlled system (Limon et al. [2006]). Feasibility of the solution can only be guaranteed if the bus is not too late (i.e. it can reach the next stop by commanding the maximum allowed velocity. If there is no feasible solution,

the maximum allowed desired velocity is used as control input as fallback. In the MPC scheme even if the solution is not feasible, only the first step of the control input sequence is used.

A key step in formulating an MPC is defining the horizon length N . In the shrinking horizon scheme it is the discretized time interval between the current time t_0 and the desired arrival time t_{arr} . The time interval between t_0 and t_{arr} is the time window for control and it is split into N equidistant steps, see Figure 4.2. In every time step the prediction horizon decreases by one. By the last time step the bus shall arrive at the desired stop. To avoid small or even negative horizon lengths (due to lateness or being close to the stop) a lower bound is introduced: $N_{min} \geq 1$. That is:

$$N = \max \left\{ N_{min}, \text{floor} \left(\frac{t_{arr} - t_0}{\Delta t} \right) \right\}. \quad (4.1)$$

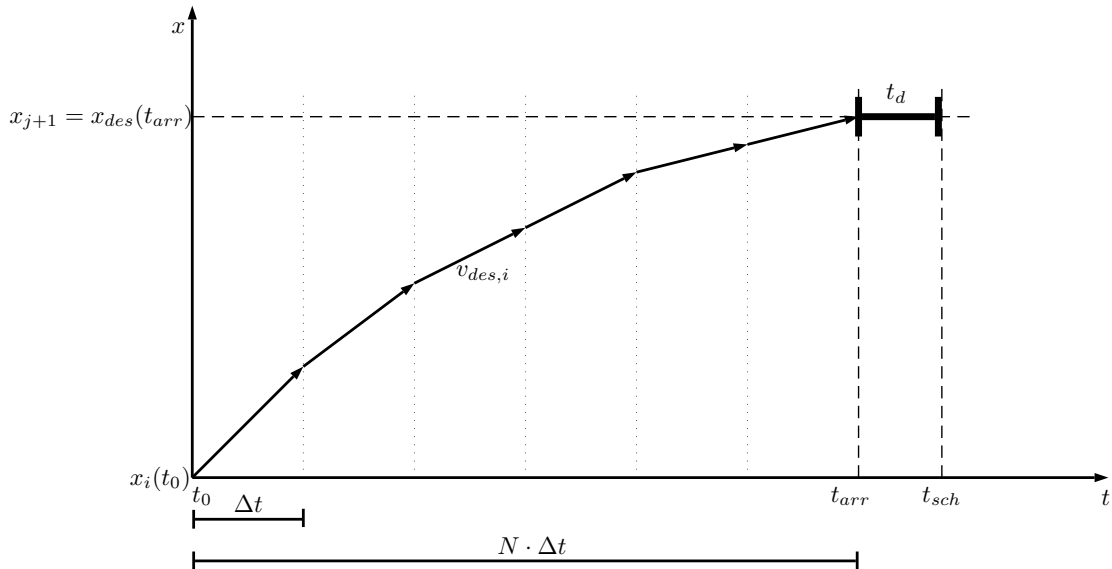


Figure 4.2: MPC horizon length calculation

The shrinking horizon control works only between bus stops. There is no control while it is at the stop. Optionally, a simple bus holding logic can be employed there too if the bus is too early. It is released from the stop when all passengers finished boarding or the holding strategy allows it to do so. Then, the shrinking horizon control can start again towards the next top. The relevant reference trajectories are selected based on the actual position of the bus in relation to the next bus stop, see Section 2.2.

4.2 Multi-objective cost function

In this section the system equations presented in Chapter 2 are extended for N horizon. These stacked matrices will serve as the basis of the cost functions in each of the conflicting objectives. In addition, tuning weights are introduced to leverage the

importance of these different objectives. Finally, the constraints imposed by vehicle dynamics and external traffic are introduced.

4.2.1 Headway and timetable tracking MPC

The first two objectives, namely headway and timetable tracking can be formulated by stacking the bus dynamics in Eq. (2.4) and the error terms Eq. (2.5) and Eq. (2.6).

4.2.1.1 Deduction of the cost function

First, introduce some nomenclature.

- $X(k)$ is the vector of state variables of a bus: $X(k) = [v(k), x(k)]^T$.
- A denotes the state matrix $A = \begin{bmatrix} 1 - \frac{\Delta t}{\tau} & 0 \\ \Delta t & 1 \end{bmatrix}$.
- B_u is the control input matrix containing coefficients for the desired velocity: $B_u = [\frac{\Delta t}{\tau}(1 - \beta), 0]^T$.
- $u(k)$ is the controlled variable (decision variable). The only control input to the system is the desired velocity of the bus $u(k) = v_{des}(k)$.
- B_w is a block diagonal disturbance matrix, consisting of $[\beta \ 0]^T$ matrices.
- $v_{mac}(k)$ is the disturbance.
- $x_{tt}(k)$ and $x_{hw}(k)$ denote the reference trajectories.
- $z_{tt}(k)$ and $z_{hw}(k)$ are the vector of performance outputs $z_{tt}(k) = z_1(k)$, $z_{hw} = [z_2(k) \ z_3(k)]^T$.
- C_{tt} and C_{hw} are the output matrices. $C_{tt} = \begin{bmatrix} 0 & -1 \\ 0 & 0 \end{bmatrix}$ and $C_{hw} = \begin{bmatrix} 0 & 0 \\ 0 & -1 \end{bmatrix}$.
- D_{tt} and D_{hw} are direct feedthrough matrices of the reference trajectories. $D_{tt} = D_{hw} = 1$.

The system state $X(k)$ is measured at time step k . Then, for a finite horizon length N the future states $X(k + \kappa|k)$ are calculated along with the corresponding control inputs $u(k + \kappa - 1|k)$ and the external reference signals $x_{tt}(k + \kappa - 1|k)$ and $x_{hw}(k + \kappa - 1|k)$. A predicted state is denoted as $X(k + \kappa|k)$, where time step k at the right side within the parentheses denotes the current time, and k at the left side the prediction step with running index $\kappa = 1, 2, \dots, N$. The same notation applies for the control input the external signals and the performance outputs $z_{tt}(k + \kappa|k)$ or $z_{hw}(k + \kappa|k)$.

$$\begin{bmatrix} \overbrace{X(k+1|k)}^{\underline{x}} \\ \overbrace{X(k+2|k)}^{\underline{x}} \\ \vdots \\ \overbrace{X(k+N|k)}^{\underline{x}} \end{bmatrix} = \begin{bmatrix} \overbrace{A}^{\underline{A}} \\ \overbrace{A^2}^{\underline{A}} \\ \vdots \\ \overbrace{A^N}^{\underline{A}} \end{bmatrix} \overbrace{X(k|k)}^{\underline{x}} + \begin{bmatrix} \overbrace{B_u}^{\underline{B}} & 0 & \dots & 0 \\ \overbrace{AB_u}^{\underline{B}} & \overbrace{B_u}^{\underline{B}} & & 0 \\ \vdots & \vdots & \ddots & \vdots \\ \overbrace{A^{N-1}B_u}^{\underline{B}} & \overbrace{A^{N-2}B_u}^{\underline{B}} & \dots & \overbrace{B_u}^{\underline{B}} \end{bmatrix} \begin{bmatrix} \overbrace{u(k|k)}^{\underline{u}} \\ \overbrace{u(k+1|k)}^{\underline{u}} \\ \vdots \\ \overbrace{u(k+N-1|k)}^{\underline{u}} \end{bmatrix} + \begin{bmatrix} \overbrace{B_w}^{\underline{B}} & 0 & \dots & 0 \\ \overbrace{AB_w}^{\underline{B}} & \overbrace{B_w}^{\underline{B}} & & 0 \\ \vdots & \vdots & \ddots & \vdots \\ \overbrace{A^{N-1}B_w}^{\underline{B}} & \overbrace{A^{N-2}B_w}^{\underline{B}} & \dots & \overbrace{B_w}^{\underline{B}} \end{bmatrix} \begin{bmatrix} \overbrace{v_{mac}(k)(k|k)}^{\underline{w}} \\ \overbrace{v_{mac}(k)(k+1|k)}^{\underline{w}} \\ \vdots \\ \overbrace{v_{mac}(k)(k+N-1|k)}^{\underline{w}} \end{bmatrix}, \quad (4.2)$$

$$\begin{aligned}
 \underbrace{\begin{bmatrix} z_{tt}(k+1|k) \\ z_{tt}(k+2|k) \\ \vdots \\ z_{tt}(k+N|k) \end{bmatrix}}_{\hat{\mathbf{z}}_{tt}} &= \underbrace{\begin{bmatrix} C_{tt} & 0 & \cdots & 0 \\ 0 & C_{tt} & & 0 \\ \vdots & \vdots & \ddots & \vdots \\ 0 & 0 & \cdots & C_{tt} \end{bmatrix}}_{\underline{\mathbf{C}}_{tt}} \underbrace{\begin{bmatrix} X(k+1|k) \\ X(k+2|k) \\ \vdots \\ X(k+N|k) \end{bmatrix}}_{\hat{\mathbf{x}}} + \underbrace{\begin{bmatrix} D_{tt} & 0 & \cdots & 0 \\ 0 & D_{tt} & & 0 \\ \vdots & \vdots & \ddots & \vdots \\ 0 & 0 & \cdots & D_{tt} \end{bmatrix}}_{\underline{\mathbf{D}}_{tt}} \underbrace{\begin{bmatrix} x_{tt}(k+1|k) \\ x_{tt}(k+2|k) \\ \vdots \\ x_{tt}(k+N|k) \end{bmatrix}}_{\hat{\xi}_{tt}}, \\
 \underbrace{\begin{bmatrix} z_{hw}(k+1|k) \\ z_{hw}(k+2|k) \\ \vdots \\ z_{hw}(k+N|k) \end{bmatrix}}_{\hat{\mathbf{z}}_{hw}} &= \underbrace{\begin{bmatrix} C_{hw} & 0 & \cdots & 0 \\ 0 & C_{hw} & & 0 \\ \vdots & \vdots & \ddots & \vdots \\ 0 & 0 & \cdots & C_{hw} \end{bmatrix}}_{\underline{\mathbf{C}}_{hw}} \underbrace{\begin{bmatrix} X(k+1|k) \\ X(k+2|k) \\ \vdots \\ X(k+N|k) \end{bmatrix}}_{\hat{\mathbf{x}}} + \underbrace{\begin{bmatrix} D_{hw} & 0 & \cdots & 0 \\ 0 & D_{hw} & & 0 \\ \vdots & \vdots & \ddots & \vdots \\ 0 & 0 & \cdots & D_{hw} \end{bmatrix}}_{\underline{\mathbf{D}}_{hw}} \underbrace{\begin{bmatrix} x_{hw}(k+1|k) \\ x_{hw}(k+2|k) \\ \vdots \\ x_{hw}(k+N|k) \end{bmatrix}}_{\hat{\xi}_{hw}}.
 \end{aligned} \tag{4.3}$$

The cost functions for timetable and headway tracking are sought in a quadratic form with the help of $\hat{\mathbf{z}}_{tt}$, $\hat{\mathbf{z}}_{hw}$ and \mathbf{u} :

$$J_{tt}(k) = \frac{1}{2} \left[\hat{\mathbf{z}}_{tt}^T \underline{\mathbf{Q}}_{tt} \hat{\mathbf{z}}_{tt} + \mathbf{u}^T \underline{\mathbf{R}}_{tt} \mathbf{u} \right] \tag{4.4}$$

and

$$J_{hw}(k) = \frac{1}{2} \left[\hat{\mathbf{z}}_{hw}^T \underline{\mathbf{Q}}_{hw} \hat{\mathbf{z}}_{hw} + \mathbf{u}^T \underline{\mathbf{R}}_{hw} \mathbf{u} \right], \tag{4.5}$$

respectively.

In Eq. (6.5) and Eq. (4.5) $\hat{\mathbf{x}}$, $\hat{\mathbf{z}}_{tt}$, $\hat{\mathbf{z}}_{hw}$ and \mathbf{u} denote stacked vectors of the predicted states (velocity, position), predicted reference trajectory errors, and the control input (desired velocity) at each time step. With the two cost functions the two objectives of timetable- and headway tracking are separated. Introduce positive semi-definite weighting matrices $\underline{\mathbf{Q}}_{tt} = \text{diag}(q_{z_{tt}})$ and $\underline{\mathbf{Q}}_{hw} = \text{diag}(q_{z_{hw}})$, where $q_{z_{tt}}$ and $q_{z_{hw}}$ are tuning parameters for their respective reference trajectories. Higher value on a weight means more emphasis on that tracking objective. R_{tt} and R_{hw} are scalar weights penalizing the control input $v_{des}(k)$. If the control input is cheap (R_{tt} or R_{hw} are small) the controller reacts with aggressive desired velocity changes: the desired velocity values are v_{des} either v_{min} or v_{max} . If the control input is expensive (R_{tt} or R_{hw} are large), the system responds slowly and the desired performance criteria (timetable or headway tracking) are not met. In other words, if R_{tt} or R_{hw} is large, demanding high velocity would result in high cost function values. Minimum of such a function would be at small control inputs over good performance.

In the MPC scheme these weights are also extended for N horizon: $\underline{\mathbf{Q}}_{tt} = \text{diag}(\underline{\mathbf{Q}}_{tt}) \in \mathbb{R}^{2N \times 2N}$, $\underline{\mathbf{Q}}_{hw} = \text{diag}(\underline{\mathbf{Q}}_{hw}) \in \mathbb{R}^{2N \times 2N}$, $\underline{\mathbf{R}}_{tt} = \text{diag}(\underline{\mathbf{R}}_{tt}) \in \mathbb{R}^{N \times N}$ and $\underline{\mathbf{R}}_{hw} = \text{diag}(\underline{\mathbf{R}}_{hw}) \in \mathbb{R}^{N \times N}$. A quadratic formula means that it penalizes both positive and negative deviations from the reference (i.e. not only late but also early arrival).

Note that $\hat{\mathbf{x}}$ does not appear directly in the cost function. Penalizing the kinetic energy of the bus (i.e. velocity state) is handled more carefully via a more accurate energy consumption model. The state $x(k)$ is the absolute position of the bus. Minimizing absolute position would be an unreasonable choice.

Next, organize the terms as coefficients of \mathbf{u} , \mathbf{u}^T , and $\mathbf{u}^T(\star)\mathbf{u}$:

$$\begin{aligned}
 J_{tt}(k) = & \frac{1}{2} \left[\left(\mathbf{x}^T \underline{\underline{A}}^T \underline{\underline{C}}^T \underline{\underline{Q}}_{tt} \underline{\underline{C}}_{tt} \underline{\underline{B}}_u + \mathbf{w}^T \underline{\underline{B}}_w^T \underline{\underline{C}}^T \underline{\underline{Q}}_{tt} \underline{\underline{C}}_{tt} \underline{\underline{B}}_u + \hat{\zeta}_{tt}^T \underline{\underline{D}}^T \underline{\underline{Q}}_{tt} \underline{\underline{C}}_{tt} \underline{\underline{B}}_u \right) \mathbf{u} \right. \\
 & + \mathbf{u}^T \left(\underline{\underline{B}}_u^T \underline{\underline{C}}^T \underline{\underline{Q}}_{tt} \underline{\underline{C}}_{tt} \underline{\underline{A}} \mathbf{x} + \underline{\underline{B}}_u^T \underline{\underline{C}}^T \underline{\underline{Q}}_{tt} \underline{\underline{C}}_{tt} \underline{\underline{B}}_w \mathbf{w} + \underline{\underline{B}}_u^T \underline{\underline{C}}^T \underline{\underline{Q}}_{tt} \underline{\underline{D}}_{tt} \hat{\zeta}_{tt} \right) \\
 & + \mathbf{u}^T \left(\underline{\underline{B}}_u^T \underline{\underline{C}}^T \underline{\underline{Q}}_{tt} \underline{\underline{C}}_{tt} \underline{\underline{B}}_u + \underline{\underline{R}}_{tt} \right) \mathbf{u} \\
 & + \left(\mathbf{x}^T \underline{\underline{A}}^T \underline{\underline{C}}^T \underline{\underline{Q}}_{tt} \underline{\underline{C}}_{tt} \underline{\underline{A}} \mathbf{x} + \mathbf{x}^T \underline{\underline{A}}^T \underline{\underline{C}}^T \underline{\underline{Q}}_{tt} \underline{\underline{C}}_{tt} \underline{\underline{B}}_w \mathbf{w} + \mathbf{x}^T \underline{\underline{A}}^T \underline{\underline{C}}^T \underline{\underline{Q}}_{tt} \underline{\underline{D}}_{tt} \hat{\zeta}_{tt} \right. \\
 & + \mathbf{w}^T \underline{\underline{B}}_w^T \underline{\underline{C}}^T \underline{\underline{Q}}_{tt} \underline{\underline{C}}_{tt} \underline{\underline{A}} \mathbf{x} + \mathbf{w}^T \underline{\underline{B}}_w^T \underline{\underline{C}}^T \underline{\underline{Q}}_{tt} \underline{\underline{C}}_{tt} \underline{\underline{B}}_w \mathbf{w} + \mathbf{w}^T \underline{\underline{B}}_w^T \underline{\underline{C}}^T \underline{\underline{Q}}_{tt} \underline{\underline{D}}_{tt} \hat{\zeta}_{tt} \\
 & \left. \left. + \hat{\zeta}_{tt}^T \underline{\underline{D}}^T \underline{\underline{Q}}_{tt} \underline{\underline{C}}_{tt} \underline{\underline{A}} \mathbf{x} + \hat{\zeta}_{tt}^T \underline{\underline{D}}^T \underline{\underline{Q}}_{tt} \underline{\underline{C}}_{tt} \underline{\underline{B}}_w \mathbf{w} + \hat{\zeta}_{tt}^T \underline{\underline{D}}^T \underline{\underline{Q}}_{tt} \underline{\underline{D}}_{tt} \hat{\zeta}_{tt} \right) \right], \tag{4.12}
 \end{aligned}$$

$$\begin{aligned}
 J_{hw}(k) = & \frac{1}{2} \left[\left(\mathbf{x}^T \underline{\underline{A}}^T \underline{\underline{C}}^T \underline{\underline{Q}}_{hw} \underline{\underline{C}}_{hw} \underline{\underline{B}}_u + \mathbf{w}^T \underline{\underline{B}}_w^T \underline{\underline{C}}^T \underline{\underline{Q}}_{hw} \underline{\underline{C}}_{hw} \underline{\underline{B}}_u + \hat{\zeta}_{hw}^T \underline{\underline{D}}^T \underline{\underline{Q}}_{hw} \underline{\underline{C}}_{hw} \underline{\underline{B}}_u \right) \mathbf{u} \right. \\
 & + \mathbf{u}^T \left(\underline{\underline{B}}_u^T \underline{\underline{C}}^T \underline{\underline{Q}}_{hw} \underline{\underline{C}}_{hw} \underline{\underline{A}} \mathbf{x} + \underline{\underline{B}}_u^T \underline{\underline{C}}^T \underline{\underline{Q}}_{hw} \underline{\underline{C}}_{hw} \underline{\underline{B}}_w \mathbf{w} + \underline{\underline{B}}_u^T \underline{\underline{C}}^T \underline{\underline{Q}}_{hw} \underline{\underline{D}}_{hw} \hat{\zeta}_{hw} \right) \\
 & + \mathbf{u}^T \left(\underline{\underline{B}}_u^T \underline{\underline{C}}^T \underline{\underline{Q}}_{hw} \underline{\underline{C}}_{hw} \underline{\underline{B}}_u + \underline{\underline{R}}_{hw} \right) \mathbf{u} \\
 & + \left(\mathbf{x}^T \underline{\underline{A}}^T \underline{\underline{C}}^T \underline{\underline{Q}}_{hw} \underline{\underline{C}}_{hw} \underline{\underline{A}} \mathbf{x} + \mathbf{x}^T \underline{\underline{A}}^T \underline{\underline{C}}^T \underline{\underline{Q}}_{hw} \underline{\underline{C}}_{hw} \underline{\underline{B}}_w \mathbf{w} + \mathbf{x}^T \underline{\underline{A}}^T \underline{\underline{C}}^T \underline{\underline{Q}}_{hw} \underline{\underline{D}}_{hw} \hat{\zeta}_{hw} \right. \\
 & + \mathbf{w}^T \underline{\underline{B}}_w^T \underline{\underline{C}}^T \underline{\underline{Q}}_{hw} \underline{\underline{C}}_{hw} \underline{\underline{A}} \mathbf{x} + \mathbf{w}^T \underline{\underline{B}}_w^T \underline{\underline{C}}^T \underline{\underline{Q}}_{hw} \underline{\underline{C}}_{hw} \underline{\underline{B}}_w \mathbf{w} + \mathbf{w}^T \underline{\underline{B}}_w^T \underline{\underline{C}}^T \underline{\underline{Q}}_{hw} \underline{\underline{D}}_{hw} \hat{\zeta}_{hw} \\
 & \left. \left. + \hat{\zeta}_{hw}^T \underline{\underline{D}}^T \underline{\underline{Q}}_{hw} \underline{\underline{C}}_{hw} \underline{\underline{A}} \mathbf{x} + \hat{\zeta}_{hw}^T \underline{\underline{D}}^T \underline{\underline{Q}}_{hw} \underline{\underline{C}}_{hw} \underline{\underline{B}}_w \mathbf{w} + \hat{\zeta}_{hw}^T \underline{\underline{D}}^T \underline{\underline{Q}}_{hw} \underline{\underline{D}}_{hw} \hat{\zeta}_{hw} \right) \right], \tag{4.13}
 \end{aligned}$$

The first and second terms in Eq. (4.12) and in Eq. (4.13) are equal. Furthermore, the last term is constant and can be removed from the cost function. The objective function shall be minimized and a constant term does not influence the outcome of the minimization problem, just offsets the cost. The objective function to be minimized becomes:

$$\begin{aligned}
 J_{tt}(k) = & \frac{1}{2} \mathbf{u}^T \left(\underline{\underline{B}}_u^T \underline{\underline{C}}^T \underline{\underline{Q}}_{tt} \underline{\underline{C}}_{tt} \underline{\underline{B}}_u + \underline{\underline{R}}_{tt} \right) \mathbf{u} \\
 & + \left(\mathbf{x}^T \underline{\underline{A}}^T \underline{\underline{C}}^T \underline{\underline{Q}}_{tt} \underline{\underline{C}}_{tt} \underline{\underline{B}}_u + \mathbf{w}^T \underline{\underline{B}}_w^T \underline{\underline{C}}^T \underline{\underline{Q}}_{tt} \underline{\underline{C}}_{tt} \underline{\underline{B}}_u + \hat{\zeta}_{tt}^T \underline{\underline{D}}^T \underline{\underline{Q}}_{tt} \underline{\underline{C}}_{tt} \underline{\underline{B}}_u \right) \mathbf{u}, \tag{4.14}
 \end{aligned}$$

$$\begin{aligned}
 J_{hw}(k) = & \frac{1}{2} \mathbf{u}^T \left(\underline{\underline{B}}_u^T \underline{\underline{C}}^T \underline{\underline{Q}}_{hw} \underline{\underline{C}}_{hw} \underline{\underline{B}}_u + \underline{\underline{R}}_{hw} \right) \mathbf{u} \\
 & + \left(\mathbf{x}^T \underline{\underline{A}}^T \underline{\underline{C}}^T \underline{\underline{Q}}_{hw} \underline{\underline{C}}_{hw} \underline{\underline{B}}_u + \mathbf{w}^T \underline{\underline{B}}_w^T \underline{\underline{C}}^T \underline{\underline{Q}}_{hw} \underline{\underline{C}}_{hw} \underline{\underline{B}}_u + \hat{\zeta}_{hw}^T \underline{\underline{D}}^T \underline{\underline{Q}}_{hw} \underline{\underline{C}}_{hw} \underline{\underline{B}}_u \right) \mathbf{u}. \tag{4.15}
 \end{aligned}$$

For brevity, introduce the following notation for the coefficients of the control input prediction: Φ_{tt} , Φ_{hw} , Ω_{tt}^T and Ω_{hw}^T . Finally,

$$J_{tt}(k) = \frac{1}{2} \mathbf{u}^T \Phi_{tt} \mathbf{u} + \Omega_{tt}^T \mathbf{u}, \tag{4.16}$$

and

$$J_{hw}(k) = \frac{1}{2} \mathbf{u}^T \Phi_{hw} \mathbf{u} + \Omega_{hw}^T \mathbf{u}. \tag{4.17}$$

subject to:

$$|z_{tt}(k + N|k)| < \varepsilon, \quad (4.18)$$

$$|v(k + N|k)| < \varepsilon, \quad (4.19)$$

$$v_{min} \leq v_{des} \leq v_{max}. \quad (4.20)$$

In other words, by the last time step the bus shall be at the bus stop and it shall stop there. ε denotes numerical tolerance. It is assumed that the control input is constrained: the lower limit $v_{min} = 0$ km/h, since negative velocity is not allowed. The desired velocity has an upper bound too: it is either constrained by the legal speed limit on the link (e.g. $v_{lim} = 50$ km/h) or if the link is congested, the bottleneck speed $v_{btl}(k)$ imposed by other vehicles: $v_{max} = \min(v_{btl}(k), v_{lim})$.

4.2.1.2 Proving the convexity of the control problem

Convexity of the problem is guaranteed by the positive definiteness of the quadratic terms Φ_{tt} and Φ_{hw} , i.e. $\Phi_{tt} \succ 0$ and $\Phi_{hw} \succ 0$, (Horn and Johnson [1990]).

Theorem 3. *Positive semidefiniteness and positive definiteness are defined as follows: any symmetric $n \times n$ real matrix $\underline{\underline{\Lambda}}$ is said to be positive semidefinite if $\underline{u}^T \underline{\underline{\Lambda}} \underline{u} \geq 0$, and positive definite if $\underline{u}^T \underline{\underline{\Lambda}} \underline{u} > 0$ for any non-zero vector \underline{u} of n real numbers.*

Proof. In both of the cost functions Q_{tt} and Q_{hw} are positive definite matrices. The control weights q_{tt} and q_{hw} are positive numbers.

Next, the positive semidefiniteness of

$$\Phi_{tt} = \underline{\underline{\mathcal{B}}}_u^T \underline{\underline{\mathcal{C}}}_{tt}^T \underline{\underline{\mathcal{Q}}}_{tt} \underline{\underline{\mathcal{C}}}_{tt} \underline{\underline{\mathcal{B}}}_u + \underline{\underline{\mathcal{R}}}_{tt} \quad (4.21)$$

and

$$\Phi_{hw} = \underline{\underline{\mathcal{B}}}_u^T \underline{\underline{\mathcal{C}}}_{hw}^T \underline{\underline{\mathcal{Q}}}_{hw} \underline{\underline{\mathcal{C}}}_{hw} \underline{\underline{\mathcal{B}}}_u + \underline{\underline{\mathcal{R}}}_{hw} \quad (4.22)$$

are shown.

If a matrix $\underline{\underline{\Gamma}}$ has only real entries, then the product $\underline{\underline{\Gamma}}^T \underline{\underline{\Gamma}}$ gives a positive semidefinite matrix. As $\underline{\underline{\mathcal{Q}}}_{tt}$ and $\underline{\underline{\mathcal{Q}}}_{hw}$ were proven to be a positive definite diagonal matrices:

$$\left(\underline{\underline{\mathcal{B}}}_u \underline{\underline{\mathcal{C}}}_{tt} \underline{\underline{\mathcal{Q}}}_{tt}^{\frac{1}{2}} \right)^T \left(\underline{\underline{\mathcal{Q}}}_{tt}^{\frac{1}{2}} \underline{\underline{\mathcal{C}}}_{tt} \underline{\underline{\mathcal{B}}}_u \right) \succeq 0 \quad (4.23)$$

and

$$\left(\underline{\underline{\mathcal{B}}}_u \underline{\underline{\mathcal{C}}}_{hw} \underline{\underline{\mathcal{Q}}}_{hw}^{\frac{1}{2}} \right)^T \left(\underline{\underline{\mathcal{Q}}}_{hw}^{\frac{1}{2}} \underline{\underline{\mathcal{C}}}_{hw} \underline{\underline{\mathcal{B}}}_u \right) \succeq 0. \quad (4.24)$$

QED

4.2.2 Energy-aware MPC

The next aim is to reformulate the energy consumption model, proposed in Section 2.3, in a way it can be fit into a cost function to penalize energy consumption of a vehicle

along its route. The power required to move the vehicle equals the energy consumption in one time step:

$$P(k) = \frac{P_{roll}(k) + P_{drag}(k) + P_g(k) + P_{acc}(k)}{\eta_{batt} \cdot \eta_{pe} \cdot \eta_{mot} \cdot \eta_{pt}} + P_{regen}(k) \cdot \eta_{batt} \cdot \eta_{pe} \cdot \eta_{mot} \cdot \eta_{pt}. \quad (4.25)$$

In Eq. (4.25) the rolling resistance $P_{roll}(k)$, the resistance due to upgrade $P_g(k)$ and air drag $P_{drag}(k)$ are independent from the control input $v_{des}(k)$. In the quadratic minimization problem constants do not affect the result of the optimization, they just offset the cost, therefore they can be omitted. Furthermore, it makes the optimization much easier for two reasons: i) keeping terms with second or third order power of the velocity (state) would result in higher order polynomial as a cost function; ii) weighting the cost function is much easier when only the significant term (i.e. acceleration) is left. Weighting the total energy consumption would work towards slowing down the bus as lower velocity means lower energy consumption (neglecting auxiliary losses). On the other hand, weighting acceleration directly penalizes rapid accelerations and decelerations which is the most significant portion of energy consumption.

The acceleration (and deceleration) $a(k)$ can be written based on the car following model (Section 2.1). Next, substitute Eq. (2.3) into Eq. (4.25) and group efficiencies into two parameters $\eta_{acc} = \eta_{batt} \cdot \eta_{pe} \cdot \eta_{mot} \cdot \eta_{pt}$ and $\eta_{reg} = \eta_{batt} \cdot \eta_{pe} \cdot \eta_{mot} \cdot \eta_{pt} \cdot \eta_{regen}$ for $P_{acc}(k)$ and $P_{regen}(k)$, respectively. The equations become:

$$P_{acc}(k) = -\frac{m \cdot v^2(k)}{\tau \cdot \eta_{acc}} + \frac{m \cdot v(k)}{\tau \cdot \eta_{acc}} \cdot v_{des}(k), \quad (4.26)$$

$$P_{regen}(k) = -\frac{\eta_{reg} \cdot m \cdot v^2(k)}{\tau} + \frac{\eta_{reg} \cdot m \cdot v(k)}{\tau} \cdot v_{des}(k). \quad (4.27)$$

In Eq. (4.26) and Eq. (4.27) the first two terms are also independent from $v_{des}(k)$. The last term is linearly dependent.

In the finite horizon optimization problem velocity of the bus $v(k)$ is contained in the predicted state vector $\hat{\mathbf{x}}$. The control input dependent part of $\underline{P}'_{acc}(k)$ and $\underline{P}'_{reg}(k)$ for N horizon are:

$$\underline{P}'_{acc}(k) = \mathbf{u}^T \cdot \frac{m}{\tau \cdot \eta_{acc}} \cdot \underline{\mathcal{S}} \cdot \hat{\mathbf{x}}, \quad (4.28)$$

$$\underline{P}'_{reg}(k) = \mathbf{u}^T \cdot \frac{\eta_{reg} \cdot m}{\tau} \cdot \underline{\mathcal{S}} \cdot \hat{\mathbf{x}}, \quad (4.29)$$

where $\underline{\mathcal{S}}$ is a row selector matrix for the velocity $v(k)$ over the prediction horizon:

$$\underline{v}(k) = \underline{\mathcal{S}} \hat{\mathbf{x}} = \begin{bmatrix} S & 0 & \dots & 0 \\ 0 & S & & 0 \\ \vdots & \vdots & \ddots & \vdots \\ 0 & 0 & \dots & S \end{bmatrix} \begin{bmatrix} X(k+1|k) \\ X(k+2|k) \\ \vdots \\ X(k+N|k) \end{bmatrix}, \quad S = [1, 0]. \quad (4.30)$$

For the sake of simplicity, define $\underline{\mathcal{K}}_{acc}$ and $\underline{\mathcal{K}}_{reg}$ as the time independent coefficient of $\hat{\mathbf{x}}$ in $\underline{P}'_{acc}(k)$ and $\underline{P}'_{reg}(k)$ respectively:

$$\underline{\mathcal{K}}_{acc} = \frac{m}{\tau \cdot \eta_{acc}} \cdot \underline{\mathcal{S}}, \quad (4.31)$$

$$\underline{\mathcal{K}}_{reg} = \frac{\eta_{reg} \cdot m}{\tau} \cdot \underline{\mathcal{S}}. \quad (4.32)$$

Furthermore, from Eq. (4.2) $\hat{\mathbf{x}}$ is

$$\hat{\mathbf{x}} = \underline{\mathcal{A}} \mathbf{x} + \underline{\mathcal{B}} \mathbf{u}. \quad (4.33)$$

Next, substitute Eq. (4.33) into Eq. (4.28) and Eq. (4.29) and organize the resulting equations by \mathbf{u} :

$$\underline{P}'_{acc}(k) = \mathbf{u}^T \underline{\mathcal{K}}_{acc} \underline{\mathcal{A}} \mathbf{x} + \mathbf{u}^T \underline{\mathcal{K}}_{acc} \underline{\mathcal{B}}_u \mathbf{u}, \quad (4.34)$$

$$\underline{P}'_{reg}(k) = \mathbf{u}^T \underline{\mathcal{K}}_{reg} \underline{\mathcal{A}} \mathbf{x} + \mathbf{u}^T \underline{\mathcal{K}}_{reg} \underline{\mathcal{B}}_u \mathbf{u}. \quad (4.35)$$

The power to accelerate and the regenerated power are quadratic polynomials of the control input \mathbf{u} . Similar to Eq. (6.5), the cost function is sought in a quadratic form. The results of Eq. (4.34) and Eq. (4.35) can be written as two separate quadratic cost functions: $J_e^+(k)$ and $J_e^-(k)$ for accelerating and regenerative braking respectively. In order to penalize rapid accelerations or decelerations four weighting parameters are introduced: $\underline{\mathcal{W}}_{acc}$, $\underline{\mathcal{W}}_{reg}$, $\underline{\mathcal{V}}_{acc}$ and $\underline{\mathcal{V}}_{reg}$. $\underline{\mathcal{V}}_{acc}$ is the coefficient for the first order part and $\underline{\mathcal{W}}_{acc}^{N \times N}$ is the diagonal, positive semi-definite coefficient matrix for the quadratic part of the cost function. The same rationale can be applied to $\underline{\mathcal{W}}_{reg}$ and $\underline{\mathcal{V}}_{reg}$. Since the regeneration P_{reg} is an energy gain, it has negative sign and decreases the cost. With the two additional quadratic cost functions $J_e^+(k)$ and $J_e^-(k)$ the optimization results in a non-smooth problem.

$$J_e^+(k) = \frac{1}{2} \mathbf{u}^T \underline{\mathcal{K}}_{acc} \underline{\mathcal{B}} \underline{\mathcal{W}}_{acc} \mathbf{u} + \mathbf{x}^T \underline{\mathcal{A}}^T \underline{\mathcal{K}}_{acc}^T \underline{\mathcal{V}}_{acc} \mathbf{u}, \quad (4.36)$$

$$J_e^-(k) = -\frac{1}{2} \mathbf{u}^T \underline{\mathcal{K}}_{reg} \underline{\mathcal{B}} \underline{\mathcal{W}}_{reg} \mathbf{u} - \mathbf{x}^T \underline{\mathcal{A}}^T \underline{\mathcal{K}}_{reg}^T \underline{\mathcal{V}}_{reg} \mathbf{u}. \quad (4.37)$$

Switching between objective functions in Eq. (4.36) and Eq. (4.37) is formulated mathematically as follows. A selection between the cost functions shall be made for every time iteration in the prediction horizon. Exploiting some features of the matrices a simple solution can be given. First, consider the quadratic part in Eq. (4.36) or Eq. (4.37). In the cost function $\underline{\mathcal{B}}$ is a lower triangular matrix, $\underline{\mathcal{K}}_{acc}$ and $\underline{\mathcal{K}}_{reg}$ are non-square matrices with entries only in at $[i, 2i]$. Due to their special structure, the result of their multiplication will be a diagonal $N \times N$ matrix. In the linear part of the cost functions $\underline{\mathcal{K}}_{acc}$ and $\underline{\mathcal{K}}_{reg}$ act as row selector matrices, yielding two $1 \times N$ vectors. For the sake of simplicity the selection between $J_e^+(k)$ and $J_e^-(k)$ is depending on the acceleration or deceleration (the relation of $v(k)$ and v_{des}) at the κ^{th} iteration at time step k . The piecewise quadratic cost function can be written as follows:

$$\min_{\mathbf{u}} \begin{cases} J_e^+(k) & v(k + \kappa|k) < v_{des}(k + \kappa|k) - \nu \\ 0 & v(k + \kappa|k) \in (v_{des}(k + \kappa|k) - \nu, v_{des}(k + \kappa|k) + \nu), \quad \forall \kappa = 1 \dots N, \\ J_e^-(k) & v(k + \kappa|k) > v_{des}(k + \kappa|k) + \nu \end{cases} \quad (4.38)$$

subject to:

$$v_{min} \leq v_{des}(k + \kappa|k) \leq v_{max}, \quad \forall \kappa = 1 \dots N, \quad (4.39)$$

$$a_{min} \leq \frac{1}{\tau}(v_{des}(k + \kappa|k) - v(k + \kappa|k)) \leq a_{max}, \quad \forall \kappa = 1 \dots N. \quad (4.40)$$

The acceleration and deceleration are bounded by a_{min} and a_{max} for ride comfort and to avoid physically infeasible values. Furthermore, for numerical reasons a sufficiently small threshold parameter ν is introduced. The addition of energy consumption enables varying passenger load too. Furthermore, rapid accelerations can be penalized while considering energy regeneration.

4.2.3 Passenger wait costing

The final part of the multi-objective cost function is penalizing the number of passengers waiting for the bus at a stop. The cost $J_p(k)$ is based on the passenger wait model introduced in Section 2.4.3. In order to formulate an adequate cost function from the preliminary model (Eq. (2.19)), it shall be extended for N horizon length too. The notations used for stacking the wait time model are:

- $\chi(k)$ is the state vector: $\chi(k) = [t_w(k) \ p(k)]^T$.
- Λ denotes the state matrix as $\Lambda = \begin{bmatrix} 1 & 0 \\ \Delta t & 1 \end{bmatrix}$.
- \mathcal{E} is the coefficient matrix for the passenger arrivals: $\mathcal{E} = [0 \ \Delta t]^T$.
- $\lambda(k)$ is the passenger arrival rate.
- Υ is the coefficient matrix for passenger exchange $[0 \ -\frac{\Delta t}{t_b}]^T$.
- $\xi(k)$ is the integer state for boarding.

Then, the evolution of passenger wait time and the number of passengers at a stop over a finite N prediction horizon becomes:

$$\begin{aligned} \underbrace{\begin{bmatrix} \chi(k+1|k) \\ \chi(k+2|k) \\ \vdots \\ \chi(k+N|k) \end{bmatrix}}_{\hat{\chi}} &= \underbrace{\begin{bmatrix} \Lambda \\ \Lambda^2 \\ \vdots \\ \Lambda^N \end{bmatrix}}_{\hat{\Lambda}} \underbrace{\chi(k)}_{\hat{\chi}} + \underbrace{\begin{bmatrix} \mathcal{E} & 0 & \dots & 0 \\ \Lambda \mathcal{E} & \mathcal{E} & & 0 \\ \vdots & \vdots & \ddots & \vdots \\ \Lambda^{N-1} \mathcal{E} & \Lambda^{N-2} \mathcal{E} & \dots & \mathcal{E} \end{bmatrix}}_{\hat{\mathcal{E}}} \underbrace{\begin{bmatrix} \lambda(k|k) \\ \lambda(k+1|k) \\ \vdots \\ \lambda(k+N-1|k) \end{bmatrix}}_{\hat{\lambda}} + \\ &\quad \underbrace{\begin{bmatrix} \Upsilon & 0 & \dots & 0 \\ \Lambda \Upsilon & \Upsilon & & 0 \\ \vdots & \vdots & \ddots & \vdots \\ \Lambda^{N-1} \Upsilon & \Lambda^{N-2} \Upsilon & \dots & \Upsilon \end{bmatrix}}_{\hat{\Upsilon}} \underbrace{\begin{bmatrix} \xi(k|k) \\ \xi(k+1|k) \\ \vdots \\ \xi(k+N-1|k) \end{bmatrix}}_{\hat{\xi}} \end{aligned} \quad (4.41)$$

The passenger wait cost cannot be directly influenced by the decision variable (v_{des}). The cost function is sought in a linear form where the objective is minimizing passenger waiting time:

$$J_p(k) = \underline{\mathcal{P}} \underline{\chi} \quad (4.42)$$

subject to:

$$\hat{\chi} = \underline{\Lambda} \underline{\chi} + \underline{\mathcal{E}} \underline{\lambda} + \underline{\Upsilon} \underline{\xi}, \quad (4.43)$$

$$p(k + \kappa|k) \geq 0, \quad \forall \kappa = 1 \dots N. \quad (4.44)$$

The weighting parameter $\underline{\mathcal{P}}$ is a diagonal semi-definite matrix of appropriate size. Practically, it shall only penalize passenger wait t_w and not the passenger count p .

It is possible to consider multiple bus stops along the route of a bus, for example every bus between the controlled one and its leader. Even though the rolling horizon MPC targets only the next stop, the accumulation of waiting passengers at downstream stops can be considered over the prediction horizon (see Figure 4.3). In this case the optimization becomes less ego-centric. Decisions are made based on the status of a larger piece of the public transport network. In that case the cost function becomes the sum of the cost functions for each relevant bus stop ($j = 1..Y$):

$$J_p^*(k) = \sum_{j=1}^Y \underline{\mathcal{P}} \underline{\chi}. \quad (4.45)$$

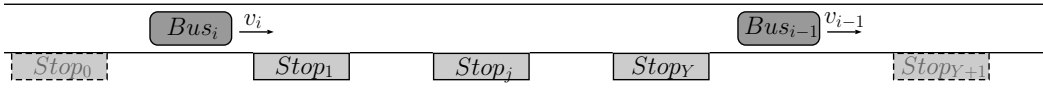


Figure 4.3: Relevant bus stops for the passenger waiting time model ($Stop_1 \dots Stop_Y$)

4.2.4 Multi-objective cost function

This section connects the results of the previous sections. The four objectives and the optimization constraints are combined into a single multi-objective cost function. By means of balancing between these conflicting goals, an optimal velocity profile is formulated for a single bus traveling along a public transport corridor.

$$\min_{v_{des}(k) \dots v_{des}(k+N)} J(k) = J_{tt}(k) + J_{hw}(k) + J_e(k) + J_p(k), \quad (4.46)$$

subject to:

$$\hat{\chi} = \underline{\Lambda} \underline{\chi} + \underline{\mathcal{E}} \underline{\lambda} + \underline{\Upsilon} \underline{\xi}, \quad (4.47)$$

$$|z_{tt}(k + N|k)| < \varepsilon, \quad (4.48)$$

$$|v(k + N|k)| = \varepsilon, \quad (4.49)$$

$$v_{min} \leq v_{des}(k + \kappa|k) \leq v_{max}, \quad \forall \kappa = 1 \dots N, \quad (4.50)$$

$$a_{min} \leq \frac{1}{\tau} (v_{des}(k + \kappa|k) - v(k + \kappa|k)) \leq a_{max}, \quad \forall \kappa = 1 \dots N, \quad (4.51)$$

$$p(k + \kappa|k) \geq 0, \quad \forall \kappa = 1 \dots N. \quad (4.52)$$

The cost function in Eq. (4.46) creates a relationship between the four conflicting objectives. The free parameter in the optimization is the desired velocity of the bus over the prediction horizon. The bus shall obey the timetable, keep equidistant headway from the bus ahead in an energy efficient way. In addition, the wait time of passengers at bus stops shall be kept low too. These objectives shall be achieved in an environment where traffic and traffic lights are considered a bottlenecks. The velocity of the bus is constrained by external circumstances: the prevailing speed on the traffic link or the legal speed limit. By prescribing level of service constraints the maximum acceleration and deceleration is bounded. Although, jerk (the derivative of acceleration) is an important factor for passenger comfort, for simplicity, it is not considered as a constraint.

Since $J_e(k)$ and $J_p(k)$ are nonlinear cost functions (i.e. they depend on integer parameters), the resulting cost function will also be nonlinear. $J_e(k)$ is piecewise due to the separation of acceleration and deceleration. Furthermore, the passenger waiting model introduced a boarding state which is depending on a state variable $x(k)$. Due to the multiple decisions, the problem is non-smooth. However, when these decisions are eliminated, the problem turns into a quadratic optimization which is analytically convenient. The non-convex problem can be solved with sequential quadratic programming (SQP) (Nocedal and Wright [2006]). It is an iterative procedure that boils down the nonlinearity into repetitive sequence of quadratic approximations by QP. Furthermore, due to the varying horizon length N , computational demand can vary. With increasing prediction horizon length increasing number of equations shall be solved and increasing number of decisions to be made.

Initially, weighting scalars and matrices are chosen in such a way that each cost has a similar magnitude. By alternative selection of the weighting parameters one can formulate different control strategies (e.g. preferring objective J_e over J_p). Alternatively, with proper weighting, public transport delay can be minimized in an energy-optimal way. The formulation of different weighting strategies and their effect on service performance will be addressed in the further sections.

4.2.5 Weighting strategies

The four specified control objectives can be taken into account with different importance. Putting more emphasis on an objective over another leads to different bus trajectories and influences the performance of the bus level of service. Weighting is done in two steps. First, the four cost functions are scaled with the help of the tuning matrices incorporated into them. That is to have the cost parts in the same magnitude range. This can be achieved with the help of the inverse square law (Bryson's rule, Bryson et al. [1979]): the weights are normalized with the reciprocal of the squared expected maximum values of the states.

Second, coefficients are introduced to each of the cost parts weighting their relevance in the optimization. In this vein, 6+1 strategies are proposed. Six static ones presented in Figure 4.4 and one dynamic, adaptive control strategy.

- a) Timetable tracking with J_{tt} being the only considered cost. Only the reference

trajectory x_{tt} is tracked by the bus, obeying the prescribed timetable and disregarding every other objective.

- b) Headway tracking, where only J_{hw} is taken into account. The goal is to mimic the trajectory of the leading bus via reference trajectory x_{hw} .
- c) Balanced, where headway and timetable tracking are equally important, i.e. $J = 0.5J_{tt} + 0.5J_{hw}$.
- d) Passenger demand driven: on frequent lines passengers usually do not consult the timetable (Dessouky et al. [2003]). In order to avoid bunching (causing increased waiting times (Fonzone et al. [2015])) and minimize passenger waiting time the two objectives to be considered are headway tracking and passenger wait time minimization. $J = J_{hw} + J_p$.
- e) Cheap service driven. From the service providers' perspective minimizing energy consumption of their fleet is crucial as it has direct impact on their expenses. In addition, running buses based on a periodic timetable is the simplest in terms of planning. $J = J_{tt} + J_e$.
- f) The balanced strategy (c) is augmented with the two nonlinear objectives, taking into account all four: $J = J_{tt} + J_{hw} + 0.5J_e + 0.5J_p$.
- g) Adaptive control, incorporating varying control weights, depending on the magnitude of timetable and headway errors: $J = \phi J_{tt} + J_{hw}$.

4.2.5.1 Adaptive control

The adaptive control strategy uses varying control weights based on the magnitude of timetable or headway errors. By means of this adaptive weight selection it is possible to match headways more efficiently depending on the delay (timetable) and the level of bunching (headway). To this end a metric is introduced that describes the bunching level given by

$$\phi(k + \kappa|k) = \left| \frac{z_{hw}(k + \kappa|k)}{z_{tt}(k + \kappa|k)} \right|, \quad (4.53)$$

where $\kappa = 1, \dots, N$ and $\phi(k + \kappa|k) \in [0, \phi_{max}]$. To apply this scaling other numerical considerations have to be taken into account: (i) ϕ is saturated with $\phi_{max} = 10$ to avoid enormous control weights, (ii) to circumvent division by zero $\phi = 1$ if $z_{tt} = 0$. The scaling parameter is calculated at the first step and frozen for the entire prediction horizon. It is necessary to freeze the value of ϕ in order to avoid algebraic loop in the solution. With this scaling if headway error z_{hw} is low $\phi \approx 0$, timetable schedule is tracked by means of weight selection. If there is a large deviation in headway, $\phi \gg 0$, headway error will play dominating role in the cost. It is sufficient to scale only J_{tt} , since the ratio of J_{tt} and J_{hw} determine which objective is more important to track.

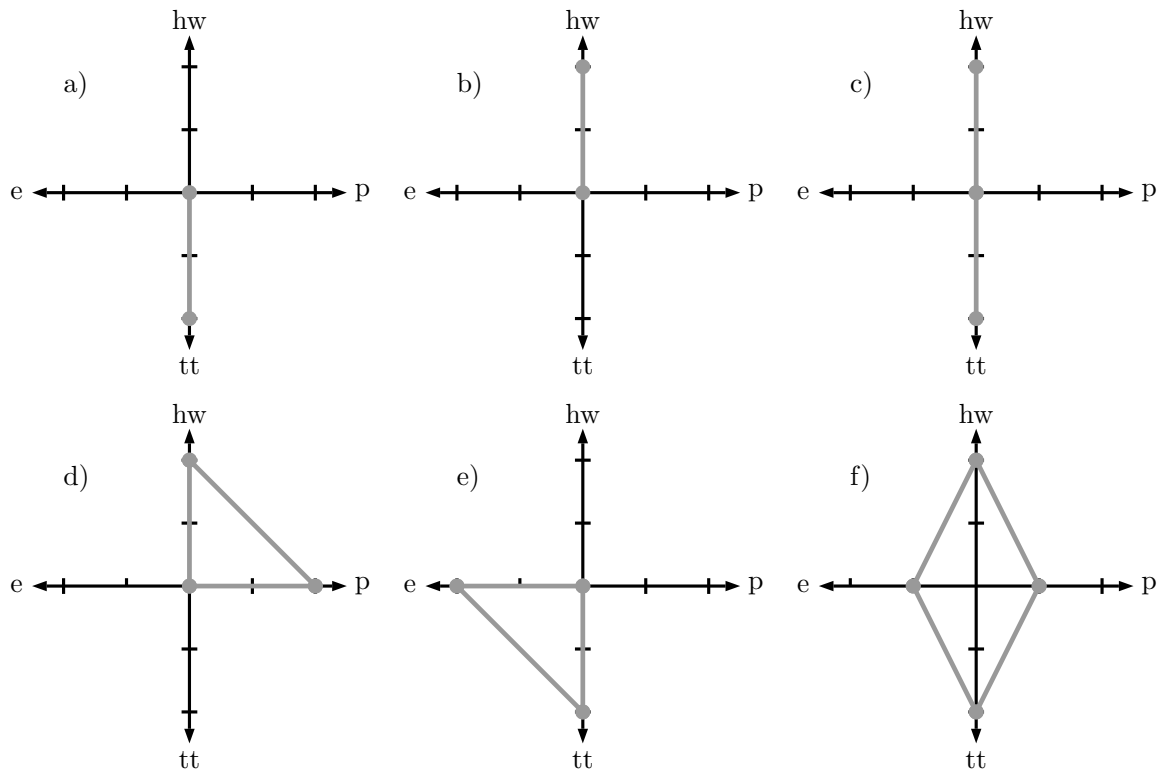


Figure 4.4: Proposed weighting strategies. *a)* Timetable tracking only, *b)* Headway tracking only, *c)* Balanced - timetable and headway tracking, *d)* Passenger demand driven - headway tracking and waiting time minimization, *e)* Cheap service driven - timetable tracking and energy consumption minimization, *f)* Balanced, advanced - timetable and headway tracking plus energy consumption and waiting time minimization. Abbreviations at each direction match the subscript of the respective cost function element

4.2.5.2 Pareto Front

A multi-objective optimization can have an infinite number of optimal solutions (i.e. the minimum cost can be achieved by a linear combination of the cost parts). This set is called the Pareto Front ([Veldhuizen and Lamont \[1998\]](#)). With the Pareto analysis, the gain of different weighting strategies can be quantified.

In this subsection the two convex cost parts (headway- and timetable tracking) are analyzed through the first three control strategies: *a)* Timetable tracking, *b)* Headway tracking and *c)* Balanced control. Since in the timetable tracking and headway tracking strategies only one objective is considered the solution of the Pareto front is trivial. To this end, a slight modification is made to these two strategies via weighting. In the headway tracking strategy 90% of the weight is assigned to the headway objective and 10% to the timetable tracking objective. In the timetable tracking control case it is the other way round. The balanced control strategy has 50 – 50% weight split. This way the two objectives do not have a unique solution but a set of optimal solutions. The two sub-cost functions J_{tt} and J_{hw} will be used to demonstrate the Pareto Front. The methodology for obtaining the Pareto front is the following: from a selected initial

state $X(k)$ and errors $z_{tt}(k)$, $z_{hw}(k)$ and prediction horizon N an optimization is started. Since the aim of the analysis is only the evaluation of the cost, not real-time control a genetic algorithm is chosen (Horn et al. [1994]). Due to the heuristic nature of the genetic algorithm, it gives solutions very close to the optimum but in a way scattered along a curve. Candidate solutions of the genetic algorithm with the lowest cost will form the Pareto Front.

The Pareto Front is illustrated for one bus at a fixed time instant considering the three different weighting strategies (timetable tracking, headway tracking and balanced), see Figure 4.5. In this example the prediction horizon is $N = 10$ and the states are: $X = [5.4, 614.8]^T$, $z_{tt} = 3.3 m$, $z_{hw} = 269.9 m$. If timetable tracking is preferred, the absolute value of J_{tt} is larger than J_{hw} . Moreover, for the headway tracking strategy, the absolute value of J_{hw} cost is more significant compared to J_{tt} . In the balanced strategy, the two costs are roughly equal. Interestingly, the results in the Pareto Front for the balanced strategy scatter much less. The balanced control policy returns with lower cost value for the timetable/headway error compared to only-headway/only-timetable policy in most of the cases (i.e. initial states plus prediction horizons). This suggests, the overall performance is better in terms of punctuality and bunching compared to single objective strategies.

4.2.5.3 Trajectory shapes

In this part, the proposed control strategies are evaluated from a fixed initial state. The aim is drawing conclusions from the shapes of the trajectory predictions in each weighting strategy. Figure 4.6 depicts the predicted control input sequences for one vehicle from a fixed location. In accordance with the rules of the MPC, only the first control input is applied to the real system. In this example the time headway is $T_{hw} = 60 s$ and the prediction horizon is $N = 100$. According to the timetable reference x_{tt} , the buses (the leader and the controlled) are running late.

The first strategy is timetable tracking (Figure 4.6 (a)). Here, the only objective is following the trajectory predefined by an ideal schedule x_{tt} , which is done accurately. Next, headway tracking strategy is shown in Figure 4.6 (b). The predicted trajectory accurately follows the sole prescribed reference trajectory x_{hw} . Next, the balanced strategy is shown in Figure 4.6 (c). In this case, both timetable and headway objectives are considered. The predicted trajectory lies between the two references. Spatial distances (tracking errors) are proportional to the set control weights. In the passenger demand-driven scenario headway homogeneity and passenger waiting times are considered. Compared to the headway tracking scenario (Figure 4.6 (d)), costing passenger wait will result in steeper accelerations and higher speeds due to passengers accumulating at stops. When energy consumption is penalized in the timetable tracking strategy, as shown in Figure 4.6 (e), accelerations and decelerations will become smoother suggesting energy savings. At the same time it causes minor delays. Finally, all four objectives are considered, however, passenger waiting time and energy consumption with 50% weight (Figure 4.6 (f)). Results are similar to the balanced (c) strategy, only with slower acceleration profiles. In addition, the predicted trajectory is knurled because regenerative braking is exploited. In a complete trajectory realization this effect cannot be observed. These trajectory predictions are for only one point in

the space-time diagram, however, the aforementioned conclusions hold true for whole bus trajectories too. Using different weighting strategies, the value of each cost function changes based on its significance. The cost function values in the optimization shown in Figure 4.6 are summarized in Table 4.1. Cost values increase as more conflicting objectives are considered.

Table 4.1: Cost function values with different weighting strategies

	J_{tt}	J_{hw}	J_e	J_p
a) Timetable tracking	16	-	-	-
b) Headway tracking	-	149	-	-
c) Balanced	175	167	-	-
d) Passenger demand driven	-	166	-	268
e) Cheap service driven	717	-	430	-
f) Advanced balanced	877	879	473	129

The proposed control framework provides a flexible selection of objectives, depending on the prevailing traffic situation. Deciding among the proposed control strategies brings in several factors such as passenger demand, frequency of buses, network layout, potential disturbances, etc. The next sections of this chapter provides numerical analyses of the proposed control strategies exploring which strategy works best in which situation.

4.3 Numerical simulations

4.3.1 Service homogeneity performance

The performance of the headway and timetable tracking objectives (control strategies *a*), *b*) and *c*)) are analyzed in depth. The basis of the results is the simulation model presented in Appendix A.1. First, one bus trajectory with balanced control strategy is explained in detail, see Figure 4.7. The blue circles represent the ideal departure times at each stop based on the bus schedule. The blue line x_{des} represents the ideal trajectory for timetable tracking. The red line x_{ref} is the trajectory of the leading bus, shifted by one time headway (3 minutes). In this balanced strategy the follower (controlled) bus tries to minimize bunching (i.e. match the trajectory of the leading bus) and keep the timetable. For the next bus the reference headway will be the trajectory of the current bus. Eventually, the trajectories will converge to the original timetable while reducing bunching. The leading bus travels slowly between *Stop 1* and *Stop 2* (due to some disturbance). The controlled bus also slows down to avoid bunching. This results in lateness but it is recovered by the end of the route. The bus holding strategy is also efficient in this scenario, the bus always departs from stops at the scheduled time instants but occupies stops for long periods. However, the bus holding cannot cope with severe disturbances. Figure 4.7 also shows the timetable and headway errors at every time instant. The desired velocity profile is not followed accurately because the bus has its own dynamics, plus it has to adjust its own velocity to the surrounding traffic.

Studying a single bus in the network does not reveal the performance of the algorithm. A sequence of bus trajectories shall be analyzed instead. To this end, the Göteborg simulation example (Appendix A.1) is used. The entry of the second bus to the network is perturbed: it arrives with one minute delay. The benchmark control strategies are bus holding and PI control, see Figure 4.8. For brevity, PI control is omitted from the plot. Holding strategy can remedy bunching and adhere to the schedule at the cost of spending long times at the stop. For example, *Stop 6* is almost always occupied by a bus with holding control. If the stop is shared among multiple bus lines the stop becomes congested adding delay to buses serving that stop. The PI control can efficiently reduce bunching and adhere to the schedule with smaller computational demand than the MPC. However, it cannot cope well with disturbances: for example if the leading bus was stopped by a traffic light, the controlled bus will also slow down regardless what the traffic light indicates. On the other hand, the MPC controllers consider a long trajectory ahead and buses can optimally adjust their velocity considering such obstacles (with the example of the traffic light - the MPC controller takes into account how long the leading bus was blocked by the traffic light).

The timetable tracking control strategy can keep the schedule few headways downstream the delay. Since the timetable is periodic, headways will converge to the prescribed timetable. With this control strategy, both headway and timetable adherence can be achieved. Next, headway tracking MPC solution is implemented. With this algorithm bunching is reduced, headway error is decreasing for consecutive buses. However, since the timetable objective is neglected, bus trajectories become out of sync with the schedule. The average velocity of the vehicles tend to decrease too, leading to further delays. A conclusion can be drawn here. Adjusting solely the headway of vehicles is not sufficient to achieve service homogeneity. On the other hand, a periodic timetable forces both timetable and headway adherence. The balanced control solution has the best of two worlds: the actual and reference trajectories overlap, meaning no bunching, while the timetable is kept too.

Next, the response of each control strategy to extreme disturbance is evaluated. The traffic is stopped between *Stop 4* and *Stop 5* for ten minutes (i.e. in the Gothenburg network Götaälvbron (bridge) is opened). Over this period congestion is formed, delays increase. After, traffic is released and congestion starts to dissipate. In Figure 4.9 the space-time diagrams of the buses with different control strategies are shown. The speed of congestion dissipation (i.e. the normalization of service periodicity) is denoted with dashed lines in Figure 4.9 and summarized in Table 4.2. Congestion dissipation speed is the forward traveling shockwave of the controlled buses at the bridge. It is the slope between the stopping point (in time-space) of the last bus affected by the perturbation and the point when service (headway periodicity) is fully recovered.

In the benchmark holding scenario five buses are affected by the service perturbation. The buses stopped at the bridge will remain bunched. Since there is no timetable or headway objective, vehicles leave the network as fast as possible, resulting in the fastest congestion dissipation. As stated in Newell [1977], delays remain so high that the scheduling cannot recover from bunching. In order for the holding strategy to work in case of large disturbances, other measures, such as stop skipping, pulling out or inserting buses shall be employed. The benchmark PI controller can dissipate the

Table 4.2: Congestion dissipation speed (m/s)

Holding	2.004
PI control	0.7268
Headway tracking	0.469
Timetable tracking	1.915
Balanced	0.608

congestion faster than the balanced controller but the system cannot recover well from the service perturbation, the buses leave the network bunched.

With headway tracking strategy bunching is completely eliminated but buses arrive with large delays at the next stop, not obeying the timetable. This strategy results in slow service between the bridge and *Stop 5* in order to equalize headways. Congestion dissipation is very slow. Timetable tracking solution cannot cope with the severe perturbation either. The buses that got caught by the opening of the bridge stick together and cannot recover. The large difference between the desired trajectory based on the timetable and the actual trajectory (i.e. large delay) forces the velocity controller to demand maximum velocity. Therefore, in order to recover, another policy (e.g. slack times, stop skipping, dynamic timetable) has to be used. The balanced technique reduces bunching compared to the timetable tracking but cannot eliminate it as well as headway tracking. Recovery of the timetable takes more time compared to the timetable tracking policy. The trade-off between headway and timetable tracking can also be observed in the congestion dissipation speed. In the multi-objective control approaches, given enough time both timetable keeping and bunching can be remedied.

Table 4.3 compares headway reliability in the different simulation scenarios based on statistical results. Headways are compared at two sections of the network: after *Stop 4* and after *Stop 6*. The mean value is close to the ideal headway of 180 seconds (3 min) except for the headway tracking and balanced control strategies after the perturbation. The reason is that after the traffic is released from the bridge there is a huge headway gap between two buses which corrupts the mean value. On the other hand in those strategies where headway tracking is not addressed this huge gap is counterbalanced by the small headways of the congested buses. Furthermore, headway standard deviations are smallest in the headway tracking and balanced scenarios. Finally, the Kullback-Liebler (KL) divergence is given between the ideal headway, and the simulation results, see [Kullback and Leibler \[1951\]](#). The ideal headway represents a uniform distribution with mean of 180 seconds and 0 variance. The KL distance is significantly smaller with the MPC compared to the holding control strategy after the service disruption. This means headways are more uniformly distributed.

Table 4.3: Statistics of the trajectories for headway reliability (target headway: 180 s)

Without service perturbation						
	After <i>Stop 4</i>			After <i>Stop 6</i>		
	Mean (s)	Std (s)	KL dist.	Mean (s)	Std (s)	KL dist.
Holding	179.647	7.026	0.0073	176.290	27.670	0.0123
PI control	183.333	13.637	0.0060	176.000	34.935	0.0204
Headway tracking	179.130	17.808	0.0037	179.130	22.347	0.0057
Timetable tracking	178.706	7.728	0.0088	176.400	47.042	0.0180
Balanced	179.647	10.386	0.0061	180.403	31.297	0.0068
With service perturbation						
Holding	181.923	9.962	0.0104	180.153	175.506	0.3581
PI control	182.832	15.077	0.0071	186.73	149.680	0.2124
Headway tracking	179.600	24.233	0.0035	236.450	134.797	0.1072
Timetable tracking	178.118	6.499	0.0063	176.401	141.494	0.2332
Balanced	179.881	15.530	0.0069	192.133	133.873	0.1640

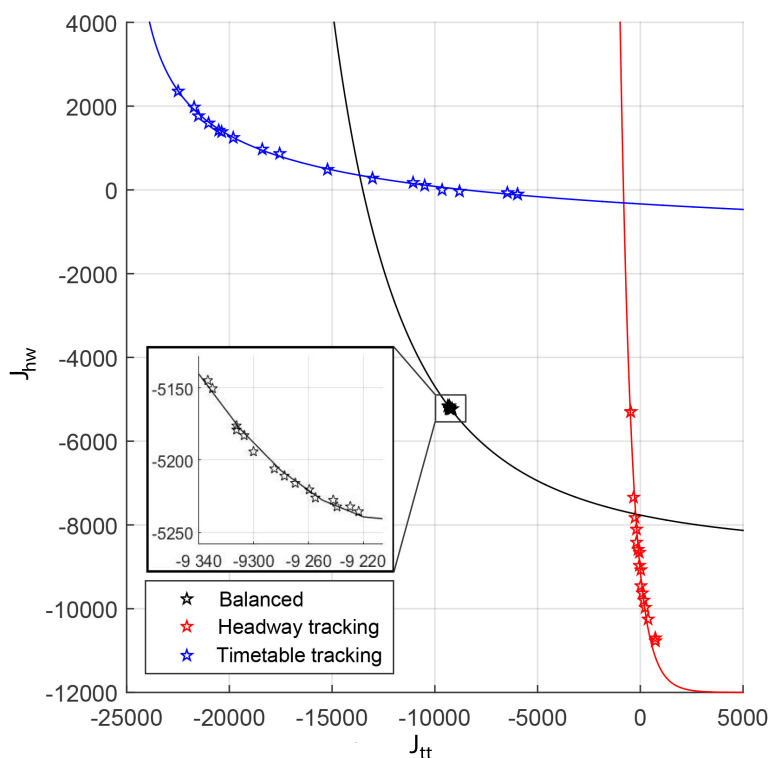


Figure 4.5: Pareto Front

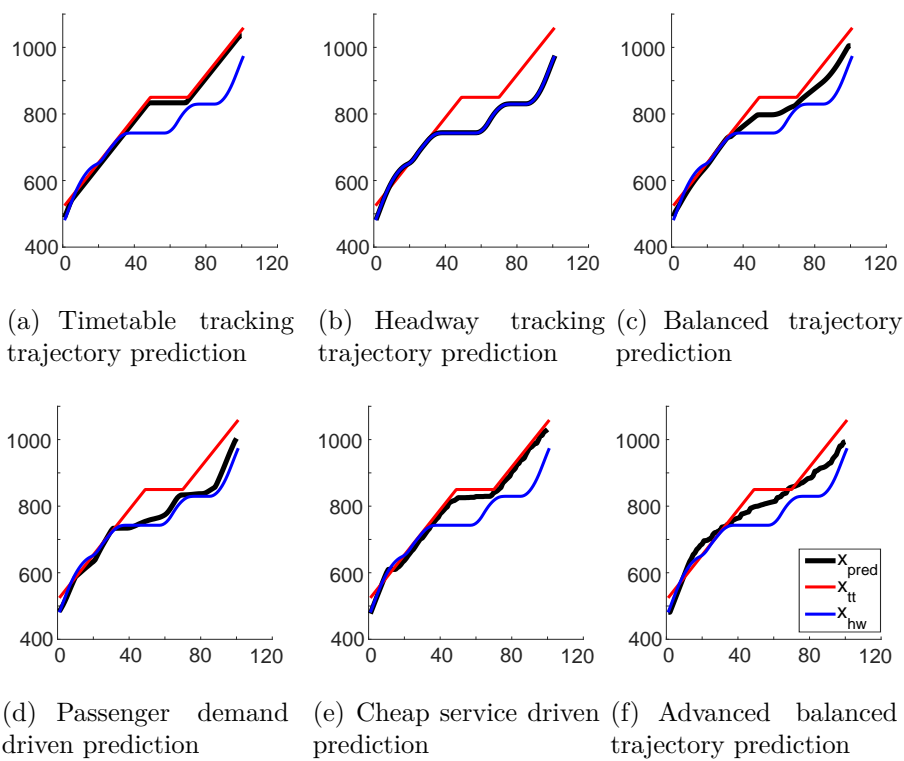


Figure 4.6: Trajectory predictions from a fixed initial state with different weighting strategies compared to the reference trajectories (vertical axis: Position (m), horizontal axis: Time (s))

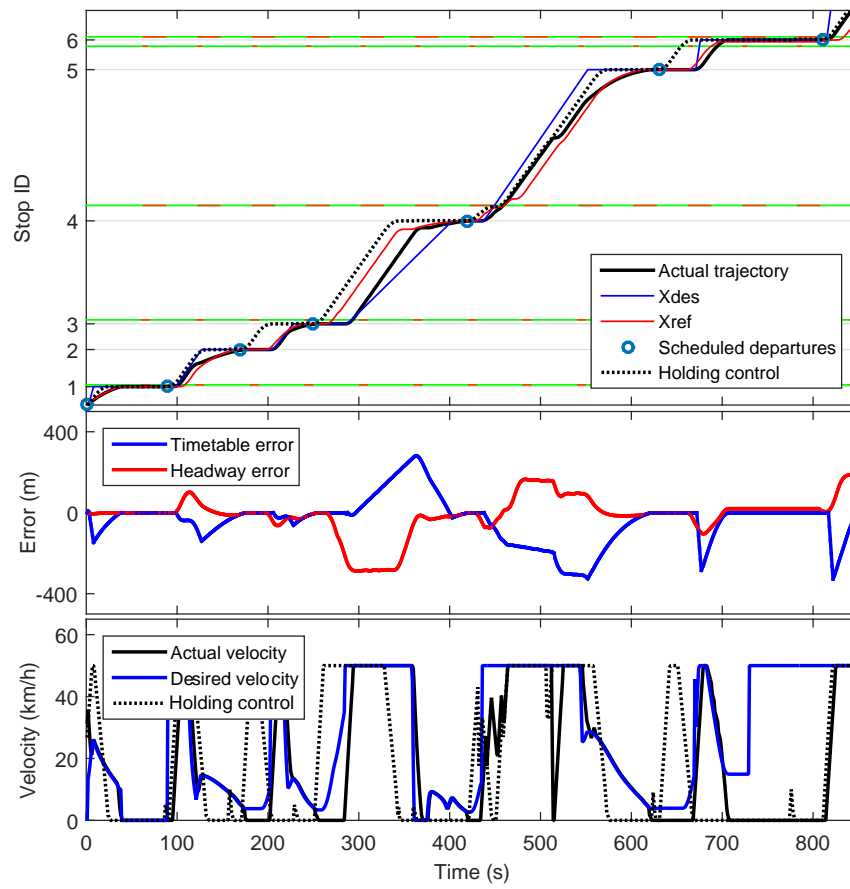


Figure 4.7: Trajectory of a single bus and its velocity profile

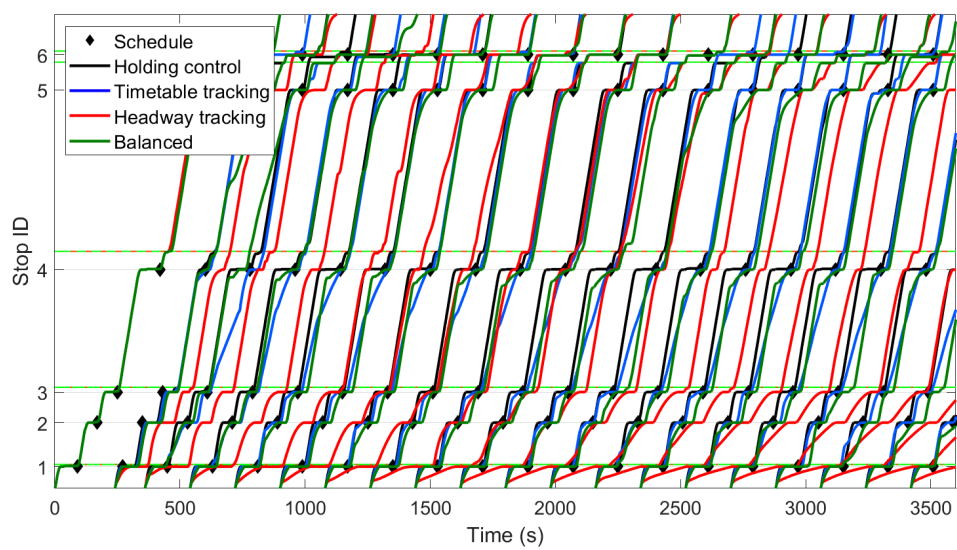


Figure 4.8: Trajectories of consecutive buses with different control strategies

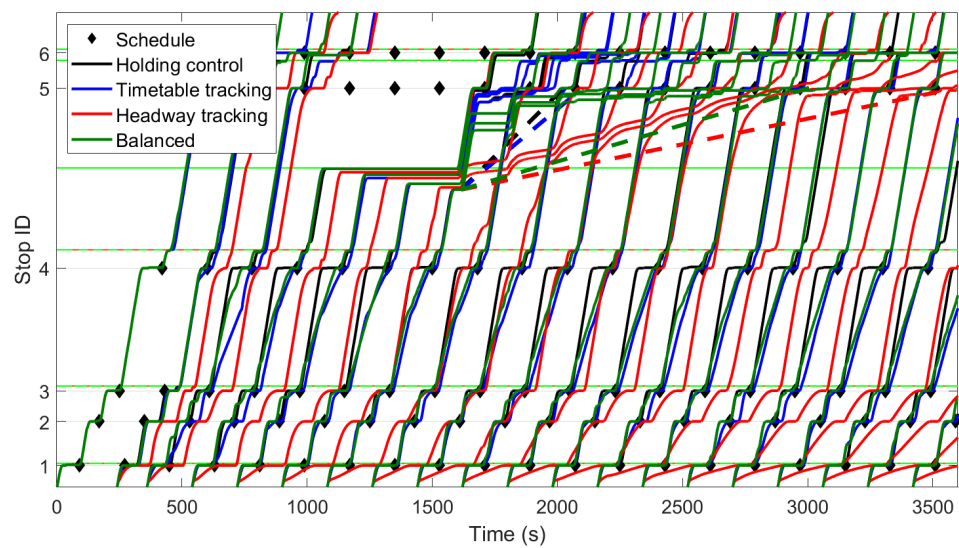


Figure 4.9: Trajectories of consecutive buses with different control strategies - 10 minute service perturbation. Dashed lines denote the speed of congestion dissipation

4.3.2 Energy consumption

In this part, the energy consumption performance metric is analyzed. First, one bus is selected from the Budapest simulation scenario (Appendix A.2) and its individual energy consumption is analyzed with different control strategies. In Figure 4.10 four bus trajectories are compared: holding control, PI control, energy-aware cheap control (d), and advanced balanced velocity control (f). The energy consumption is the lowest in the cheap control strategy. The advanced balanced velocity control has smaller average velocity (spends more time in the network) thus it has lower energy consumption compared to holding. If energy cost is not taken into account the decelerations are steeper. In the energy consumption aware scenarios when regenerative braking is considered, velocity profiles become smoother with a coasting phase before each stop. The average energy consumption is 9.5% smaller in the cheap velocity control and 4.3% smaller in the advanced balanced strategy compared to the holding strategy (Figure 4.11). The standard deviations of energy consumption (Figure 4.11) are similar to each other.

By arbitrarily selecting one vehicle does not say much about the total energy consumption of a public transport line. One bus may have good energy efficiency while it hinders following buses resulting in worse energy efficiency for the follower. To this end, the energy consumption of individual buses is summed in a simulation scenario (Figure 4.12). Simulation results suggest that the total energy consumption in the long run is as expected: the greedy holding control strategy and the PI controller consume the most energy. The holding control tries to always reach the highest permitted velocity on the link, while the PI controller only considers headway deviations. On the other hand, the energy-aware cheap control (d), and advanced balanced velocity control (f) have better energy efficiency. Using the holding control as a benchmark (100%), the energy-aware strategy consumes 8% less, while the advanced balanced velocity control consumes 3% less, considering a 3 km public transport line for 30 minutes. The PI controlled buses consume 3% more compared to holding. Note that between 500 – 1100 s the total energy consumption of the balanced strategy is the lowest. Longer simulations can smooth such deviations.

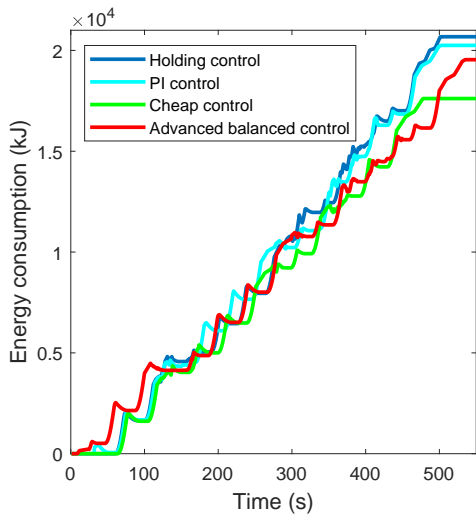


Figure 4.10: Energy consumption profile of one vehicle

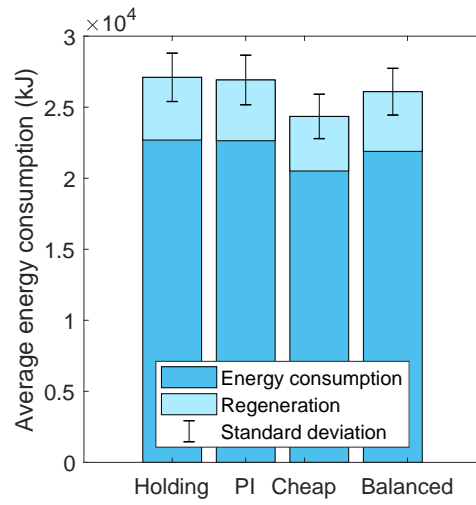


Figure 4.11: Average energy consumption and regeneration

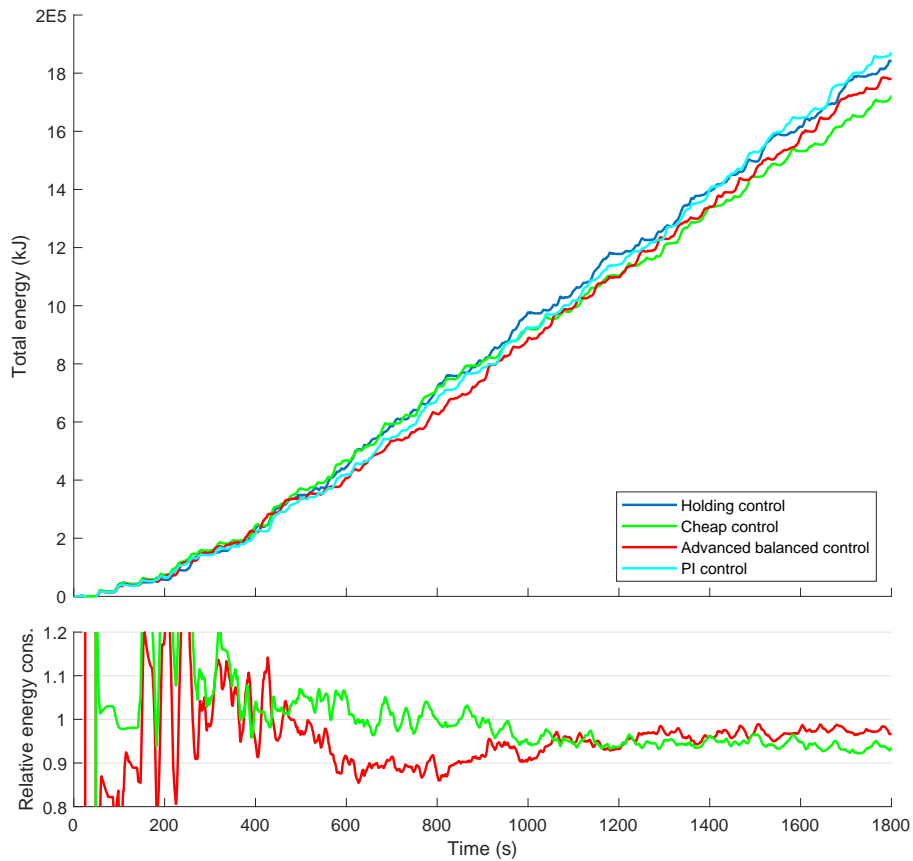


Figure 4.12: Total energy consumption on the bus line. The relative energy consumptions are normalized with the holding control strategy

4.3.3 Average passenger waiting times

Finally, the effect of considering passenger waiting times is analyzed. Average passenger waiting time relates directly to bus headways (Wu et al. [2017]). If buses arrive irregularly, passenger waiting times will deviate more and the total waiting time will increase. Again, four scenarios are considered: the benchmark holding control, PI control, passenger driven (e) and the advanced balanced (f) strategy. In terms of total (cumulated) passenger waiting times at each stop, the balanced control performs worst. The passenger driven strategy performs slightly better than the holding control. It performs well in this metric because buses spend less time between stops and more time waiting at each stop. So passengers who just arrived can board the bus instantly. The PI control performs similarly to the balanced control. The passenger driven scenario performs well if there are several passengers waiting at a stop far ahead as passengers draw the vehicle towards the stop. On the other hand, the passenger driven strategy considers the adverse effect of bus bunching too. Therefore, it can happen that the two objectives considered in this strategy (i.e. minimizing passenger wait and maintaining equidistant headways) are in conflict. Although it is possible for some stops that the strategy falls behind, in the long run, on network level it provides the least passenger wait. The average passenger waiting times for the bus at each stop are summarized in Table 4.4.

Table 4.4: Average total waiting time (in seconds) of passengers at each stop

Stop ID	Holding control	PI control	P Pass. driven	Adv. balanced control
Stop 1	50.7	51.1	52.6	48.5
Stop 2	49.7	50.9	50.5	48.8
Stop 3	289.4	334.8	300.6	341.7
Stop 4	58.4	57.8	52.1	60.1
Stop 5	65.5	63.7	57.0	62.7
Stop 6	492.0	511.6	423.7	508.3
Stop 7	237.5	343.0	251.7	330.8
Mean	177.63	201.8	169.77	200.17

4.4 Contribution

Thesis 3

Decentralized, multi-objective model predictive control strategies were formulated for public transport velocity control. The four (often) conflicting objectives considered in the optimization are timetable adherence, equidistant headways, energy efficiency, and minimal passenger waiting time. The controller operates in a shrinking horizon way meaning that trajectories are predicted until the vehicle reaches the next stop. The four objectives can be cast into control strategies via different weighting of the cost function.

Based on the control oriented public transport system models in Chapter 2 a multi-objective model predictive velocity controller was created. The aim is calculating an optimal velocity profile between the actual position of the vehicle and the next stop, while taking into account several uncertainties. First, the shrinking horizon strategy was introduced: the bus shall arrive at the next bus stop by the end of the prediction horizon. This way, as the scheduled arrival time becomes closer, the prediction horizon length shrinks. By the prediction time step the bus shall arrive at the desired stop. This also establishes a terminal set of system states, guaranteeing stability of the solution. With stacking states and inputs of the linear headway and timetable tracking models two convex objective parts were obtained. Convexity of the problem enables fast optimization. Next, the energy consumption model was adapted to the model predictive velocity control framework. Based on the acceleration and deceleration terms a piecewise objective was constructed. Then, a passenger waiting times objective was constructed.

The four control objectives were fused into a single multi-objective cost function subject to constraints that characterize a public transport line. The proposed control algorithm can deal with bus bunching, timetable adherence, energy efficiency and passenger waiting time minimization in a flexible way. To this end, different control strategies were introduced via assigning different weights to the cost function parts.

With the help of numerical simulations the performance of the proposed control strategies were analyzed and benchmarked against reference controllers borrowed from the literature. The model predictive controllers outperform the PI controller in the event of extreme disturbance in both timetable and headway tracking. If there are minor disturbances, the controllers are on par. Each strategy has its advantage and disadvantage. Timetable tracking solution is efficient during off-peak hours when bunching is not significant or when it is desirable to empty the network quickly after a major disturbance. Headway tracking is capable of eliminating bunching at the cost of abandoning the timetable. This strategy can work well if headways are short and buses tend to bunch - in case of short headways passengers are less likely to consult the timetable. The balanced strategy strikes equilibrium between the objective of headway and timetable tracking, granting good performance in both aspects. When energy efficiency is considered, the proposed energy-aware solution outperforms the benchmark holding control by 8% in terms of total energy consumed. The advanced balanced velocity control consumes 3% less compared to holding on network level. In long-run, this

suggests significant energy savings. In the passenger waiting time metric the holding control performs well, as it spends significantly more time at stops compared to other strategies. From the proposed control strategies only passenger driven solution can outperform it, as it is capable of planning ahead several stops. Other MPC strategies perform significantly worse.

The proposed control framework provides a flexible selection of objectives, depending on the prevailing traffic situation. Deciding which of the proposed control strategies brings in several factors such as passenger demand, frequency of buses, network layout, potential disturbances, etc.

Related publications:

The bi-objective (headway tracking and timetable tracking) control was formulated in [Varga et al. \[2018b\]](#) and [Varga et al. \[2018c\]](#). The two objectives were extended with the energy consumption objective based on [Varga \[2018\]](#). Then, the four objectives with the different control strategies was proposed in [Varga et al. \[2019a\]](#).

Chapter 5

Chance-constrained trajectory control

For more accurate trajectory prediction the adverse effect of traffic lights shall be considered too. In this chapter, the proposed model predictive controller in Chapter 4 is extended with additional constraints based on the stochastic shockwave profile model (Chapter 3). This means, the resulting controller becomes a chance-constrained MPC. After introducing chance-constraints and relaxing them with the help of the sampling and discarding method (Campi and Garatti [2011]) the controlled system is analyzed through numerical simulations.

5.1 Chance-constraints

Chance-constraints are based on the stochastic shockwave profile model presented in Chapter 3. If the controlled bus is in the queue upstream a traffic light $R_J(t, \omega)$, it cannot move. If it is in the queue discharge $R_C(t, \omega)$, its velocity is constrained by the surrounding traffic, see Figure 3.3. For simplicity, instead of considering acceleration fans (Laval and Leclercq [2010]) for the moving queue, the critical velocity v_C is assumed in this region. The two stochastic traffic regions can be expressed mathematically as:

$$x(k) \in R_J(t, \omega) \text{ if } \begin{cases} x(k) < l_l, \\ x(k) > l_l + W_2(t - (t_2 + ct_{cyc})), \\ x(k) < l_{s,c}(t_{s,c}, \omega) + W_3(t, \omega)(t - t_{s,c}(t, \omega)), \\ x(k) > l_l + W_4(t - (t_1 + (c + 1)t_{cyc})). \end{cases} \quad (5.1)$$

Similarly,

$$x(k) \in R_C(t, \omega) \text{ if } \begin{cases} x(k) < l_l, \\ x(k) > l_l + W_4(t - (t_1 + ct_{cyc})), \\ x(k) > l_{r,c-1}(t_{r,c}, \omega) + W_1(t, \omega)(t - t_{r,c-1}(t, \omega)), \\ x(k) < l_l + W_2(t - (t_2 + ct_{cyc})). \end{cases} \quad (5.2)$$

The conditional probability $\mathbb{P}(\cdot)$ of $x(k)$ being in $R_C(t, \omega)$ can be written as follows:

$$\begin{aligned} & \mathbb{P}\{\omega : x(k) \in R_C(t, \omega)\} = \\ & \mathbb{P}\{\{\omega : l_{r,c-1}(t_{r,c}, \omega) + W_1(t - t_{r,c-1}(t, \omega)) > x(k)\} \mid \{x(k) < l_l\} \wedge \\ & \wedge \{x(k) > l_l + W_4(t - (t_1 + ct_{cyc}))\} \wedge \{x(k) < l_l + W_2(t - (t_2 + ct_{cyc}))\}\}. \end{aligned} \quad (5.3)$$

Similarly,

$$\begin{aligned} & \mathbb{P}\{\omega : x(k) \in R_J(t, \omega)\} = \\ & \mathbb{P}\{\{\omega : l_{s,c}(t_{s,c}, \omega) + W_3(t, \omega)(t - t_{s,c}(t, \omega)) > x(k)\} \mid \{x(k) < l_l\} \wedge \\ & \wedge \{x(k) > l_l + W_2(t - (t_2 + ct_{cyc}))\} \wedge \{x(k) > l_l + W_4(t - (t_1 + (c + 1)t_{cyc}))\}\}. \end{aligned} \quad (5.4)$$

The CDFs $F_{x(k) \in R_J(t, \omega)}(\varphi)$ and $F_{x(k) \in R_C(t, \omega)}(\varphi)$ for the probabilities of a point is within region $R_C(t, \omega)$ or $R_J(t, \omega)$ can be determined, however, numerically challenging. The discrete time MPC takes samples from the continuous time shockwave profile model. Note that stochasticity only arises in the third case which describes the tail of the queue in both Eq. (5.1) and Eq. (5.2), the other lines bounding the regions $R_J(t, \omega)$ and $R_C(t, \omega)$ are deterministic (Figure 3.2). The stochastic nature of the regions $R_J(t, \omega)$ and $R_C(t, \omega)$ turns the optimization into a chance-constrained MPC (Campi et al. [2009]). A continuous distribution for the queue length imposes infinite number of constraints on the optimization on the domain Ω . Campi and Garatti [2011] provided a reformulation method for a chance-constrained optimization problem into its sample-based counterpart. A continuous stochastic event can be replaced with a finite sample of independent instances $\omega^{(1)}, \omega^{(2)}, \dots, \omega^{(M)} \in \Omega$, distributed according to \mathbb{P} where Ω is the sample-space. The optimization is then solved for M chance-constraints and the additional non-chance-constraints for every discrete time step k . In addition, Campi and Garatti [2011] studied the effect of constraint removal: what is the trade-off between performance (cost value) and constraint violation (feasibility) if m constraints are removed. Sample-based problems are solved via Monte-Carlo simulations by varying the probability level based on the distribution function (Campi et al. [2009]). Monte-Carlo simulation is used as a tool for analysis: a probability level is sought where the predicted trajectory remains feasible without the control being too conservative. Under feasibility the existence of a control input that satisfies all the constraints of the optimization (Stephen Boyd [2019]).

Next, the probability sampling and discarding approach in Campi and Garatti [2011] is translated into the problem of stochastic queue lengths in the trajectory optimization. The continuous stochastic shockwave profile model in Section 3.2 has a natural discretization. Queue length discretization is done by discretizing the vehicle arrival rate $Q_A(t, \omega)$ according to $F_{Q_A}(t, \varphi)$ (i.e. discrete number of vehicles). Then, the continuous $R_J(t, \omega)$, $R_C(t, \omega)$ regions turn into discrete ones denoted by $\hat{R}_J(t, \omega)$, $\hat{R}_C(t, \omega)$ respectively. The spatially discretized traffic flow state regions $\hat{R}_J(t, \omega)$ and $\hat{R}_C(t, \omega)$ impose finite number of nonlinear constraints on the optimization through fixed probability levels for every prediction step. Finally, the two chance-constraints to be appended to the final optimization problem are:

$$v(k + \kappa | k) = v_J = 0, \text{ if } x(k + \kappa | k) \in \hat{R}_J(t, \omega), \forall \kappa = 1 \dots N, \quad (5.5)$$

$$v(k + \kappa | k) = v_C, \text{ if } x(k + \kappa | k) \in \hat{R}_C(t, \omega), \forall \kappa = 1 \dots N. \quad (5.6)$$

For simplicity, in the chance-constrained optimization, only the timetable tracking objective is considered (i.e. weighting strategy a) in Section 4.2.5).

$$\min_{v_{des}(k) \dots v_{des}(k+N)} J_{tt}(k), \quad (5.7)$$

subject to:

$$\hat{\chi} = \underline{\Lambda} \underline{\chi} + \underline{\mathcal{E}} \underline{\lambda} + \underline{\Upsilon} \underline{\xi}, \quad (5.8)$$

$$|z_{tt}(k + N|k)| < \varepsilon, \quad (5.9)$$

$$|v(k + N|k)| = \varepsilon, \quad (5.10)$$

$$v_{min} \leq v_{des}(k + \kappa|k) \leq v_{max}, \quad \forall \kappa = 1 \dots N, \quad (5.11)$$

$$a_{min} \leq \frac{1}{\tau} (v_{des}(k + \kappa|k) - v(k + \kappa|k)) \leq a_{max}, \quad \forall \kappa = 1 \dots N, \quad (5.12)$$

$$v(k + \kappa|k) = v_J = 0, \quad \text{if } x(k + \kappa|k) \in \hat{R}_J(t, \omega), \quad \forall \kappa = 1 \dots N, \quad (5.13)$$

$$v(k + \kappa|k) = v_C, \quad \text{if } x(k + \kappa|k) \in \hat{R}_C(t, \omega), \quad \forall \kappa = 1 \dots N. \quad (5.14)$$

The stochasticity in the constraints will inevitably propagate to the solution of the minimization problem (i.e. the predicted trajectory). Although the stochastic properties of the constraints are known, the explicit connection of stochastic properties between the constraints and the solution fades away. It can only be recovered via numerical simulations. Although, the cost function is quadratic the introduced chance-constraints are non-convex: a decision shall be made based on the location of the bus. Once the chance-constraints are relaxed (albeit still non-convex), the problem can be solved with the SPQ method in a more efficient way (Nocedal and Wright [2006]).

5.2 Numerical simulations

The proposed model predictive controller is analyzed from two aspects. First, feasibility of the predicted trajectories from a deterministic starting point is studied. Second, based on a microscopic traffic simulator the proposed chance-constrained optimal velocity control is compared to other benchmark strategies.

5.2.1 Feasibility study

The goal of this analysis is finding a probabilistic measure to quantify the validity of the result. A confidence level is sought where the predicted trajectory remains feasible without the control being too conservative.

The bus predicts its trajectory towards the next stop from a given deterministic initial condition. There are three traffic lights between the bus and the next stop. The signal timings and traffic flow rates upstream each traffic light is summarized in Table 5.1. The experimental network is the upper part of the Budapest network (Appendix A.2) with slightly modified signal programs. In the fixed initial condition prediction the distance from the target bus stop is 500 m and the desired arrival time is 70 s . Assuming $\Delta t = 2$ s this results in $N = 35$.

Table 5.1: Signal program and vehicle flow upstream each traffic light

Light ID	Location l_l (m)	Cycle time t_{cyc} (s)	Green time t_{green} (s)	Switch time t_1 (s)	Mean arrival rate Q_A (veh/h)
#1	220	60	40	50	550
#2	370	100	40	0	550
#3	470	60	40	10	550

The aim of this simulation is evaluating predicted trajectories when queue lengths are randomly generated in a Monte Carlo simulation. That is, the inflow volumes $Q_A(t, \omega)$ are randomly chosen from their distribution function $F_{Q_A}(t, \varphi)$. To keep the demonstration simple, vehicle inflows to the network follow independent Poisson distributions with constant (time-independent) arrival rate (Table 5.1). By varying the magnitude of the input traffic volumes, shockwave profiles and traffic state regions change too. The regions $\hat{R}_J(t, \omega)$ and $\hat{R}_C(t, \omega)$ play part in the trajectory prediction as chance-constraints. Figure 5.1 presents the set of predicted trajectories in the Monte Carlo simulation (with 1000 runs). The planned trajectories arrive at the desired position by the end of the prediction with some tolerance. The predicted desired velocities are zero at the jam region and vehicles arrive at the destination on time, obeying the constraints imposed by the SPM. According to Figure 5.1, the vehicles would slow down and wait upstream the queue and only enter it for a short time, resulting in somewhat counter-intuitive trajectory shapes. Despite being counter-intuitive, the solutions are feasible, since there are infinitely many feasible solutions. Note that, due to the sparse sampling ($\Delta t = 2$ s) it is possible that the predicted trajectory does not stop exactly upon arriving at a queue but slightly after. Furthermore, Figure 5.1 also presents two trajectories: bus holding and an MPC that does not consider traffic lights, thus they violate constraints.

As a metric for analysis, the spatial standard deviations are calculated at every time instance and shown in Figure 5.2. The prediction horizon is split in three intervals depending on the predicted position of the bus relative to traffic lights. In time interval $0 - 32$ s the standard deviation of the queue in front of the first traffic light, between $32 - 52$ s the standard deviation upstream the second traffic light are shown. Finally, between $52 - 68$ s there are no random events considered so the standard deviation is assumed to be 0.

According to Figure 5.2 there is correlation between the queue lengths and predicted trajectories. When the standard deviation of the queue length σ_{queue} increases so does the standard deviation of the predicted trajectories σ_{traj} and peaks when entering the queue. The uncertainty in the queue length prediction (i.e. larger variance) amplifies the variance of the predicted trajectories too. When there is no stochastic queue (after 52 s) the predicted trajectories converge and their standard deviation decreases. In addition, the trajectory standard deviation starts decreasing upstream Light #2, since the queue forces the vehicles to stop. Figures 5.3-5.4 suggest negative correlation between the queue length and the predicted trajectory samples. As the predicted queue increases the bus slows down (being farther from the traffic lights), trying to avoid coming to a full stop in the queue.s

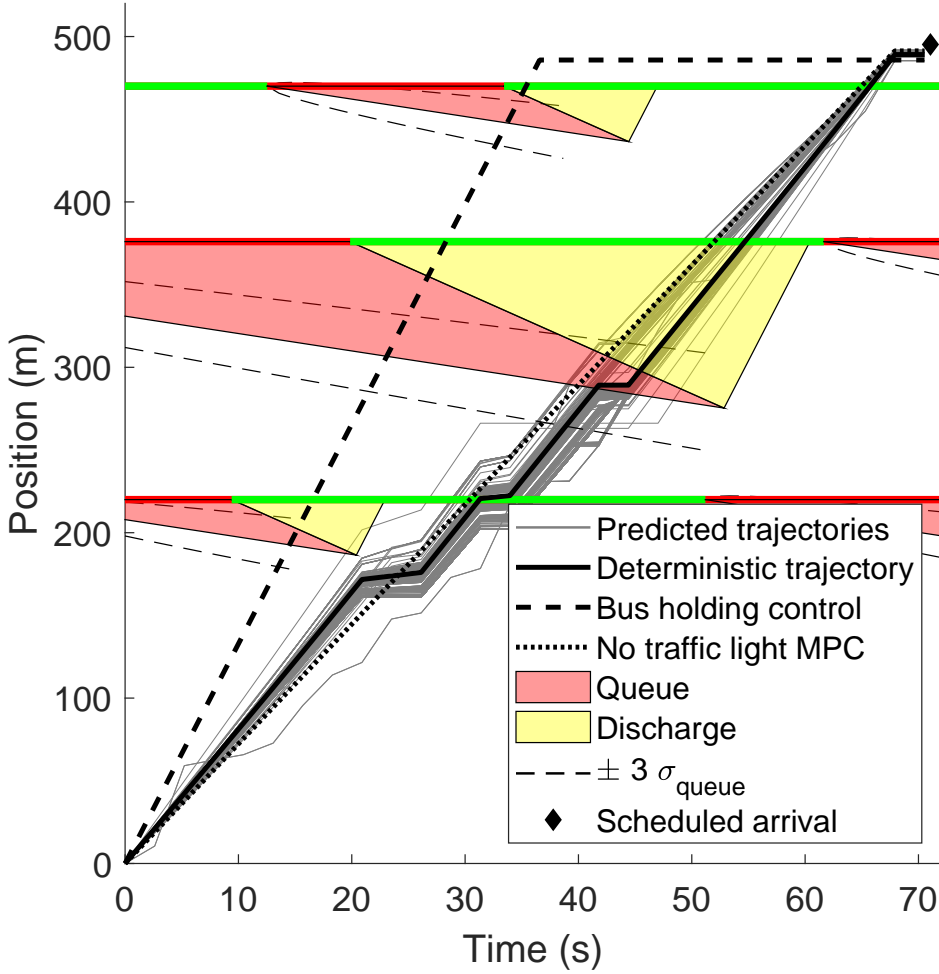


Figure 5.1: Trajectory prediction distribution. Red areas indicate jam regions $R_J(t, \omega)$, yellow areas indicate queue discharge regions $R_C(t, \omega)$. Dashed lines at the shockwave profiles indicate the queue length distribution with $\pm 3\sigma_{queue}$.

Next, the feasibility of the prediction is checked. Trajectories are predicted from a deterministic initial position for different probability levels. The method is translated from the sampling and discarding approach in [Campi and Garatti \[2011\]](#). Selecting a fixed probability level means that constraints imposed by less likely events (i.e. queue lengths) are discarded. The input flow has Poisson distribution with mean value 700 veh/h (per lane). One trajectory is predicted for confidence levels: $mean$, $mean - 2\sigma$, $mean + 2\sigma$ (Figure 5.5). The prediction horizon is 50 s long and the target distance is 150 m . In the feasibility analysis it is checked if the results are feasible by calculating the relative constraint violation as follows:

$$V = \frac{1}{N} \sum_{k=1}^N \left| \frac{v_{des}(k) - v_*(k)}{v_{des}(k)} \right|, \quad (5.15)$$

where $v_*(k)$ equals $v_{des}(k)$, v_J , v_C , depending on which region the k^{th} step of the

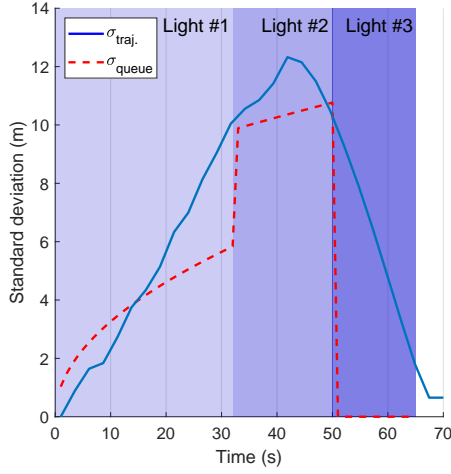


Figure 5.2: Standard deviations of the queue length σ_{queue} and the predicted trajectories σ_{traj} .

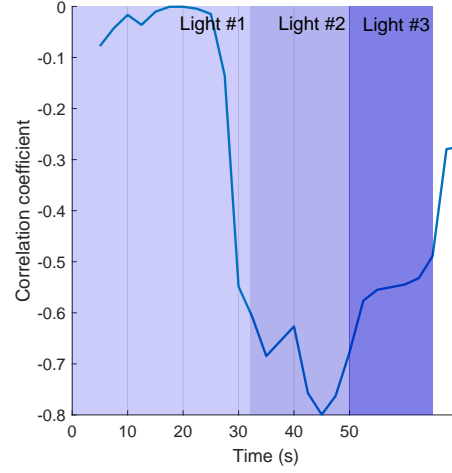


Figure 5.3: Correlation coefficient between the queue lengths and the predicted trajectories over the prediction horizon

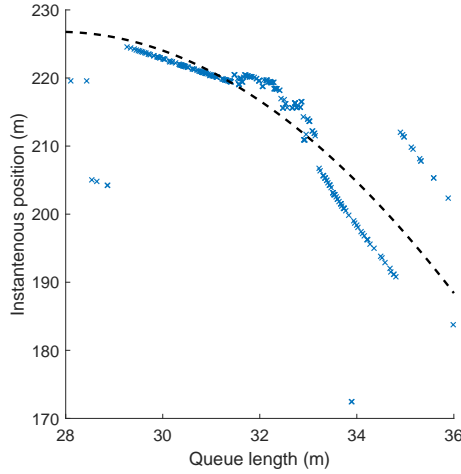


Figure 5.4: Scatter plot of the queue length vs the instantaneous position samples at prediction time 35 s

predicted trajectory is in. The value of V at each test is summarized in Table 5.2. The constraint violation value V is not zero in the tested cases. Results in Table 5.2 point towards a trivial conclusion: when the actual (measured) queue length is larger than the queue length used for prediction, prediction results tend to be less feasible and vice versa. When the queue length used for prediction is larger than actual queue lengths, it would cause unnecessary stops (Figure 5.5). However, accounting for larger inflow rate (i.e. larger probability than the actual queue length) leads to more robust results, more room for correction along the vehicle's trajectory and more reliable bus arrivals at a stop.

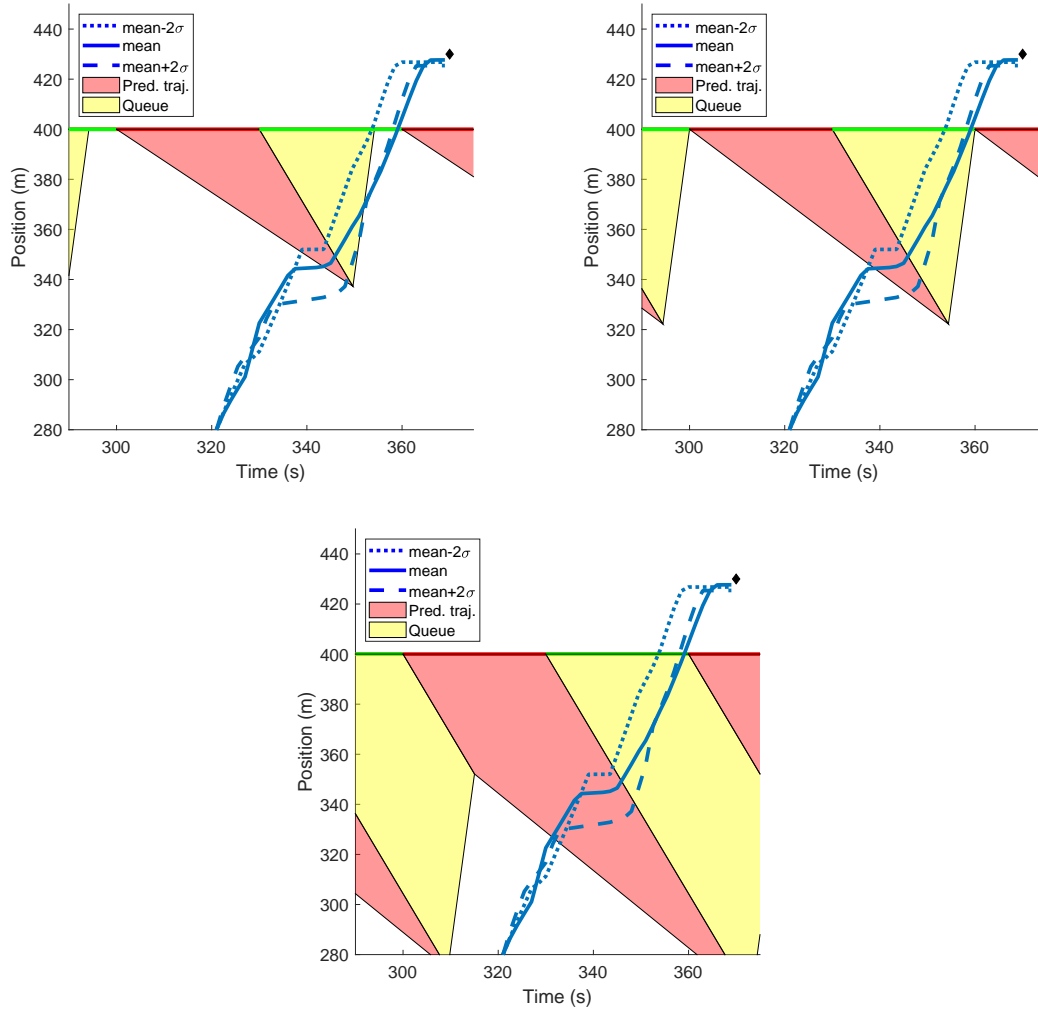


Figure 5.5: Predicted trajectories for -2σ (dotted line) – 700 (solid line) – $+2\sigma$ (dashed line) *veh/h* compared to the SPM at 647 (*mean* – 2σ) (top left) – 700 (top right) – 753 (*mean* + 2σ) (bottom) *veh/h*

Table 5.2: Constraint violation metric V . Horizontal: actual arrival rate, vertical: presumed arrival rate.

Volume	647 <i>veh/h</i>	700 <i>veh/h</i>	753 <i>veh/h</i>
647 <i>veh/h</i>	0.132	0.202	0.354
700 <i>veh/h</i>	0.059	0.163	0.323
753 <i>veh/h</i>	0	0.148	0.254

Although, Table 5.2 suggests that predictions from a deterministic initial state are not feasible they are adequate. In the rolling horizon MPC scheme only the first step of the prediction is used. Simulation results suggest that the first prediction step is feasible if the constraints are not too restrictive for the trajectory planning.

5.2.2 Microscopic traffic simulation

The traffic-light aware trajectory planning algorithm is tested in VISSIM (PTV [2011]) too. The modeled network is a 1 *km* long section of the Budapest network (Appendix A.2). The fixed probability level for queue length estimation is set to 70%, i.e. the queue lengths will be overestimated for guaranteed avoidance of stopping. The proposed MPC algorithm is compared to three benchmark controllers:

- i) bus holding strategy,
- ii) timetable tracking control strategy *a*) which does not consider traffic lights, and
- iii) an MPC that only considers traffic signal states without queue length information, similar to Kural et al. [2014a].

The trajectories generated by the four control strategies in space-time diagram are presented in Figure 5.6.

The holding strategy is greedy, as the set desired velocity for buses between bus stops is 50 *km/h*, thus they try to get to the next stop as fast as possible. At stops, they wait until their scheduled departure time. Compared to other strategies there are steeper decelerations and accelerations when entering or leaving queues, respectively. Steep accelerations decrease ride comfort and increase energy consumption. In addition, buses following this strategy are more likely to be held in queues for longer times. When not considering traffic lights at all (timetable tracking strategy *a*)), buses go slower and may miss the green traffic light window where it has to cross the intersection in order to arrive on time. Therefore, for an urban velocity control strategy to work, it is crucial to take into account downstream obstacles, such as traffic lights. The benchmark algorithm that operates without queue length information can hold the timetable and be faster than the proposed chance-constrained MPC. The controller assumes there are no queues at traffic lights and can cross the intersection right after the light turns green. Without assuming queues, it has to often come to a full stop at traffic lights. Finally, buses with the chance-constrained MPC take traffic light cycles and queue lengths into account and drive accordingly. Buses slow down before entering the queue or even try to elude it, avoiding coming at a full stop, saving energy. In Figure 5.7, at the third traffic light the measured queue is shorter than the predicted. The queue length aware bus slows down so it may avoid the predicted queue. This finding suggests that, it is not sufficient only to predict queue lengths, queue lengths shall be continuously adjusted with the actual measured queue lengths if they are available. Without proper traffic light information such velocity control algorithms may fail, as seen in the case of the “no queue MPC” or “timetable tracking” velocity controllers. Chance-constraints are therefore adding efficient probabilistic guarantees to velocity control algorithms.

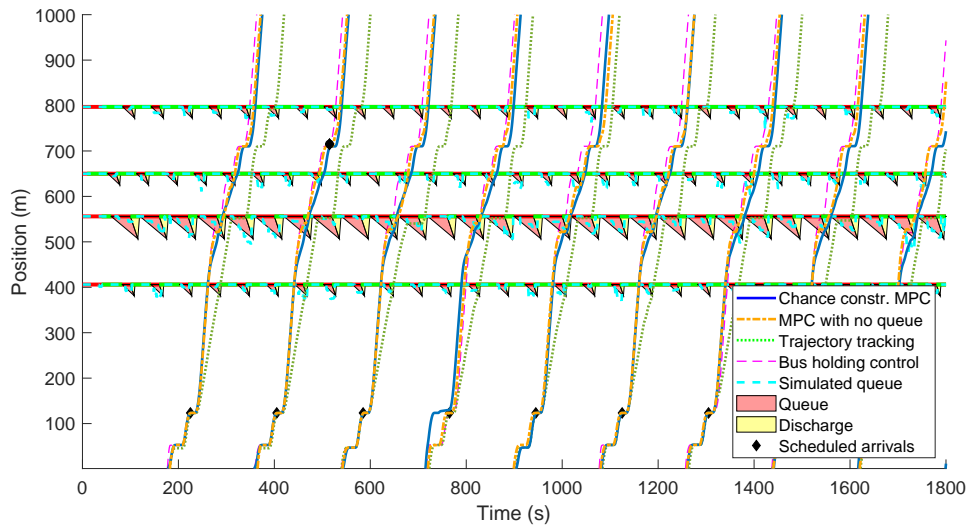


Figure 5.6: Bus trajectories. A detailed section of this figure can be seen in Figure 5.7

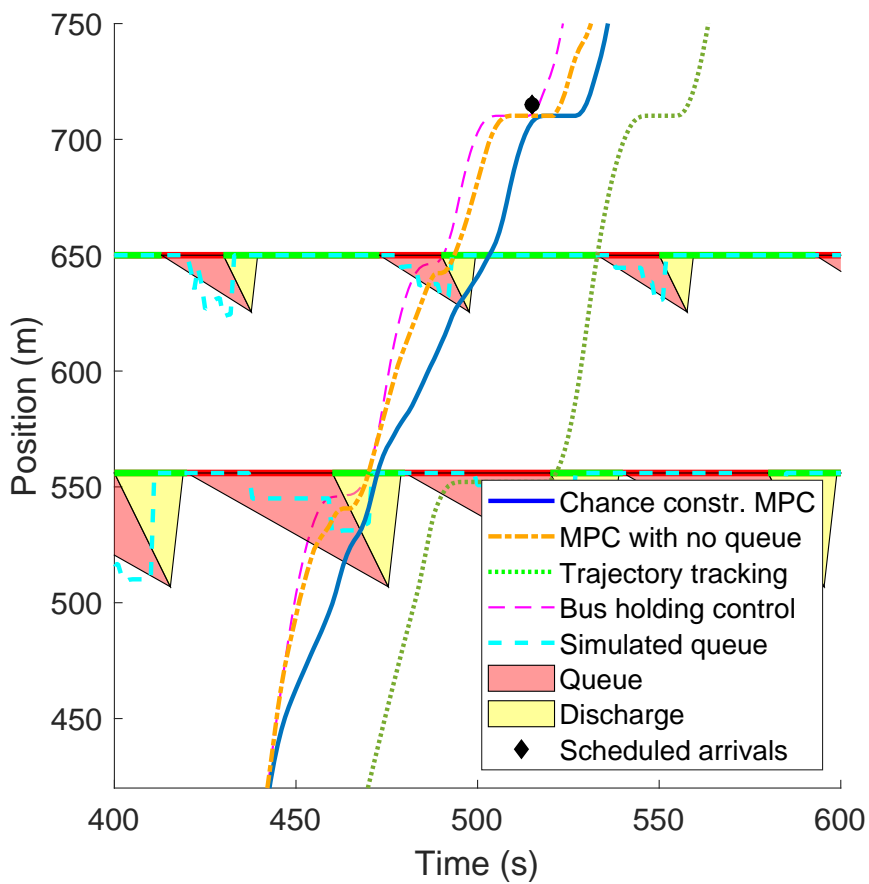


Figure 5.7: Bus trajectories - zoomed

5.3 Contribution

Thesis 4

To improve the performance of green-wave cruise control systems, a trajectory planning algorithm was augmented with the stochastic shockwave profile model. The controller considers traffic signal states and queue lengths at signalized intersections in a stochastic way. In the optimization, stochasticity arises in the form of chance-constraints which are alleviated with the sampling and discarding method.

The velocity control algorithm was augmented with the adverse effect of vehicle queues at signalized intersections. The stochastic shockwave profile model was incorporated into the optimization as chance-constraints. The SSPM model distinguishes different traffic regions (in a probabilistic sense). If the controlled vehicle's predicted trajectory is in either of these regions, its velocity is constrained (e.g. if it is in the stationary queue its velocity shall be zero).

Stochasticity in the constraints was alleviated via the sampling and discarding approach. First, the shockwave profiles were discretized, then a fixed probability level was selected, based on the results of multiple simulation runs (Monte Carlo simulation). For example, setting the probability level to 70% means that the algorithm will overestimate queue lengths in 70% of the cases. The optimization may yield infeasible solution due to long queue lengths (many velocity constraints) or short prediction length (delay). Due to the rolling horizon nature of the controller it is not critical: if the first element of the control input sequence yields feasible solution, the algorithm can function adequately.

Numerical simulations suggest that there is negative correlation between the queue length and the predicted trajectory samples. Resultantly, longer queues mean that the bus is farther from the desired stop, as it tries to avoid the queue and approach it slower. The proposed controller tries to avoid stopping the vehicle in front of signalized intersections, vehicles try to avoid the queue. This suggests improvement in energy efficiency.

Related publications:

The reference tracking foundation of the control algorithm was described in [Varga et al. \[2018c\]](#). Then, the stochastic shockwave profile was outlined in [Varga et al. \[2018b\]](#) and [Varga and Tettamanti \[2019\]](#). Finally, the realization of the chance-constrained model predictive control was published in [Varga et al. \[2019b\]](#) and [Varga et al. \[2020b\]](#).

Chapter 6

Centralized public transport network velocity control

This chapter gives a different approach for the bus network control. Section 2.5.2 introduced a centralized model for urban public transport. Section 6.2 places this model into a model predictive framework. Then, the system is analyzed and the strengths and weaknesses of the centralized control are highlighted. When the public transport network is considered several other factors shall be considered too. These factors boil down to the interaction of buses on different lines and passengers waiting for these buses. On top of equidistant headways and energy efficiency on common bus lines, service quality becomes a more complex question. Accounting for passengers at a stop waiting for different bus lines are briefly discussed in Section 2.4. An additional service quality related objective is formulating the timetable considering transfers and connections. This can be done explicitly via bus holding constraints or implicitly by formulating the timetable reference signals with this objective in mind. In the proposed public transport network control, the latter is assumed.

6.1 Network MPC

The piecewise affine network model can be used as a basis of a rolling horizon optimization. This approach, however, is different from the previous approach in several aspects: handling the system in a centralized way significantly increases the dimension of the state space model. Furthermore, the controller design is based on an NP-hard mixed integer optimization. Although control design for high-dimensional mixed-integer systems is well-established, systematic analysis techniques for such systems are limited. The decentralized control in the previous sections pinpointed a fixed point in the state-space, serving as a terminal set. This shrinking horizon approach, i.e. the bus shall be at the next stop by the end of the prediction horizon does not work. To this end, the horizon length N is chosen as large as computational capacity permits. This means, the proposed MPC does not have a terminal set, therefore, closed-loop behavior shall be checked separately. In addition, due to computational burdens, the energy consumption objective is not considered. Introducing additional integer variables to the problem (acceleration or braking state for every bus) would considerably increase the

computational complexity of the problem.

In order to formulate an optimization problem based on the model in Eq. (2.22) and Eq. (2.23), it shall be extended for N horizon. The shorthand writing of the aforementioned equations are

$$X_N(k+1) = A_N X_N(k) + B_{N,u} u_N(k) + B_{N,\xi} \xi_N(k) + B_{N,w} w_N(k), \quad (6.1)$$

$$Z_N(k+1) = C_N X_N(k+1) + D_N \zeta_N(k). \quad (6.2)$$

Introduce the following nomenclature for the extension of the model:

- $X_N(k)$ is the vector of network states (bus positions $x_{i=1..M_B}$, velocities $v_{i=1..M_B}$ and passenger numbers at stops $p_{j=1..M_S}$).
- A_N denotes the state matrix combining the bus and stop dynamics.
- $B_{N,u}$ is the coefficient matrix for the control inputs (bus desired velocities).
- $u_N(k)$ collects the control input for each bus at time step k :
 $u_N(k) = [v_{des,1}(k), v_{des,2}(k), \dots, v_{des,M_B}(k)]^T$.
- $B_{N,\xi}$ is a block diagonal matrix for the boarding status coefficients.
- $\xi_N(k)$ is the vector of boarding states at each bus stop
 $\xi_N(k) = [\xi_1(k), \xi_2(k), \dots, \xi_{M_B}(k)]^T$.
- $B_{N,w}$ is the coefficient matrix for external signals (velocity disturbance for buses and passenger arrival rates for stops).
- $w_N(k)$ external signals:
 $w_N(k) = [v_{mac,1}(k), v_{mac,2}(k), \dots, v_{mac,M_B}(k), \lambda_1(k), \lambda_2(k), \dots, \lambda_{M_B}(k)]^T$.
- $Z_N(k)$ is the vector of tracking errors $z_{tt,i=1..M_B}$ and $z_{hw,i=1..M_B}$.
- C_N is the output matrix.
- D_N is the direct feedthrough matrix of the reference trajectories.
- $\zeta_N(k)$ contains the reference trajectories for the buses $x_{tt,i=1..M_B}$, $x_{hw,i=1..M_B}$.

The stacking is done in the same vein as in the previous sections:

$$\begin{aligned}
 & \overbrace{\begin{bmatrix} X_N(k+1|k) \\ X_N(k+2|k) \\ \vdots \\ X_N(k+N|k) \end{bmatrix}}^{\underline{\mathbf{x}}_N} = \overbrace{\begin{bmatrix} A_N \\ A_N^2 \\ \vdots \\ A_N^N \end{bmatrix}}^{\underline{\mathbf{A}}_N} \overbrace{X(k|k)}^{\underline{\mathbf{x}}_N} + \overbrace{\begin{bmatrix} B_{N,u} & 0 & \cdots & 0 \\ A_N B_{N,u} & B_{N,u} & & 0 \\ \vdots & \vdots & \ddots & \vdots \\ A_N^{N-1} B_{N,u} & A_N^{N-2} B_{N,u} & \cdots & B_{N,u} \end{bmatrix}}^{\underline{\mathbf{B}}_{N,u}} \overbrace{\begin{bmatrix} u_N(k|k) \\ u_N(k+1|k) \\ \vdots \\ u_N(k+N-1|k) \end{bmatrix}}^{\underline{\mathbf{u}}_N} \\
 & + \overbrace{\begin{bmatrix} B_{N,\xi} & 0 & \cdots & 0 \\ A_N B_{N,\xi} & B_{N,\xi} & & 0 \\ \vdots & \vdots & \ddots & \vdots \\ A_N^{N-1} B_{N,\xi} & A_N^{N-2} B_{N,\xi} & \cdots & B_{N,\xi} \end{bmatrix}}^{\underline{\mathbf{B}}_{N,\xi}} \overbrace{\begin{bmatrix} \xi_N(k|k) \\ \xi_N(k+1|k) \\ \vdots \\ \xi_N(k+N-1|k) \end{bmatrix}}^{\underline{\xi}_N} + \overbrace{\begin{bmatrix} B_{N,w} & 0 & \cdots & 0 \\ A_N B_{N,w} & B_{N,w} & & 0 \\ \vdots & \vdots & \ddots & \vdots \\ A_N^{N-1} B_{N,w} & A_N^{N-2} B_{N,w} & \cdots & B_{N,w} \end{bmatrix}}^{\underline{\mathbf{B}}_{N,w}} \overbrace{\begin{bmatrix} w_N(k|k) \\ w_N(k+1|k) \\ \vdots \\ w_N(k+N-1|k) \end{bmatrix}}^{\underline{\mathbf{w}}_N}, \quad (6.3)
 \end{aligned}$$

$$\begin{bmatrix} \hat{\mathbf{z}}_N \\ Z_N(k+1|k) \\ Z_N(k+2|k) \\ \vdots \\ Z_N(k+N|k) \end{bmatrix} = \begin{bmatrix} \underline{\mathbf{C}}_N & 0 & \cdots & 0 \\ 0 & C_N & & 0 \\ \vdots & \vdots & \ddots & \vdots \\ 0 & 0 & \cdots & C_N \end{bmatrix} \begin{bmatrix} \hat{\mathbf{x}} \\ X_N(k+1|k) \\ X_N(k+2|k) \\ \vdots \\ X_N(k+N|k) \end{bmatrix} + \begin{bmatrix} \underline{\mathbf{D}}_N & 0 & \cdots & 0 \\ 0 & D_N & & 0 \\ \vdots & \vdots & \ddots & \vdots \\ 0 & 0 & \cdots & D_N \end{bmatrix} \begin{bmatrix} \hat{\boldsymbol{\zeta}}_N \\ \zeta_N(k+1|k) \\ \zeta_N(k+2|k) \\ \vdots \\ \zeta_N(k+N|k) \end{bmatrix}. \quad (6.4)$$

Again, the cost function is sought in a quadratic form:

$$J_N(k) = \frac{1}{2} \left[\hat{\mathbf{x}}_N^T \underline{\mathbf{Q}}_{N,x} \hat{\mathbf{x}}_N + \hat{\mathbf{z}}_N^T \underline{\mathbf{Q}}_{N,z} \hat{\mathbf{z}}_N + \mathbf{u}_N^T \underline{\mathbf{R}}_N \mathbf{u}_N \right], \quad (6.5)$$

where $\underline{\mathbf{Q}}_{N,x}$, $\underline{\mathbf{Q}}_{N,z}$ and $\underline{\mathbf{R}}_N$ are diagonal, positive semi-definite matrices as weighting parameters. Each row in the weighting matrices correspond to one (predicted) state or control input. The mathematical steps in towards the final form of the cost function are the same as in Section 4.2.1.1. The final form of the cost function becomes:

$$J_N(k) = \frac{1}{2} \mathbf{u}_N^T \Phi_N \mathbf{u}_N + \Omega_N^T \mathbf{u}_N, \quad (6.6)$$

where Φ_N and Ω_N^T denote the quadratic and linear coefficients of the control input. The cost function is subject to the following constraints:

$$\xi_j(k) \in \mathbb{Z}^* \quad \forall j, \quad (6.7a)$$

$$p_j(k) \geq 0 \quad \forall j, \quad (6.7b)$$

$$v_{min} \leq v_{des,i}(k) \leq v_{max} \quad \forall i, \quad (6.7c)$$

$$\lambda_i = \min\{\lambda_{i,max}, p_i(k)\} \quad \forall i, \quad (6.7d)$$

$$v_{des,i}(k) = 0 \text{ if } \eta_i = 1 \quad \forall i. \quad (6.7e)$$

In other words, a desired velocity profile shall be predicted for every bus in the network considering the reference trajectories $x_{tt,i}(k \dots k+N)$, $x_{hw,i+1}(k \dots k+N)$ obeying the following constraints. $\xi_j(k)$ denotes passenger exchange at stop j . Its value equals the number of buses at the stop. The number of passengers at a stop cannot be smaller than zero. To this end, the passenger boarding rate is constrained. The desired velocities of the buses are bounded too. The purpose of the last constraint is to force the bus to stop to perform passenger exchange. A bus is performing passenger exchange if it is at the stop, its velocity is zero and there are passengers at the stop. To this end a logical variable is introduced:

$$\eta_i(k) : \exists j : (|x_i(k) - x_{stop,j}|) < \epsilon \ \& \ p_j(k) \geq \epsilon. \quad (6.8)$$

The above logical variable will activate together with one of the boarding states ξ_j (see its definition is Eq. (2.16)). The bus will be held at the stop until all the passengers at that stop have boarded, i.e. $p_j(k)$ is reduced to zero. In the expression above (Eq. (6.8)) $p_j(k)$ relates to the stop where the bus i is. ϵ denote numerical tolerances.

The system is loosely coupled through the integer states: since the control input is computed in a centralized way, the passenger numbers are calculated in relation of

the buses of the network. If one bus takes passengers from a stop, the trajectory of the following bus is planned accordingly (e.g. less dwell time required). The proposed optimization problem is a standard mixed integer quadratic problem (MIQP) which can efficiently be solved by existing solvers (e.g. [Gurobi \[2014\]](#)). The complexity of the problem, however, grows exponentially with additional system states or by increasing the prediction horizon.

6.2 Analysis

In this section the centralized control algorithm is analyzed. First, simple case studies are constructed to test the controller in practical situations. Second, the feasibility of the bus network control is analyzed. Third, a comparison is made with the decentralized control in Chapter 4. Finally, the computational demand of the network controller compared to the other model predictive approaches is studied.

6.2.1 Experimental results

In this section two simulation examples are given. First, the simulation results are analyzed from the relationship of one bus and a bus stop, i.e. how the system states behave when a bus enters a stop. Then, an experimental network consisting of two circular bus lines, six buses and six stops is analyzed. In the first simulation, in [Figure 6.1](#), a bus travels towards a stop, located at 500 m and stops. When its speed is reduced to zero, passenger boarding can start (ξ is set to 1). When there are no passengers at the stop, the bus can continue its route. The prediction horizon is fixed: $N = 15$.

Next, the system performance is analyzed through an arbitrary public transport network ([Figure 6.2](#)) consisting of two circular bus lines (2000 m and 2500 m) long, respectively. Three buses serve each line with four stops each. Two stops are shared. The time headway on both lines is 200 s , therefore, the headway on the common corridor is $\frac{200\text{ s} \cdot 200\text{ s}}{200\text{ s} + 200\text{ s}} = 100\text{ s}$.

[Figure 6.3](#) depicts a single bus performing three laps on Line 1. In the first lap the tracking errors are bigger due to initialization. As time progresses, tracking performance becomes better. At 1200 m the headway reference changes, since the bus enters the common route section and starts following a bus from Line 2. Next, every bus in the network is analyzed in time-space diagram ([Figure 6.4](#)). The trajectories of bus Line 1 are shifted by 500 m , so stops III and IV are situated in the same places. After initialization, buses start to equalize their headways, they arrive to the common section precisely, only minor speed adjustment is required after merging. Finally, [Figure 6.5](#) shows the evolution of passenger numbers over time at one bus stop. The time when passenger numbers are decreasing are exactly the same times, when there is a bus from Line 1 at Stop II in [Figure 6.4](#).

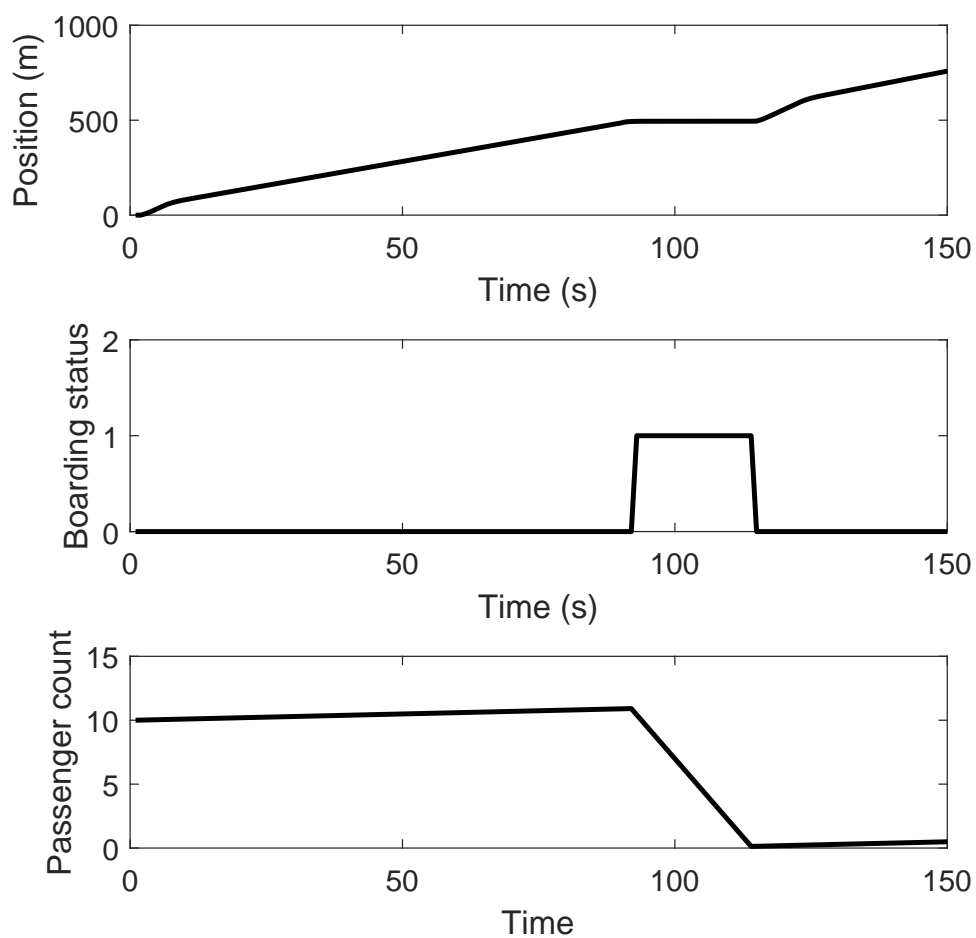


Figure 6.1: System states upon a bus approaching a bus stop

Table 6.1: Bus stops on the experimental network

	Location Line 1 (m)	Location Line 2 (m)	Arrival rate (pass/s)
Stop I	500		0.05
Stop II	1000		0.05
Stop III	1200	800	0.1
Stop IV	1800	1400	0.1
Stop V		1700	0.02
Stop VI		2300	0.02

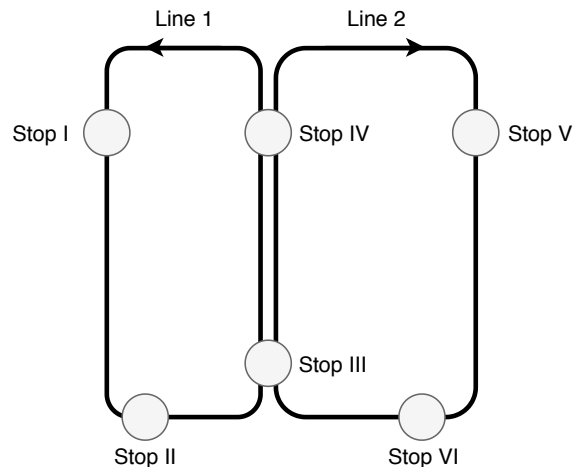


Figure 6.2: Experimental network

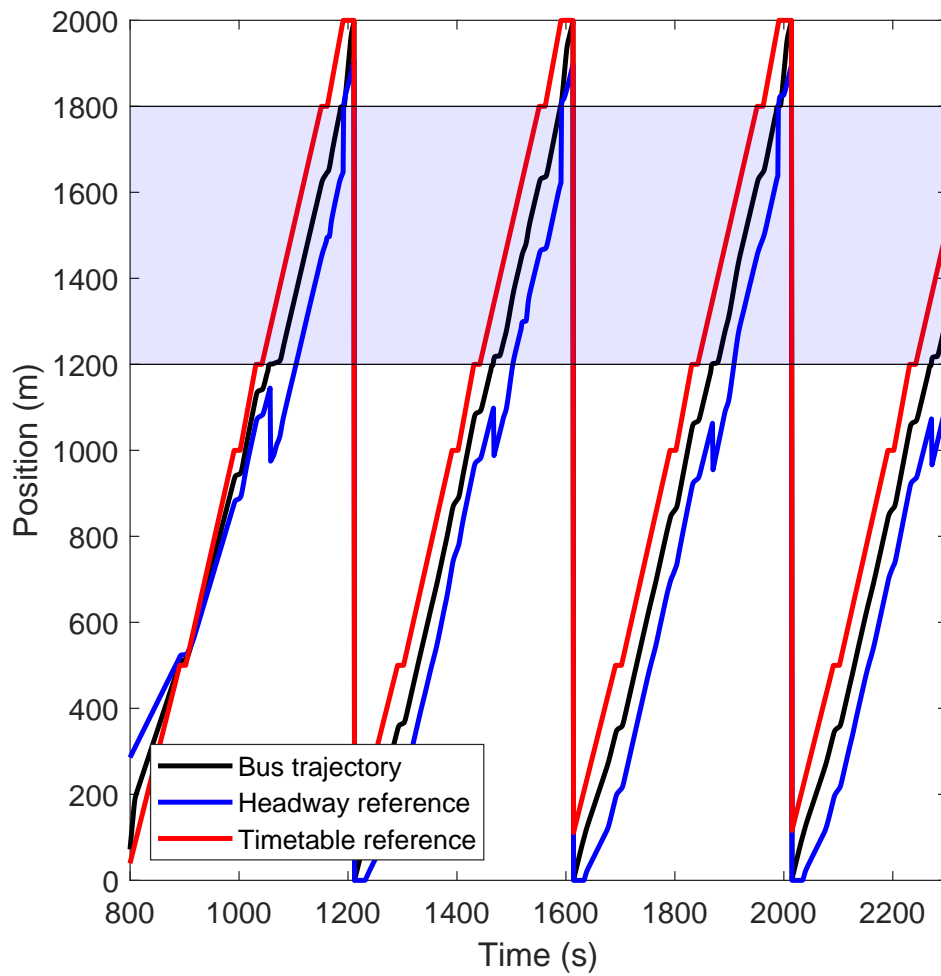


Figure 6.3: Trajectory of one bus in the experimental network with its reference trajectories. The bus makes three laps. The shaded area denotes the common line section.

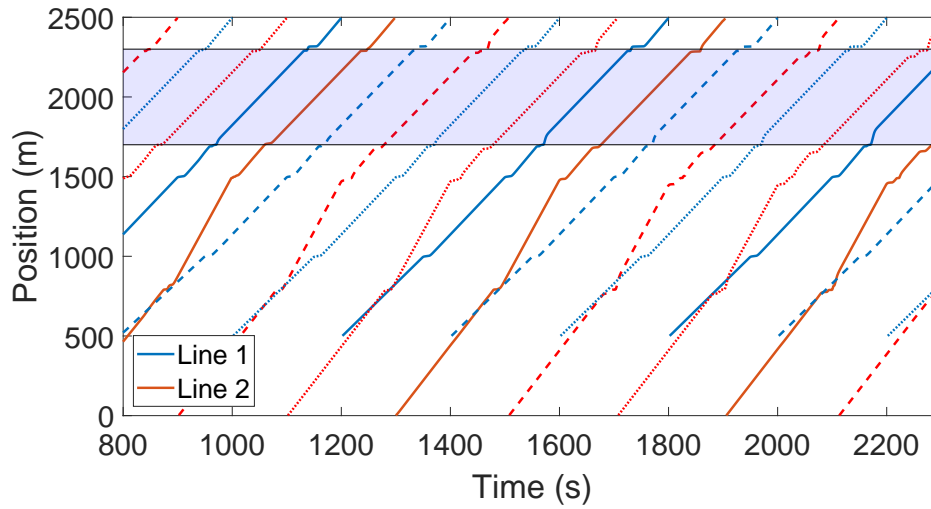


Figure 6.4: Trajectory of every bus in the network. Different line styles are used to distinguish individual buses. Trajectories of Line 1 are shifted so positions match in the common line section.

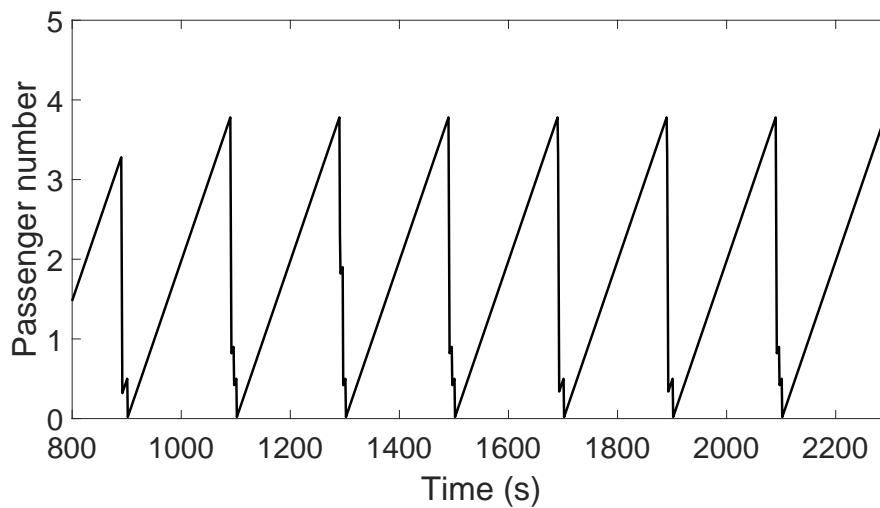


Figure 6.5: Passenger numbers at Stop II

6.2.2 Feasibility study

6.2.2.1 Random simulations

In this analysis step, several numerical simulations are launched from random initial conditions with the same model settings. The goal is to get quantitative information on the maximal passenger number, which is a practically relevant performance metric of the controlled bus network. Probabilistic measure is computed to quantify the validity of the result. More refined simulation based analysis can be performed by using the recent results of the scenario approach (Campi et al. [2009]).

Here, the same example network is used as in Section 6.2.1. In such a high dimensional system varying every initial condition is especially exhausting. As a simplification, one scenario is defined with identical bus initial conditions (positions, velocities) and constant disturbances. The passenger number initial conditions are generated randomly (between 5 – 20 passengers) at each stop. The length of one simulation run is 500 s. The method involved $S = 500$ simulations with randomized (uniformly distributed) initial passenger numbers. Figure 6.6 depicts the sum of passenger numbers waiting at bus stops in the whole network. The red dotted line shows the last order statistics of the scenarios (David and Nagaraja [2004]). The probability of more passengers waiting than the simulated maximum is $\frac{1}{S+1} = 0.2\%$.

Simulation results suggest that after the buses reach their subsequent stop the passengers generated as the initial condition are taken and the periodicity is recovered. Remark: as there are no constraints on the passenger numbers, feasible (but high cost) solution will always be found regardless of the initial conditions.

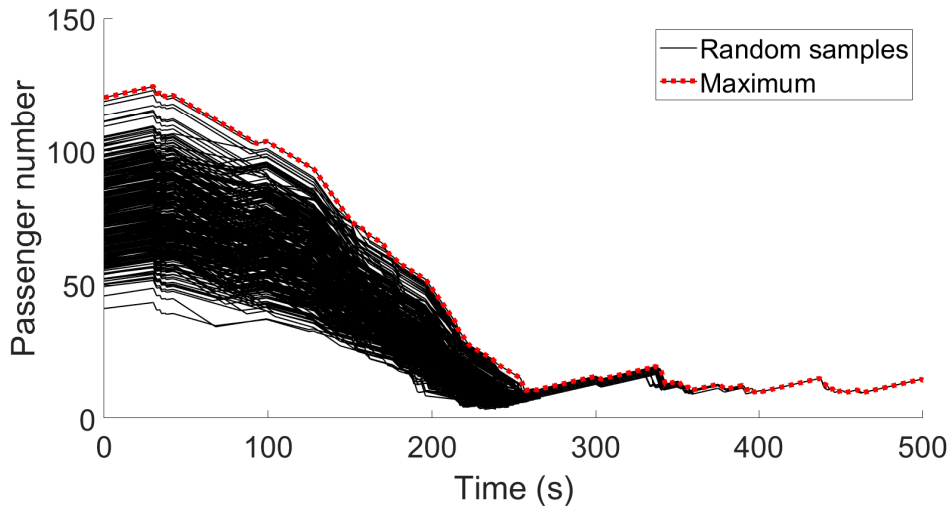


Figure 6.6: Sum of accumulated passengers at every stop for every scenario

6.2.2.2 Set theory

In this section the aim is to characterize the feasibility region of the MPC algorithm and analyze how its shape and size are changing when explicit constraints are prescribed

for the maximal allowed passenger number. The approach is based on computing the explicit solution of the MPC problem in Eq. (6.6).

Definition 1. *The explicit MPC (EMPC) computes the optimal control action offline as an “explicit” function of the state and reference vectors, so that online operations reduce to a simple function evaluation. Such a function is piecewise affine in most cases, so that the MPC controller maps into a lookup table of linear gains (Alessio and Bemporad [2009]).*

The existence of an explicit MPC controller can guarantee feasibility of the system. Since the computation of the EMPC (especially for hybrid systems) is NP-hard (Borrelli [2003]) and therefore the available methods (Herceg et al. [2013]) works only for systems of moderate size. Therefore, this analysis step is performed on a simplified (3 buses, 2 stops) network model.

As the first step, the mixed integer problem is be rewritten into a Piecewise-affine (PWA) system by separating Eq. (2.22) into different subsystems, depending on which binary state $\xi_i(k)$ is 1. Not only the state equations shall be separated but constraints too: when a bus is performing passenger exchange, it shall be stationary at the stop, therefore when a given affine system is active, the respective constraint shall be chosen too.

Then, the EMPC is designed for the bus network, considering the same constraints as the original controller. When formulating the EMPC controller the reference signals for the buses are set to the end of the network. This way, when testing the system in closed-loop the control input is other than zero. The goal of the set based analysis is to check which regions of the state space yield feasible solution. If the EMPC cannot cover a partition of the state space, that means the solution is infeasible. To this end, a hypercube \mathcal{X} is defined bounding the valid system states (i.e. velocities from 0 to 13.5 m/s, bus positions from 0 to 2500 m and passenger number from 0 to 50 passengers per stop). Then, the intersection of the hypercube and the EMPC controller is calculated. If the intersection is equal to the initial polytope, the original MPC controller can cover the whole relevant state space. The steps of this analysis is summarized below.

Results show that there are no infeasible solutions. As a next step, two extra constraints are introduced to the system that may cause infeasibility: the maximum allowed number of passengers is constrained. If the number of allowed passengers at the stop is small, there may be bus states where buses cannot reach the stop before the stop overflows with passengers. Figure 6.7 depicts the projection of the EMPC controller’s polyhedron to the to the state plane of the first bus ($[v_1, x_1]$). According to the figure, there exist feasible solution from every system state combination. On the other hand, when constraining the maximum allowed passengers strictly to 2 passengers per stop (Figure 6.8), the resulting EMPC controller yields feasible solution on a smaller set.

Algorithm 1: Feasibility analysis with EMPC

Define: \mathcal{X} as a polytope of relevant states.

Compute an EMPC for Eq. (2.22).

Define: \mathcal{E} as the feasibility domain of the EMPC.

$\mathcal{J} = \mathcal{X} \cap \mathcal{E}$.

if $\mathcal{E} \setminus \mathcal{J} = \emptyset$ **then**

there are no infeasible states.

else

There are infeasible states.

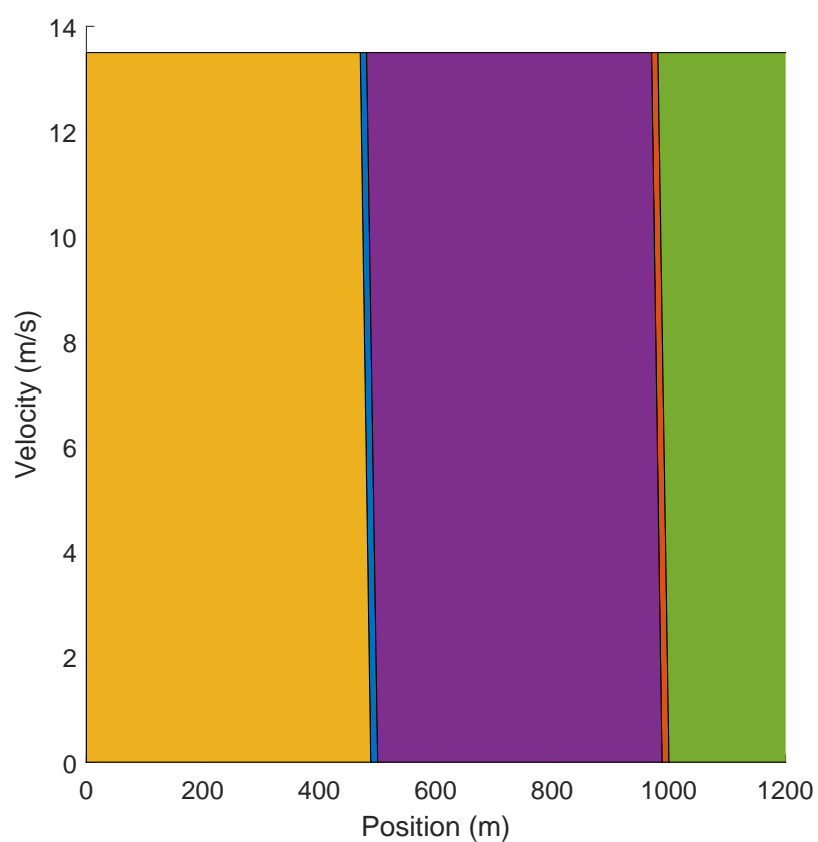


Figure 6.7: EMPC projection to the state plane of the 1st bus with 12 passengers limit at stops

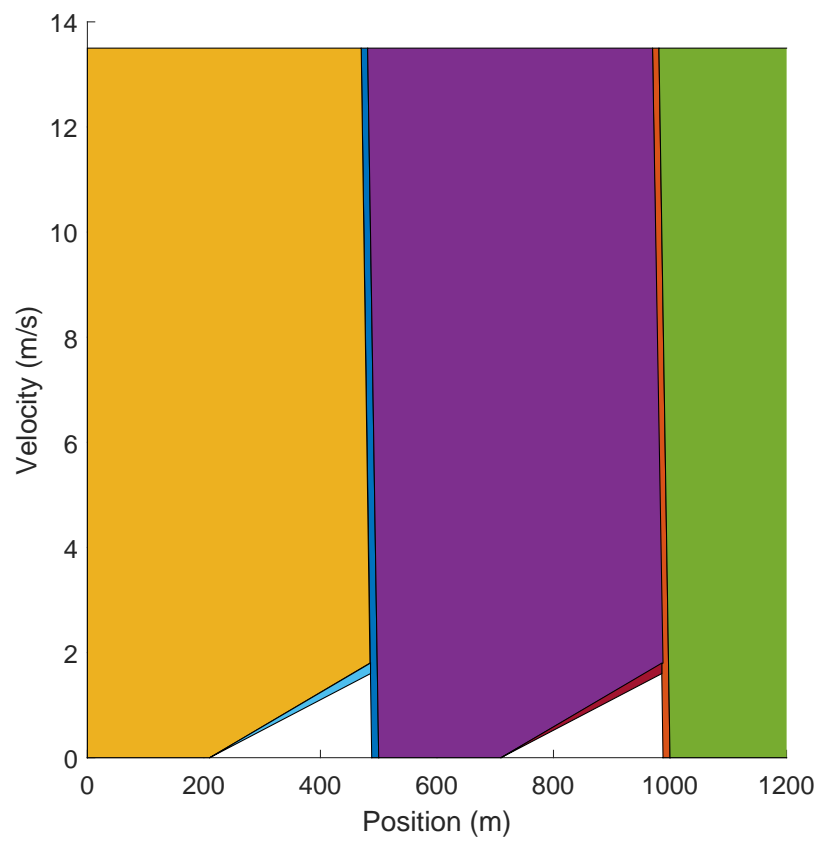


Figure 6.8: EMPC projection to the state plane of the 1st bus with 2 passengers limit at stops

6.2.3 Comparison to the decentralized model

To compare the performance of the centralized network MPC to the decentralized strategy, the balanced control (control strategy c) from Chapter 4 is used as benchmark. It is an adequate choice, since it is already compared to other benchmark strategies and the weighting strategy is similar: timetable and headway adherence is equally costed. Contrarily, passenger waiting time and the interconnection of buses are incorporated into the network model too.

The public transport line used in this experiment is the Göteborg network (Appendix A.1) with and without the 10 minute service perturbation. This network was chosen, since it is interesting to see how a centralized controller can diminish congestion on the public transport line.

Due to the high dimension of the network model ($M_B = 20$ and $M_S = 6$), the horizon length had to be chosen $N = 2$ in order for the optimization to run in tolerable time.

The results of the traffic simulation without perturbation is shown in Figure 6.9. The realized trajectories are similar between the stops, the main difference is at the stops. Buses with the network control arrive at stops earlier. This can be due to the passenger wait time minimization objective. Figure 6.10 depicts the case when the traffic is jammed for 10 minutes. According to the figure, the congestion can be dissipated 17% faster with the centralized controller compared to the decentralized balanced control.

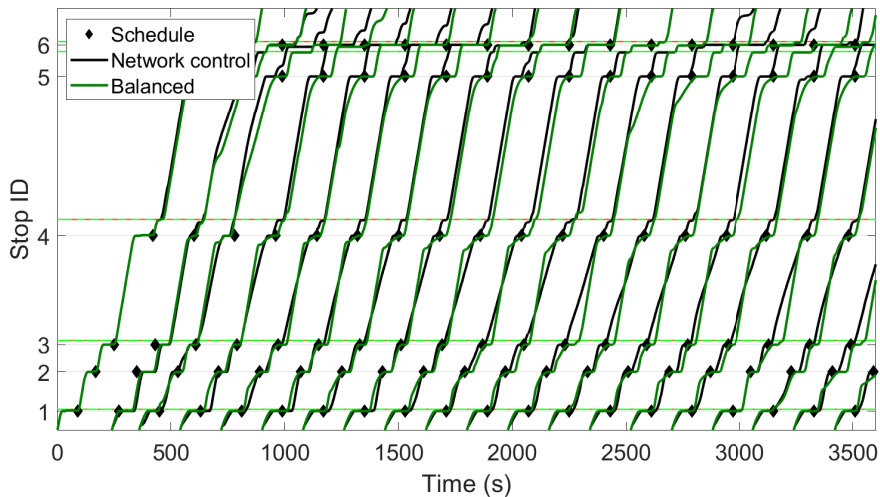


Figure 6.9: Trajectories of consecutive buses with centralized and decentralized control

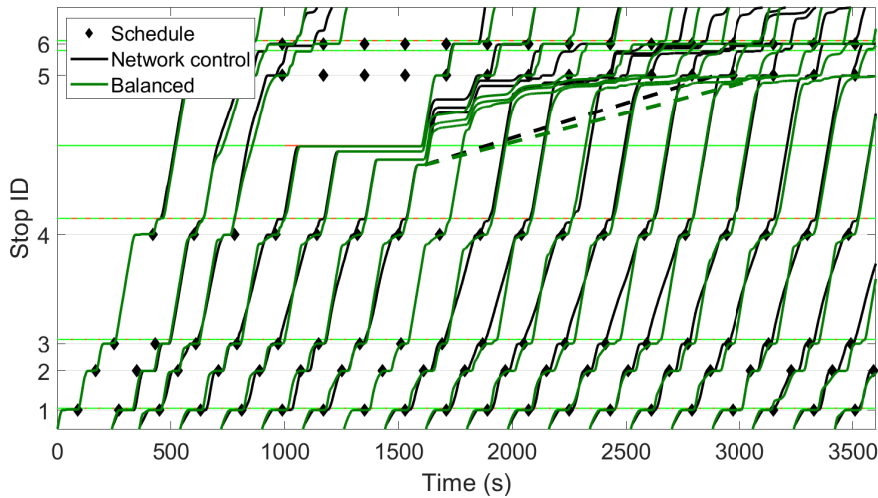


Figure 6.10: Trajectories of consecutive buses with centralized and decentralized control with service perturbation

6.2.4 Computational demand

This section compares the computational demand of the proposed public transport velocity control algorithms proposed in Chapter 4, Chapter 5 and Chapter 6.

The computational complexity of the proposed decentralized algorithms are vital, since they are supposed to run online, on-board the vehicles. Although on-board computation units have their own limitations in this regard, dedicated embedded hardware can perform much faster calculations compared to Matlab simulation. The aim is solving the problem real-time, under the discrete step time Δt . Simulation results suggest that (depending on the complexity of the problem) it can be selected between 0.5 – 2.5 s. Note that, the step time shall be smaller than the relaxation term τ in the bus dynamics model. That is, to avoid instability of the dynamic system. If $\Delta t = \tau$, the bus reacts instantly to the desired velocity v_{des} , i.e. dynamics disappear. To avoid too long horizons it is possible to adjust the step time of the controller dynamically, based on the distance from the next stop. Due to the varying horizon length N and weighting strategy, computational demand varies too. In addition, the complexity of the problem, i.e. considering non-convex objectives and traffic states call for non-convex solvers.

First, the balanced control is investigated. This control strategy employs a quadratic cost function and linear constraints. It was proven in Section 4.2.1.2 that this problem is convex. Therefore, quadratic solvers can efficiently solve this optimization even for several prediction steps ahead (Figure 6.11). Assuming $\Delta t = 1$ s, with the balanced control strategy, the trajectory can be planned ahead for two minutes. If the two non-smooth objectives (energy consumption and passenger wait) are introduced, the problem turns into a mixed-integer quadratic program (MIQP). It can be efficiently solved by existing solvers (e.g. Nocedal and Wright [2006], Gurobi [2014]). The optimization is based on sequential quadratic programming (SQP). It is an iterative procedure which that boils down the nonlinearity into repetitive sequence of quadratic

approximations by QP, converging to the optimum. According to Figure 6.12, the algorithm can predict one minute ahead in real-time. Next, analyze the timetable tracking control with the traffic light states incorporated. The chance-constraints are relaxed into a finite number of constraints (Section 5.1), however they are not smooth either (the bus is in either of the traffic regions). This is also a MIQP problem. The speed of the optimization is evaluated with increasing prediction horizon length (i.e. increasing number of equations to solve). Since the controller design is based on an NP-hard mixed integer optimization, with increasing prediction horizon the computational demand grows exponentially (Figure 6.13).

Finally, the centralized network level control is analyzed from computational demand point of view. Although this is the most computationally demanding, it does not have to be installed on individual vehicles but can operate in a control center. The network model is also based on a mixed integer quadratic problem. The complexity of the problem, however, grows not only with the prediction length but also with the number of states (i.e. number of buses and stops in the network). The number of integer states in the search space (for $N = 1$ prediction horizon) can be computed as the sum of the following geometric sequence:

$$K_{int} = \sum_{c=0}^{M_B} \binom{M_B}{c} M_S^c. \quad (6.9)$$

In other words, there can be $0 \dots M_B$ stops occupied by any combination of M_S buses. For example, in a 6 bus, 6 bus stop system, assuming every bus $M_B = 6$ can be at every stop $M_S = 6$, Eq. (6.9) gives $K_{int} = 117649$ combinations. Exploiting the network layout (not every bus serves every stop), the number of combinations can be reduced significantly. Figure 6.14 presents the computational demand of the network model. Results suggest that the centralized control is only feasible for small networks.

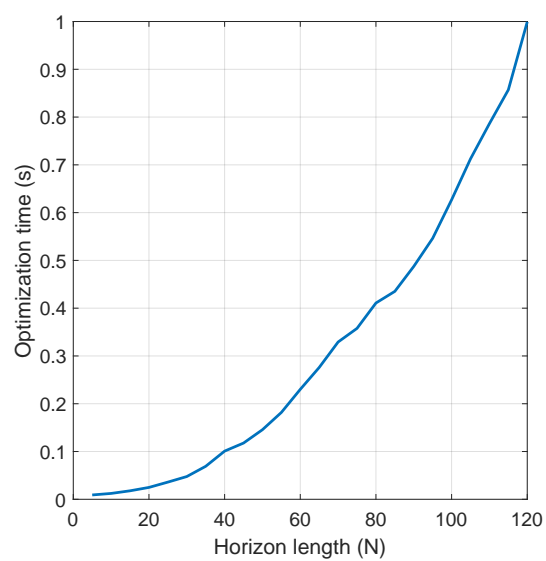


Figure 6.11: Optimization time - convex, balanced control

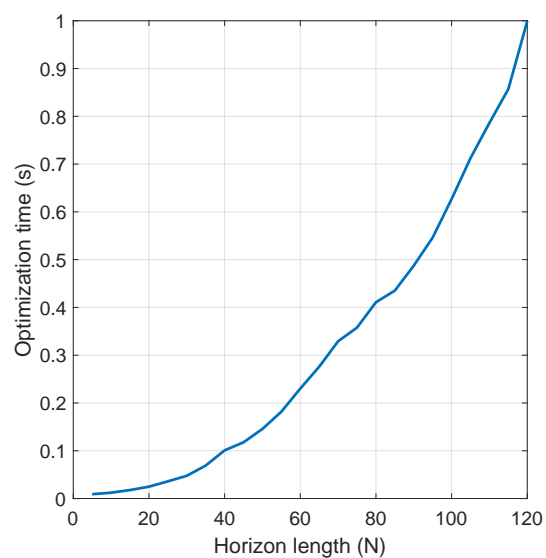


Figure 6.12: Optimization time - non-convex, timetable, headway, passenger wait and energy aware control

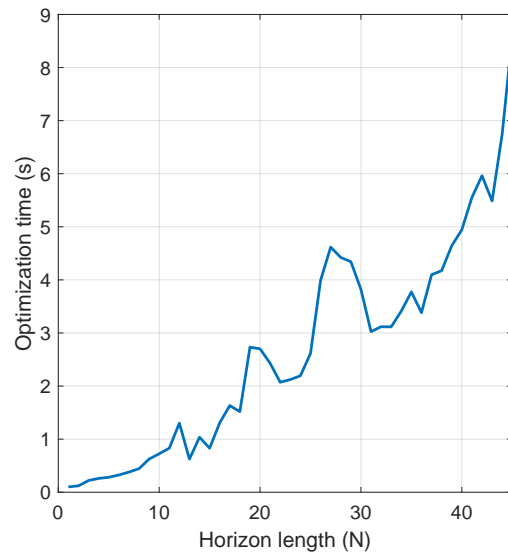


Figure 6.13: Optimization time - non-convex, traffic aware control

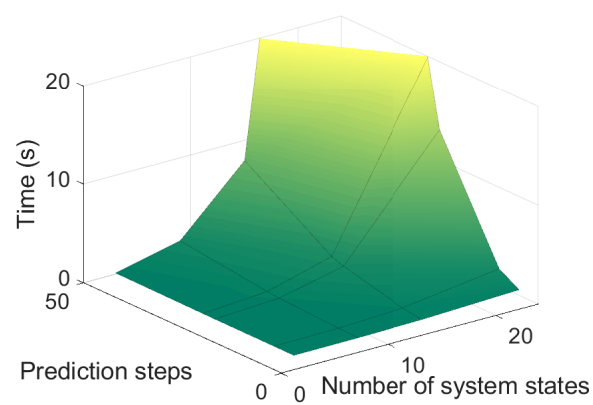


Figure 6.14: Optimization time - centralized control

Thesis 5

Methods for feasibility analysis of large-scale bus networks have been investigated. A centralized rolling horizon algorithm was formulated and analyzed for controlling the vehicles in a public transport network. The subsystems describing individual buses and stops can be rewritten into a single piecewise-affine system. The performance and feasibility of the bus network was analyzed with Monte Carlo simulation and set theory.

Instead of running control algorithms on individual buses, a centralized controller was formulated which calculates the velocity profile for every bus in the network simultaneously. The network model is a high dimensional piecewise affine system. Compared to the decentralized model it does not have a terminal set, as the “next bus stop” cannot be interpreted on a network level. To this end, the horizon length N was chosen as large as computational capacity permitted.

The centralized controller was compared to the decentralized approach too. Due to computational limitations, prediction can only be made for a few steps ahead, curbing the advantages of the look-ahead control. In terms of performance, it is on par with the balanced control. According to simulations, buses with the centralized control arrived at stops earlier due to the cost on passenger waiting time. In addition, when the flow of traffic was disrupted, public transport service can be recovered 17% faster with the centralized controller.

Analysis of such a high dimensional piecewise affine system is not well established. In this chapter the system was analyzed with two techniques: random simulations and set theory. The random simulations gave a probabilistic measure on the upper bound of the total passengers waiting at stops at a network. Simulation results suggest that passenger wait times converge to an equilibrium regardless of initial system state. The set theory approach attempted to search infeasible control regions via creating an EMPC controller. Results suggest that the EMPC can cover the polytope of relevant system states, thus there exist a feasible solution for network control from every initial state.

Related publications:

An algorithm to merge and split buses in a headway optimal way was proposed in [Varga et al. \[2018a\]](#). The bus network control model and its analysis were published in [Varga et al. \[2020a\]](#).

Chapter 7

Conclusions and future work

7.1 Conclusions

This dissertation proposed novel, model predictive velocity control methods for autonomous or highly automated urban public transport networks. The aim was creating a flexible, modular multi-objective optimization framework that can handle different conflicting objectives arising during the operation of public transport service. To this end, first control oriented models of the subsystems of a public transport network were created. For a reference tracking velocity controller the longitudinal model of a single public transport bus with two reference trajectories (headway and timetable tracking) were formulated. A physical based energy consumption model with regenerative braking was incorporated into the model. Then, public transport stops were modeled.

In the same vein, the model of the traffic around public transport vehicles are created. In an urban setting the flow of traffic is mainly characterized by traffic light cycles and uncertain vehicle numbers. To this end, the urban shockwave model, which is an efficient traffic model for links with signalized intersections is augmented with the randomness of vehicle arrivals. The proposed stochastic shockwave profile model can predict queue lengths and traffic flow regions in a stochastic way.

Using the proposed public transport models a decentralized, shrinking horizon multi-objective MPC was created. Shrinking horizon means that buses plan their trajectory up until the next bus stop. Consequently, as its desired arrival time approaches, the horizon length shrinks. This guarantees the stability of the controller too. Four conflicting objectives were addressed in this work: timetable and headway reliability, energy consumption and passenger waiting times. Among the four objectives different control strategies were formulated via weighting the objectives differently. The proposed controllers were compared to well established PI and holding controllers. Simulation results suggest that the proposed controllers outperform the benchmark controllers in service homogeneity, energy consumption and are on par in terms of passenger waiting times.

The proposed velocity controller was further augmented. The detailed stochastic shockwave profile model was incorporated into the optimization as chance-constraints. Thus, an eco-cruise control for urban public transport buses was obtained. The algorithm is capable of making buses avoid being stuck in queues at signalized intersections

with a preset probability, defined with the help of the sampling and discarding technique. The eco-cruise control further improves energy efficiency of public transport.

Finally, the control oriented models can be combined into a single, loosely coupled piecewise affine public transport network model. By building on this, a centralized MPC was created. The centralized MPC performs similarly to the decentralized strategies, however with a much higher computational cost.

7.2 Future work

There are multiple research directions that seem interesting for future research. The proposed stochastic shockwave profile can be extended to a whole network with signalized intersections. Considering joint probabilities emerging from the interconnection of traffic links can lead to more accurate queue length descriptions. Some limitations, such as queue spillover or gridlock shall also be further studied. In addition, benchmarking the SSPM network model against other traffic models (e.g. store-and-forward) is a logical next step.

The analysis of the centralized public transport network control is difficult to analyze due to its high dimension and non-convex nature. Analysis of such a high dimensional piecewise affine system is not well established. Reformulating the model in such a way it is better suited for analysis could lead to new conclusions on the stability of public transport networks.

The thesis has some assumptions regarding the behavior of passengers (i.e. always boarding the first bus). In addition, the occupancy of buses, the total travel time of passengers, and ride comfort are not considered in the optimization. The further assumptions could be further relaxed in the modeling step.

7.3 Implementation related questions

Implementation and evaluation of the proposed velocity control algorithms is also an interesting topic. The limitations are more related to technical and organizational difficulties rather than algorithmic. The computational demand of the algorithm can be tuned by adjusting the sampling interval of the MPC controller. In addition, the control is formulated in a modular way; unnecessary objectives can be removed, or even new ones can be added.

From practical engineering and operational perspectives, implementing a speed advisory system on buses is much cheaper and easier (an extra on-board unit) than modifying traffic controllers. Traffic controllers are often rigid, protected from any manipulation by its manufacturer, and also have to comply with strict regulations. On the other hand, the on-board unit of buses is often closed, and proprietary algorithms cannot be run. The reliability of bus-to-bus communication is also a question to be further investigated. The decentralized control is more flexible and better scalable. Service providers are often against centralization too. Merging smart traffic responsive signal control with the speed control can be problematic on an organizational level. Signalization is looked after by traffic managers while a different operator runs pub-

lic transport. They need to work together with both operators to consolidate speed control and adaptive signals.

Appendix A

Example networks

Road traffic simulation is commonly used in practice to assist design and validation of newly developed control strategies. The control algorithms are tested with the help of a high fidelity microscopic traffic simulator VISSIM too (PTV [2011]). VISSIM is based on the so-called psycho-physical driver behavior model (Wiedemann [1974]). In this appendix, two realistic networks are introduced. For the analysis of service recovery in case of a major disruption, the route of Gothenburg’s trunk bus line 16 between Lindholmen and Brunnsparcken is modeled. For energy efficiency analysis and testing the eco-cruise control, a section of Budapest’s bus line 7 is modeled. Controlled vehicles are driven by the proposed trajectory planning algorithms (via external programming (Tettamanti and Varga [2012])) while the dynamics of external traffic and signal program are determined by the simulator.

A.1 Gothenburg network

The route of Gothenburg’s trunk bus line 16 between Lindholmen and Brunnsparcken is modeled, see Figure A.1. The route is 4.3 kilometers long and includes six public transport stops. Between Lindholmen and Pumpgatan the line travels on a dedicated lane, then enters mixed traffic towards Frihamnporten. On Götaälvbron it shares tracks with other public transport lines crossing the bridge (e.g. tram lines 5 and 6). Nordstan and Brunnsparcken stops are also shared with other lines. Buses have priority at signalized intersections, shown in Figure A.1. The legal speed limit is 50 km/h on the whole route. The time headway of the buses is 3 minutes. The passenger boarding and alighting volumes during peak hours at each stop is shown in Table A.1. Furthermore, Table A.1 summarizes the total number of on-board passengers (in passenger per hour - not for individual vehicles) is summarized after each stop. In addition, the departure times from each stop is presented starting from Lindholmen stop at 0 seconds (repeating every 3 minutes).

The proposed vehicle to transport passengers on this route is a 18.75 meters long, articulated bus. The passenger capacity is approximately 4 passengers per square-meter resulting in 135 persons passenger capacity. The ratio of standees and sitting passengers is not addressed.

During the simulations two types of disturbances are distinguished. (1) Minor disturbances coming from traffic lights, other vehicles and dwell time fluctuation. (2) In order to investigate the control system under major disturbance, traffic flow is perturbed, vehicles are stopped in the middle of Göta älvbron for ten minutes (i.e. opening the bridge). The simulator is capable of generating random boarding and alighting times, serving as an additional disturbance to the system.

A.2 Budapest network

A busy arterial in Budapest's XI^{th} district serves as the basis of the analysis (Figure A.2). A 3 km long section of trunk bus line 7 is modeled, including 7 stops. In this area there is no dedicated lane, the bus travels in a mixed traffic environment along the route but there are two lanes so it can be overtaken. It is assumed that buses have priority at signalized intersections and the legal speed limit is 50 km/h. The time headway of the buses is 3 min. Table A.2 presents the hourly passenger demand at each stop and the scheduled departure times. Traffic signal program is modeled in detail between the two last stops (Figure A.3). There are three traffic lights between the stops with fixed-time signal program. The signal timings and traffic flow rates upstream each traffic light is summarized in Table A.3 The modeled buses have the same properties as in Section A.1.

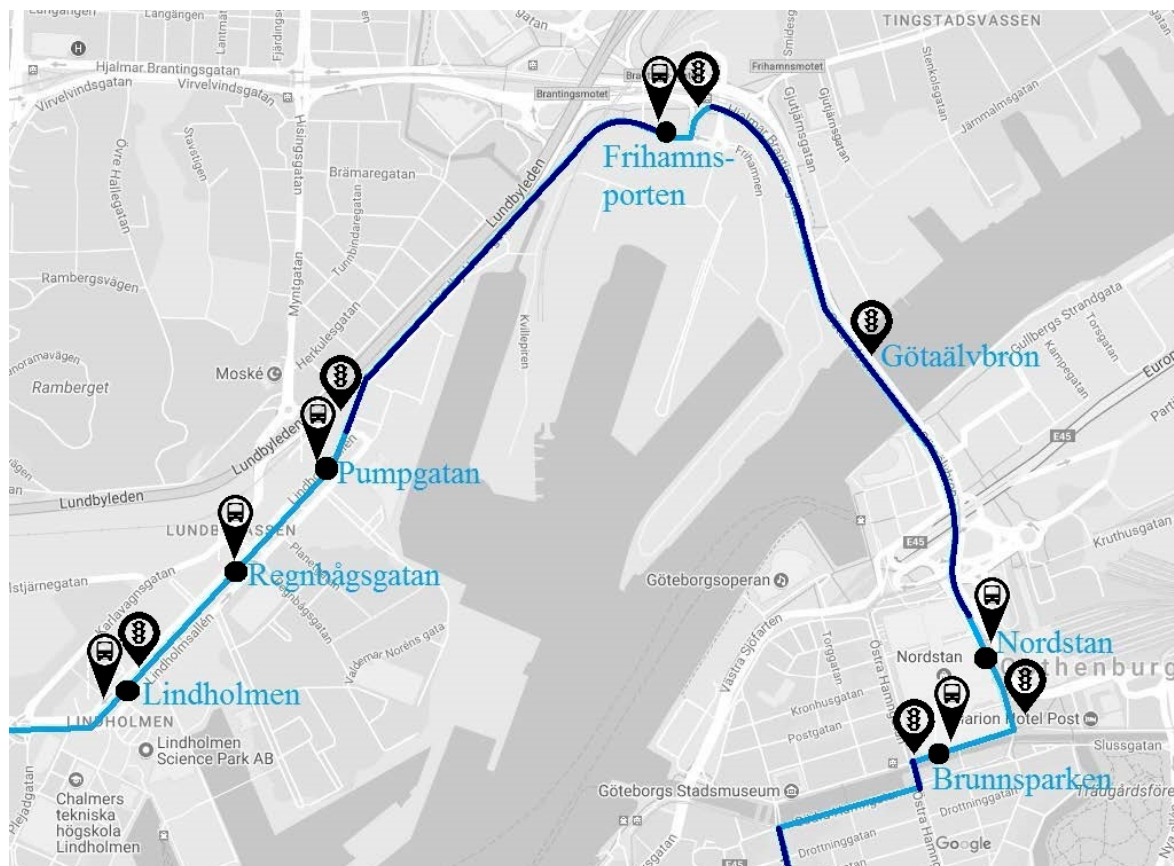


Figure A.1: Modeled route section: Gothenburg, Line 16. Dots mark stops and semaphore pictograms indicate traffic lights. The route in darker shade of blue represents mixed traffic (i.e. lack of dedicated bus lane). (GPS coordinates: 57.711 N, 11.944 E; source: Google maps)

Table A.1: Number of boarding and alighting passengers at each stop (passengers/hour), scheduled departure time (seconds)

	Boarding	Alighting	On-board	Schedule (s)
Lindholmen	1500	0	1500	0
Regnbågsgatan	600	75	2025	80
Pumpgatan	400	200	2225	160
Frihamnsporten	200	25	2400	330
Nordstan	400	600	2200	540
Brunnsparcken	1500	1300	2400	720

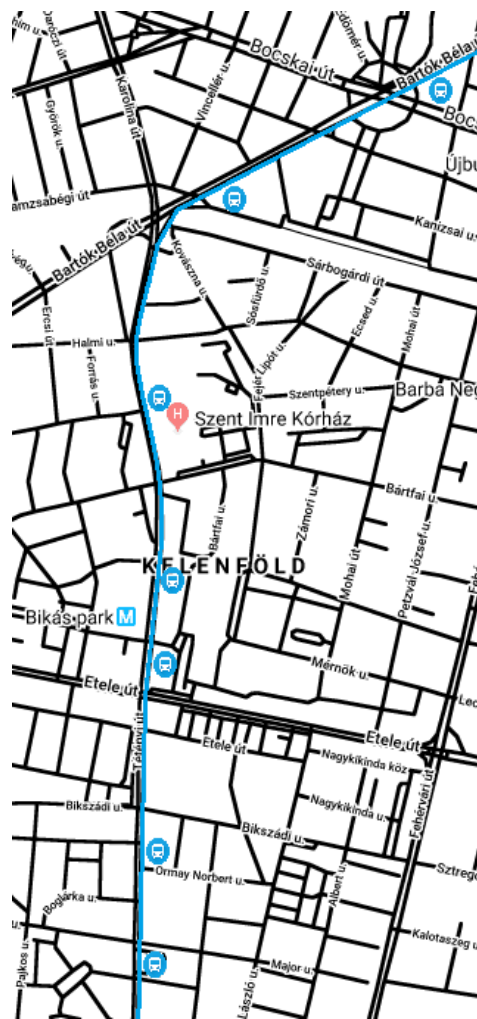


Figure A.2: Modeled real-world section (GPS coordinates: 47.465 N, 19.034 E; source: OpenStreetMap)

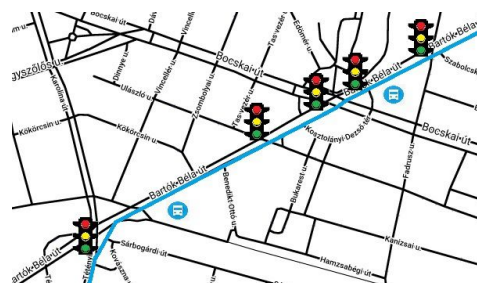


Figure A.3: Detailed route section of Figure A.2 with traffic lights; source: OpenStreetMap)

Table A.2: Bus arrival times (with entry to the network being 0, in seconds) and passenger demand at each stop (passengers/hour)

Stop ID	Location (m)	Scheduled arrival (s)	Boarding volume ($pass / h$)
Bornemissza tér	174	25	50
Puskás Tivadar utca	402	75	50
Bikás park M	829	160	300
Tétényi út 30.	1065	200	50
Szent Imre Kórház	1265	240	50
Karolina út	1887	325	300
Kosztolányi Dezső tér	2474	415	100

Table A.3: Signal program and mean traffic flow upstream each traffic light.

Light ID	Location (m)	Cycle time (s)	Green time (s)	Switch time (s)	Mean arrival rate (veh/h)
#1	2163	60	40	40	1000
#2	2313	60	20	45	900
#3	2407	60	40	10	1000

Appendix B

Benchmark control strategies

The proposed control algorithms are compared to each other and to control strategies found in the literature. Two commonly used bus bunching remedies are selected for comparative analysis: bus holding and PI velocity control.

Holding: Buses have no velocity control but they are held at stops until their scheduled departure time. The holding strategy is greedy, as vehicles try to get to the next stop as fast as possible (Wu et al. [2017]).

PI control: The PI (Proportional-Integral) controller uses the two reference trajectories proposed in Section 2.2 but does not predict the desired trajectory as the MPC, only considers the actual timetable and headway tracking errors $z_1(k)$ and $z_2(k)$ respectively. The control input for the PI controller is calculated as follows:

$$v_{des,PI}(k) = P_{des} \cdot z_1(k) + I_{des} \cdot \sum_0^k z_1(k) + P_{ref} \cdot z_2(k) + I_{ref} \cdot \sum_0^k z_2(k), \quad (\text{B.1})$$

with $P_{des} = 0.025$, $I_{des} = 0.001$, $P_{ref} = 0.025$, $I_{ref} = 0.001$ being tuning parameters for the PI controller with a balanced strategy. The controller was tuned using the Ziegler-Nichols method and also augmented with anti-windup due to the limitation of v_{des} (Skogestad and Postlethwaite [2005]). The control algorithm resembles the one proposed in Sirmatel and Geroliminis [2018].

References

- [Aboudolas et al.(2009)] Konstantinos Aboudolas, Markos Papageorgiou, and E Kosmatopoulos. Store-and-forward based methods for the signal control problem in large-scale congested urban road networks. *Transportation Research Part C: Emerging Technologies*, 17(2):163–174, 2009. doi: 10.1016/j.trc.2008.10.002.
- [Akhegaonkar et al.(2018)] Sagar Akhegaonkar, Lydie Nouveliere, Sébastien Glaser, and Frédéric Holzmann. Smart and green ACC: energy and safety optimization strategies for EVs. *IEEE Transactions on Systems, Man, and Cybernetics: Systems*, 48(1):142–153, 2018. doi: 10.1109/TSMC.2016.2600273.
- [Alessio and Bemporad(2009)] Alessandro Alessio and Alberto Bemporad. A survey on explicit model predictive control. In *Nonlinear Model Predictive Control*, pages 345–369. Springer Berlin Heidelberg, 2009. doi: 10.1007/978-3-642-01094-1_29.
- [Amini(2018)] M. Hadi Amini. A panorama of interdependent power systems and electrified transportation networks. In *Studies in Systems, Decision and Control*, pages 23–41. Springer International Publishing, dec 2018. doi: 10.1007/978-3-319-98923-5_2.
- [Ampountolas and Kring(2015)] K. Ampountolas and M. Kring. Mitigating bunching with bus-following models and bus-to-bus cooperation. In *IEEE 18th International Conference on Intelligent Transportation Systems (ITSC)*, pages 60–65, 15 - 18 September, 2015, Las Palmas, Spain, 2015.
- [Andres and Nair(2017)] Matthias Andres and Rahul Nair. A predictive-control framework to address bus bunching. *Transportation Research Part B: Methodological*, 104:123–148, 2017.
- [Ap. Sorratini et al.(2008)] José Ap. Sorratini, Ronghui Liu, and Shalini Sinha. Assessing bus transport reliability using micro-simulation. *Transportation Planning and Technology*, 31(3):303–324, 2008.
- [Arnold(2013)] Ludwig Arnold. *Random dynamical systems*. Springer Science & Business Media, 2013. ISBN 9783642083556. doi: 10.1007/978-3-662-12878-7.
- [Bando et al.(1995)] M. Bando, K. Hasebe, A. Nakayama, A. Shibata, and Y. Sugiyamai. Dynamical model of traffic congestion and numerical simulation. *Physical review E*, 51(2):1035–1043, 1995.

- [Barth and Boriboonsomsin(2009)] Matthew Barth and Kanok Boriboonsomsin. Energy and emissions impacts of a freeway-based dynamic eco-driving system. *Transportation Research Part D: Transport and Environment*, 14(6):400–410, 2009. doi: 10.1016/j.trd.2009.01.004.
- [Bartholdi and Eisenstein(2012)] J. J. Bartholdi and D. D. Eisenstein. A self-coordinating bus route to resist bus bunching. *Transportation Research Part B: Methodological*, 46(4):481–491, 2012.
- [Bi et al.(2015)] Zicheng Bi, Lingjun Song, Robert De Kleine, Chunting Chris Mi, and Gregory A Keoleian. Plug-in vs. wireless charging: Life cycle energy and greenhouse gas emissions for an electric bus system. *Applied Energy*, 146:11–19, 2015. doi: 10.1016/j.apenergy.2015.02.031.
- [Borrelli(2003)] Francesco Borrelli. *Constrained Optimal Control of Linear and Hybrid Systems*. Springer Berlin Heidelberg, 2003. ISBN 354000257X. URL https://www.ebook.de/de/product/6699691/francesco_borrelli_constrained_optimal_control_of_linear_and_hybrid_systems.html.
- [Bryson et al.(1979)] Arthur E Bryson, Yu-Chi Ho, and George M Siouris. Applied optimal control: Optimization, estimation, and control. *IEEE Transactions on Systems, Man, and Cybernetics*, 9(6):366–367, 1979.
- [Campi and Calafiore(2009)] Marco C. Campi and Giuseppe C. Calafiore. Notes on the scenario design approach. *IEEE Transactions on Automatic Control*, 54(2):382–385, feb 2009. doi: 10.1109/tac.2008.2008335.
- [Campi and Garatti(2011)] Marco C Campi and Simone Garatti. A sampling-and-discarding approach to chance-constrained optimization: feasibility and optimality. *Journal of Optimization Theory and Applications*, 148(2):257–280, 2011. doi: 10.1007/s10957-010-9754-.
- [Campi et al.(2009)] Marco C. Campi, Simone Garatti, and Maria Prandini. The scenario approach for systems and control design. *Annual Reviews in Control*, 33(2):149–157, dec 2009.
- [Cats et al.(2012)] Oded Cats, Anahid Larijani, Ásdís Ólafsdóttir, Wilco Burghout, Ingmar Andreasson, and Haris Koutsopoulos. Bus-holding control strategies: simulation-based evaluation and guidelines for implementation. *Transportation Research Record: Journal of the Transportation Research Board*, (2274):100–108, 2012.
- [Chiabaut et al.(2009)] Nicolas Chiabaut, Christine Buisson, and Ludovic Leclercq. Fundamental diagram estimation through passing rate measurements in congestion. *IEEE Transactions on Intelligent Transportation Systems*, 10(2):355–359, 2009. doi: 10.1109/TITS.2009.2018963.
- [Chow et al.(2017)] Andy HF Chow, Shuai Li, and Renxin Zhong. Multi-objective optimal control formulations for bus service reliability with traffic signals. *Transportation Research Part B: Methodological*, 103:248–268, 2017. doi: 10.1016/j.trb.2017.02.006.

-
- [Comert and Cetin(2009)] Gurcan Comert and Mecit Cetin. Queue length estimation from probe vehicle location and the impacts of sample size. *European Journal of Operational Research*, 197(1):196–202, 2009. doi: 10.1016/j.ejor.2008.06.024.
- [Daganzo(2009)] C. F. Daganzo. A headway-based approach to eliminate bus bunching: Systematic analysis and comparisons. *Transportation Research Part B: Methodological*, 43(10):913–921, 2009. doi: 10.1016/j.trb.2009.04.002.
- [Daganzo and Geroliminis(2008)] Carlos F Daganzo and Nikolas Geroliminis. An analytical approximation for the macroscopic fundamental diagram of urban traffic. *Transportation Research Part B: Methodological*, 42(9):771–781, 2008.
- [Daganzo and Lehe(2016)] Carlos F Daganzo and Lewis J Lehe. Traffic flow on signalized streets. *Transportation Research Part B: Methodological*, 90:56–69, 2016. doi: 10.1016/j.trb.2016.03.010.
- [Daganzo and Pilachowski(2011)] Carlos F Daganzo and Josh Pilachowski. Reducing bunching with bus-to-bus cooperation. *Transportation Research Part B: Methodological*, 45(1):267–277, 2011.
- [Darroch(1964)] JN Darroch. On the traffic-light queue. *The Annals of Mathematical Statistics*, 35(1):380–388, 1964. doi: 10.1214/aoms/1177703761.
- [David and Nagaraja(2004)] Herbert Aron David and Haikady Navada Nagaraja. *Order Statistics*. Wiley, 2004.
- [de Oliveira and Camponogara(2010)] L.B. de Oliveira and E. Camponogara. Multi-agent model predictive control of signaling split in urban traffic networks. *Transportation Research Part C: Emerging Technologies*, 18(1):120–139, 2010. doi: 10.1016/j.trc.2009.04.022. Information/Communication Technologies and Travel Behaviour; Agents in Traffic and Transportation.
- [Desreuveaux et al.(2019)] Anatole Desreuveaux, Alain Bouscayrol, Rochdi Trigui, Elodie Castex, and John Klein. Impact of the velocity profile on energy consumption of electric vehicles. *IEEE Transactions on Vehicular Technology*, 68(12):11420–11426, dec 2019. doi: 10.1109/tvt.2019.2949215.
- [Dessouky et al.(2003)] M. Dessouky, R. Hall, L. Zhang, and A. Singh. Real-time control of buses for schedule coordination at a terminal. *Transportation Research Part A: Policy and Practice*, 37(2):145–164, 2003.
- [Estrada et al.(2016)] Miquel Estrada, Josep Mensión, Josep M Aymamí, and Laura Torres. Bus control strategies in corridors with signalized intersections. *Transportation Research Part C: Emerging Technologies*, 71:500–520, 2016.
- [Fathy and Siyal(1998)] M Fathy and MY Siyal. A window-based image processing technique for quantitative and qualitative analysis of road traffic parameters. *IEEE Transactions on Vehicular Technology*, 47(4):1342–1349, 1998. doi: 10.1109/25.728525.

-
- [Fonzone et al.(2015)] A. Fonzone, J. D. Schmöcker, and R. Liu. A model of bus bunching under reliability-based passenger arrival patterns. *Transportation Research Procedia*, 7:276–299, 2015.
- [Gallet et al.(2018)] Marc Gallet, Tobias Massier, and Thomas Hamacher. Estimation of the energy demand of electric buses based on real-world data for large-scale public transport networks. *Applied energy*, 230:344–356, 2018. doi: 10.1016/j.apenergy.2018.08.086.
- [Garcia-Bunster and Torres-Torriti(2009)] Guillermo Garcia-Bunster and Miguel Torres-Torriti. A density-based approach for effective pedestrian counting at bus stops. In *IEEE International Conference on Systems Man and Cybernetics*, pages 3434–3439. IEEE, 2009.
- [Gu et al.(2013)] Weihua Gu, Michael J Cassidy, Vikash V Gayah, and Yanfeng Ouyang. Mitigating negative impacts of near-side bus stops on cars. *Transportation Research Part B: Methodological*, 47:42–56, 2013. doi: 10.1016/j.trb.2012.09.005.
- [Gurobi(2014)] Gurobi. Gurobi optimizer reference manual, 2014.
- [Guzzella et al.(2013)] Lino Guzzella, Antonio Sciarretta, et al. *Vehicle propulsion systems*. Vol. 3, Springer-Verlag Berlin Heidelberg, 2013. ISBN 978-3-642-35913-2. doi: 10.1007/978-3-642-35913-2.
- [Heidemann(1994)] Dirk Heidemann. Queue length and delay distributions at traffic signals. *Transportation Research Part B: Methodological*, 28(5):377–389, 1994. doi: 10.1016/0191-2615(94)90036-1.
- [Helbing and Tilch(1998)] Dirk Helbing and Benno Tilch. Generalized force model of traffic dynamics. *Physical review E*, 58(1):133, 1998. doi: 10.1103/PhysRevE.58.133.
- [Hellström et al.(2010)] E. Hellström, J. Åslund, and L. Nielsen. Design of an efficient algorithm for fuel-optimal look-ahead control. *Control Engineering Practice*, 18(11):1318–1327, 2010. doi: 10.1016/j.conengprac.2009.12.008.
- [Herceg et al.(2013)] Martin Herceg, Michal Kvasnica, Colin N. Jones, and Manfred Morari. Multi-parametric toolbox 3.0. In *2013 European Control Conference (ECC)*. IEEE, jul 2013.
- [Holroyd and Scraggs(1966)] E. M. Holroyd and D. A. Scraggs. *Waiting times for buses in central London*, volume 8. Printerhall, 1966.
- [Hoogendoorn and Bovy(2001)] Serge P Hoogendoorn and Piet HL Bovy. State-of-the-art of vehicular traffic flow modelling. *Proceedings of the Institution of Mechanical Engineers, Part I: Journal of Systems and Control Engineering*, 215(4):283–303, 2001.
- [Horn et al.(1994)] Jeffrey Horn, Nicholas Nafpliotis, and David E Goldberg. A niched pareto genetic algorithm for multiobjective optimization. In *Evolutionary Computation, 1994. IEEE World Congress on Computational Intelligence., Proceedings of the First IEEE Conference on*, pages 82–87. IEEE, 1994.

-
- [Horn and Johnson(1990)] Roger A Horn and Charles R Johnson. *Matrix analysis*. Cambridge university press, 1990.
- [Jiang et al.(2017)] Feng Jiang, Valentina Cacchiani, and Paolo Toth. Train timetabling by skip-stop planning in highly congested lines. *Transportation Research Part B: Methodological*, 104:149–174, 2017.
- [Jolliffe and Hutchinson(1975)] J. K. Jolliffe and T. P. Hutchinson. A behavioural explanation of the association between bus and passenger arrivals at a bus stop. *Transportation Science*, 9(3):248–282, 1975.
- [Karlin(1957)] Samuel Karlin. *A first course in stochastic processes*. Academic Press, 2 edition, 1957. ISBN 978-0-08-057041-9. doi: 10.1016/C2009-1-28569-8.
- [Kenworthy(2019)] Jeffrey Kenworthy. Urban transport and eco-urbanism: A global comparative study of cities with a special focus on five larger swedish urban regions. *Urban Science*, 3(1):25, feb 2019. doi: 10.3390/urbansci3010025.
- [Kesting et al.(2008)] Arne Kesting, Martin Treiber, Martin Schönhof, and Dirk Helbing. Adaptive cruise control design for active congestion avoidance. *Transportation Research Part C: Emerging Technologies*, 16(6):668–683, 2008.
- [Kittelton et al.(2003)] Kittelson, Associates, United States. Federal Transit Administration, Transit Cooperative Research Program, and Transit Development Corporation. *Transit capacity and quality of service manual*, volume 100. Transportation Research Board, 2003.
- [Kivekas et al.(2019)] Klaus Kivekas, Antti Lajunen, Francesco Baldi, Jari Vepsalainen, and Kari Tammi. Reducing the energy consumption of electric buses with design choices and predictive driving. *IEEE Transactions on Vehicular Technology*, 68(12):11409–11419, dec 2019. doi: 10.1109/tvt.2019.2936772.
- [Kullback and Leibler(1951)] Solomon Kullback and Richard A Leibler. On information and sufficiency. *The annals of mathematical statistics*, 22(1):79–86, 1951.
- [Kural et al.(2014a)] Emre Kural, Stephen Jones, Alejandro Ferreira Parrilla, and Anders Grauers. Traffic light assistant system for optimized energy consumption in an electric vehicle. In *2014 International Conference on Connected Vehicles and Expo (IC-CVE)*. IEEE, nov 2014a. doi: 10.1109/iccve.2014.7297619.
- [Kural et al.(2014b)] Emre Kural, Stephen Jones, Alejandro Ferreira Parrilla, and Anders Grauers. Traffic light assistant system for optimized energy consumption in an electric vehicle. In *International Conference on Connected Vehicles and Expo (IC-CVE)*, pages 604–611, 3-7 November, 2014, Vienna, Austria, 2014b. IEEE. doi: 10.1109/ICCVE.2014.7297619.
- [Laskaris et al.(2018)] Georgios Laskaris, Oded Cats, Erik Jenelius, Marco Rinaldi, and Francesco Viti. Multiline holding based control for lines merging to a shared transit corridor. *Transportmetrica B: Transport Dynamics*, 7(1):1062–1095, nov 2018.

- [Laval and Castrillón(2015)] Jorge A Laval and Felipe Castrillón. Stochastic approximations for the macroscopic fundamental diagram of urban networks. *Transportation Research Procedia*, 7:615–630, 2015. doi: 10.1016/j.trpro.2015.06.032.
- [Laval and Leclercq(2010)] Jorge A. Laval and Ludovic Leclercq. A mechanism to describe the formation and propagation of stop-and-go waves in congested freeway traffic. *Philosophical Transactions of the Royal Society A: Mathematical, Physical and Engineering Sciences*, 368(1928):4519–4541, oct 2010. doi: 10.1098/rsta.2010.0138.
- [Li et al.(2018)] Xiaopeng Li, Amir Ghiasi, Zhigang Xu, and Xiaobo Qu. A piecewise trajectory optimization model for connected automated vehicles: Exact optimization algorithm and queue propagation analysis. *Transportation Research Part B: Methodological*, 118:429–456, 2018. doi: 10.1016/j.trb.2018.11.002.
- [Limon et al.(2006)] D. Limon, T. Alamo, F. Salas, and E.F. Camacho. On the stability of constrained MPC without terminal constraint. *IEEE Transactions on Automatic Control*, 51(5):832–836, may 2006. doi: 10.1109/tac.2006.875014.
- [Lin et al.(2010)] Shu Lin, B De Schutter, Yugeng Xi, and H Hellendoorn. Model predictive control for urban traffic networks via MILP. In *Proceedings of the 2010 American Control Conference*. IEEE, jun 2010. doi: 10.1109/acc.2010.5530534.
- [Liu et al.(2009)] Henry X Liu, Xinkai Wu, Wenteng Ma, and Heng Hu. Real-time queue length estimation for congested signalized intersections. *Transportation Research Part C: Emerging Technologies*, 17(4):412–427, 2009. doi: 10.1016/j.trc.2009.02.003.
- [Luethi et al.(2007)] Marco Luethi, Ulrich Weidmann, and Andrew Nash. Passenger arrival rates at public transport stations. In *86th Transportation Research Board Annual Meeting (TRB 2007)*. Institute for Transport Planning and Systems, ETH Zurich, 2007.
- [Lv et al.(2018)] Chen Lv, Yang Xing, Chao Lu, Yahui Liu, Hongyan Guo, Hongbo Gao, and Dongpu Cao. Hybrid-learning-based classification and quantitative inference of driver braking intensity of an electrified vehicle. *IEEE Transactions on Vehicular Technology*, pages 1–1, 2018. doi: 10.1109/tvt.2018.2808359.
- [Lv et al.(2019)] Chen Lv, Xiaosong Hu, Alberto Sangiovanni-Vincentelli, Yutong Li, Clara Marina Martinez, and Dongpu Cao. Driving-style-based codesign optimization of an automated electric vehicle: A cyber-physical system approach. *IEEE Transactions on Industrial Electronics*, 66(4):2965–2975, apr 2019. doi: 10.1109/tie.2018.2850031.
- [Maciejowski(2002)] Jan Marian Maciejowski. *Predictive control: with constraints*. Prentice Hall, Harlow, UK, 1 edition, 2002. ISBN 201-39823-0 PPR.
- [Mandelzys and Hellinga(2010)] Michael Mandelzys and Bruce Hellinga. Identifying causes of performance issues in bus schedule adherence with automatic vehicle location and passenger count data. *Transportation Research Record: Journal of the Transportation Research Board*, (2143):9–15, 2010.

- [Mihály et al.(2018)] András Mihály, Balázs Németh, and Péter Gáspár. Real-time look-ahead cruise control simulator. *Periodica Polytechnica Transportation Engineering*, 46(1):11–16, 2018. doi: 10.3311/PPtr.9896.
- [Mohamed et al.(2017)] Moataz Mohamed, Hany Farag, Nader El-Taweel, and Mark Ferguson. Simulation of electric buses on a full transit network: Operational feasibility and grid impact analysis. *Electric Power Systems Research*, 142:163–175, jan 2017. doi: 10.1016/j.epsr.2016.09.032.
- [Mung et al.(1996)] Gregory KS Mung, Antonio CK Poon, and William HK Lam. Distributions of queue lengths at fixed time traffic signals. *Transportation Research Part B: Methodological*, 30(6):421–439, 1996. doi: 10.1016/0191-2615(96)00009-4.
- [Németh and Gáspár(2011)] B. Németh and P. Gáspár. Road inclinations in the design of lpv-based adaptive cruise control. *IFAC Proceedings Volumes*, 44(1):2202–2207, 2011. doi: 10.3182/20110828-6-IT-1002.00932.
- [Nesheli et al.(2015)] Mahmood Mahmoodi Nesheli, Avishai Avi Ceder, and Tao Liu. A robust, tactic-based, real-time framework for public-transport transfer synchronization. *Transportation Research Procedia*, 9:246–268, 2015.
- [Newell and Potts(1964)] G. F. Newell and R. B. Potts. Maintaining a bus schedule. In *Australian Road Research Board (ARRB) 2nd Conference*, volume 2, 1964, Melbourne, Australia, 1964.
- [Newell(1977)] GF Newell. Unstable brownian motion of a bus trip. In *Statistical Mechanics and Statistical Methods in Theory and Application*, pages 645–667. Springer, 1977.
- [Nocedal and Wright(2006)] Jorge Nocedal and Stephen J Wright. *Numerical optimization*. Springer, 2 edition, 2006. ISBN 978-0-387-30303-1.
- [O’Flaherty and Mangan(1970)] C. A. O’Flaherty and D. O. Mangan. Bus passenger waiting times in greater manchester. *Traffic Engineering and Control*, 11(9):419–421, 1970.
- [Olsson et al.()] Oscar Olsson, Anders Grauers, and Stefan Pettersson. Method to analyze cost effectiveness of different electric bus systems. In *EVS29 International Battery, Hybrid and Fuel Cell Electric Vehicle Symposium*, pages 1–12, 19-22 Montreal, Quebec, Canada.
- [Papageorgiou(1998)] Markos Papageorgiou. Some remarks on macroscopic traffic flow modelling. *Transportation Research Part A: Policy and Practice*, 32(5):323–329, 1998. doi: 10.1016/S0965-8564(97)00048-7.
- [Papamichail et al.(2010)] Ioannis Papamichail, Apostolos Kotsialos, Ioannis Margonis, and Markos Papageorgiou. Coordinated ramp metering for freeway networks – a model-predictive hierarchical control approach. *Transportation Research Part C: Emerging Technologies*, 18(3):311–331, jun 2010. doi: 10.1016/j.trc.2008.11.002.

- [Pariota et al.(2019)] Luigi Pariota, Luca Di Costanzo, Angelo Coppola, Claudio Daniello, and Gennaro Nicola Bifulco. Green light optimal speed advisory: a c-ITS to improve mobility and pollution. In *2019 IEEE International Conference on Environment and Electrical Engineering and 2019 IEEE Industrial and Commercial Power Systems Europe (EEEIC / I&CPS Europe)*, 11-14 June 2019. Genova, Italy, 2019. doi: 10.1109/eeeic.2019.8783573.
- [Park et al.(2011)] Sangjun Park, Hesham Rakha, Kyoungso Ahn, and Kevin Moran. Predictive eco-cruise control: Algorithm and potential benefits. In *IEEE Forum on Integrated and Sustainable Transportation Systems*, pages 394–399, 29 June - 1 July 2011, Vienna, Austria, 2011. IEEE. doi: 10.1109/FISTS.2011.5973639.
- [PTV(2011)] PTV. *VISSIM 5.30-05 User Manual*. PTV, Stumpfstrasse 1, D-76131 Karlsruhe, Germany, 2011.
- [Qu et al.(2017)] Xiaobo Qu, Jin Zhang, and Shuaian Wang. On the stochastic fundamental diagram for freeway traffic: model development, analytical properties, validation, and extensive applications. *Transportation Research Part B: Methodological*, 104: 256–271, 2017. doi: 10.1016/j.trb.2017.07.003.
- [Rajbhandari et al.(2003)] R. Rajbhandari, S. Chien, and J. Daniel. Estimation of bus dwell times with automatic passenger counter information. *Transportation Research Record: Journal of the Transportation Research Board*, (1841):120–127, 2003.
- [Rogge et al.(2015)] Matthias Rogge, Sebastian Wollny, and Dirk Sauer. Fast charging battery buses for the electrification of urban public transport—a feasibility study focusing on charging infrastructure and energy storage requirements. *Energies*, 8(5): 4587–4606, may 2015. doi: 10.3390/en8054587.
- [Rogge et al.(2018)] Matthias Rogge, Evelien van der Hurk, Allan Larsen, and Dirk Uwe Sauer. Electric bus fleet size and mix problem with optimization of charging infrastructure. *Applied Energy*, 211:282–295, 2018. doi: 10.1016/j.apenergy.2017.11.051.
- [Rupp et al.(2019)] Matthias Rupp, Nils Handschuh, Christian Rieke, and Isabel Kuperjans. Contribution of country-specific electricity mix and charging time to environmental impact of battery electric vehicles: A case study of electric buses in germany. *Applied Energy*, 237:618–634, 2019. doi: 10.1016/j.apenergy.2019.01.059.
- [Saerens et al.(2013)] Bart Saerens, Hesham A Rakha, Moritz Diehl, and Eric Van den Bulck. A methodology for assessing eco-cruise control for passenger vehicles. *Transportation Research Part D: Transport and Environment*, 19:20–27, 2013. doi: 10.1016/j.trd.2012.12.001.
- [Schmöcker et al.(2016)] Jan-Dirk Schmöcker, Wenzhe Sun, Achille Fonzone, and Ronghui Liu. Bus bunching along a corridor served by two lines. *Transportation Research Part B: Methodological*, 93:300–317, nov 2016.

- [Seo et al.(2019)] Toru Seo, Yutaka Kawasaki, Takahiko Kusakabe, and Yasuo Asakura. Fundamental diagram estimation by using trajectories of probe vehicles. *Transportation Research Part B: Methodological*, 122:40–56, 2019. doi: 10.1016/j.trb.2019.02.005.
- [Sharma et al.(2007)] Anuj Sharma, Darcy Bullock, and James Bonneson. Input-output and hybrid techniques for real-time prediction of delay and maximum queue length at signalized intersections. *Transportation Research Record: Journal of the Transportation Research Board*, (2035):69–80, 2007. doi: 10.3141/2035-08.
- [Sirmatel and Geroliminis(2018)] Isik Ilber Sirmatel and Nikolas Geroliminis. Hybrid model predictive control of public transport operations. In *18th Swiss Transport Research Conference, May 16-18, 2018, Monte Verita, Ascona, Switzerland*, 2018.
- [Skogestad and Postlethwaite(2005)] S. Skogestad and I. Postlethwaite. *Multivariable Feedback Control: Analysis and Design*. Wiley, 2005.
- [Stephen Boyd(2019)] Lieven Vandenberghe Stephen Boyd. *Convex Optimization*. Cambridge University Press, 2019. ISBN 0521833787.
- [Su et al.(2012)] Wencong Su, Habiballah Eichi, Wenteng Zeng, and Mo-Yuen Chow. A survey on the electrification of transportation in a smart grid environment. *IEEE Transactions on Industrial Informatics*, 8(1):1–10, feb 2012. doi: 10.1109/tii.2011.2172454.
- [Sun et al.(2014)] Lijun Sun, Alejandro Tirachini, Kay W. Axhausen, Alexander Erath, and Der-Hong Lee. Models of bus boarding and alighting dynamics. *Transportation Research Part A: Policy and Practice*, 69:447–460, nov 2014. doi: 10.1016/j.tra.2014.09.007.
- [Tettamanti and Varga(2010)] T. Tettamanti and I. Varga. Distributed traffic control system based on model predictive control. *Periodica Polytechnica ser. Civil Eng.*, 54(1):3–9, 2010. doi: 10.3311/pp.ci.2010-1.01.
- [Tettamanti and Varga(2012)] Tamás Tettamanti and István Varga. Development of road traffic control by using integrated VISSIM-MATLAB simulation environment. *Periodica Polytechnica Civil Engineering*, 56(1):43, 2012. doi: 10.3311/pp.ci.2012-1.05.
- [Tettamanti et al.(2014)] Tamas Tettamanti, Tamas Luszpay, Balazs Kulcsar, Tamas Peni, and Istvan Varga. Robust control for urban road traffic networks. *IEEE Transactions on Intelligent Transportation Systems*, 15(1):385–398, feb 2014. doi: 10.1109/tits.2013.2281666.
- [Tettamanti et al.(2016)] Tamás Tettamanti, István Varga, and Zsolt Szalay. Impacts of autonomous cars from a traffic engineering perspective. *Periodica Polytechnica Transportation Engineering*, 44(4):244–250, 2016. doi: 10.3311/PPtr.9464.
- [Transportation Research Board(2016)] Transportation Research Board. *Highway Capacity Manual: A Guide for Multimodal Mobility Analysis*. The National Academies Press, Washington, D.C, 6 edition, 2016. doi: 10.17226/24798.

- [Van den Berg et al.(2003)] M Van den Berg, A Hegyi, Bart De Schutter, and J Hellendoorn. A macroscopic traffic flow model for integrated control of freeway and urban traffic networks. In *Decision and Control, 2003. Proceedings. 42nd IEEE Conference on*, volume 3, pages 2774–2779. IEEE, 2003.
- [Veldhuizen and Lamont(1998)] D. A. Van Veldhuizen and G. B. Lamont. Evolutionary computation and convergence to a pareto front. In *Genetic Programming*, pages 221–228, 22-25 July, 1998, Madison, WI, USA, 1998.
- [Vreeswijk et al.(2010)] Jacob Dirk Vreeswijk, MKM Mahmod, and Bart van Arem. Energy efficient traffic management and control-the eCoMove approach and expected benefits. In *13th International IEEE Conference on Intelligent Transportation Systems*, pages 955–961, 19-22 September 2010, Funchal, Portugal, 2010. IEEE. doi: 10.1109/ITSC.2010.5625122.
- [Wiedemann(1974)] R. Wiedemann. Simulation des Straßenverkehrsflusses. *Schriftenreihe des Instituts für Verkehrswesen der Universität Karlsruhe*, 8, 1974.
- [Wu et al.(2017)] Weitiao Wu, Ronghui Liu, and Wenzhou Jin. Modelling bus bunching and holding control with vehicle overtaking and distributed passenger boarding behaviour. *Transportation Research Part B: Methodological*, 104:175–197, 2017.
- [Wu and Liu(2011)] Xinkai Wu and Henry X Liu. A shockwave profile model for traffic flow on congested urban arterials. *Transportation Research Part B: Methodological*, 45(10):1768–1786, 2011. doi: 10.1016/j.trb.2011.07.013.
- [Xuan et al.(2011)] Yiguang Xuan, Juan Argote, and Carlos F Daganzo. Dynamic bus holding strategies for schedule reliability: Optimal linear control and performance analysis. *Transportation Research Part B: Methodological*, 45(10):1831–1845, 2011.
- [Yang et al.(2017a)] Hao Yang, Hesham Rakha, and Mani Venkat Ala. Eco-cooperative adaptive cruise control at signalized intersections considering queue effects. *IEEE Transactions on Intelligent Transportation Systems*, 18(6):1575–1585, 2017a. doi: 10.1109/TITS.2016.2613740.
- [Yang et al.(2017b)] Songpo Yang, Jianjun Wu, Huijun Sun, Xin Yang, Ziyou Gao, and Anthony Chen. Bi-objective nonlinear programming with minimum energy consumption and passenger waiting time for metro systems, based on the real-world smart-card data. *Transportmetrica B: Transport Dynamics*, pages 1–18, 2017b. doi: 10.1080/21680566.2017.1320775.
- [Yi et al.(2016)] Boliang Yi, Stefan Gottschling, Jens Ferdinand, Norbert Simm, Frank Bonarens, and Christoph Stiller. Real time integrated vehicle dynamics control and trajectory planning with MPC for critical maneuvers. In *2016 IEEE Intelligent Vehicles Symposium (IV)*. IEEE, jun 2016. doi: 10.1109/ivs.2016.7535446.
- [Zheng et al.(2018)] Fangfang Zheng, Saif Eddin Jabari, Henry X Liu, and DianChao Lin. Traffic state estimation using stochastic lagrangian dynamics. *Transportation Research Part B: Methodological*, 115:143–165, 2018. doi: 10.1016/j.trb.2018.07.004.

Publications of the Author (related to the theses)

- [Kulcsár and Varga(2016)] Balázs Kulcsár and Balázs Varga. Drive us - into sustainable automatized bus trains. resreport, Chalmers University of Technology, 2016.
- [Varga(2018)] Balázs Varga. Energy aware cruise control for urban public transport buses. In *16th Mini Conference on Vehicle System Dynamics, Identification and Anomalies (VSDIA 2018)*, 5-7. November 2018, Budapest, Hungary, 2018.
- [Varga and Tettamanti(2019)] Balázs Varga and Tamás Tettamanti. Sztochasztikus lökeshullámmmodell levezetése és alkalmazási lehetőségei. *Közlekedéstudományi Szemle*, 69:45–52, 2019 (In Hungarian).
- [Varga et al.(2017)] Balázs Varga, Tamás Tettamanti, and Balázs Kulcsár. Multiobjective control to mitigate bus bunching and improve schedule reliability of public transport. In *Swedish Transportation Research Conference*, 17-18 October 2017, Stockholm, Sweden, 2017.
- [Varga et al.(2018a)] Balázs Varga, Tamás Tettamanti, and Balázs Kulcsár. Optimal headway merging for balanced public transport service in urban networks. *IFAC-PapersOnLine*, 51(9):416–421, 2018a. doi: 10.1016/j.ifacol.2018.07.068.
- [Varga et al.(2018b)] Balázs Varga, Tamás Tettamanti, and Balázs Kulcsár. Urban cruise control based on stochastic shockwaves. In *Swedish Transportation Research Conference*, 15-17 October 2018, Gothenburg, Sweden, 2018b.
- [Varga et al.(2018c)] Balázs Varga, Tamás Tettamanti, and Balázs Kulcsár. Optimally combined headway and timetable reliable public transport system. *Transportation Research Part C: Emerging Technologies*, 92:1–26, 2018c.
- [Varga et al.(2019a)] Balázs Varga, Tamás Tettamanti, and Balázs Kulcsár. Energy-aware predictive control for electrified bus networks. *Applied Energy*, 252:113477, oct 2019a. doi: 10.1016/j.apenergy.2019.113477.
- [Varga et al.(2019b)] Balázs Varga, Tamás Tettamanti, and Balázs Kulcsár. Chance-constrained trajectory planning. In *Swedish Transportation Research Conference*, 22-23 October 2019, Linköping, Sweden, 2019b.

- [Varga et al.(2020a)] Balázs Varga, Tamás Péni, Balázs Kulcsár, and Tamás Tettamanti. Network-level optimal control for public bus operation. In *21st IFAC World Congress*, 12-17 July 2020, Berlin, Germany, 2020a.
- [Varga et al.(2020b)] Balázs Varga, Tamás Tettamanti, Balázs Kulcsár, and Xiaobo Qu. Public transport trajectory planning with probabilistic guarantees (under review). *Transportation Research Part B: Methodological*, 2020b.

Publications of the Author (unrelated to the theses)

- [Horváth et al.(2019)] Márton Tamás Horváth, Tamás Tettamanti, Balázs Varga, and Zsolt Szalay. The scenario-in-the-loop (scil) automotive simulation concept and its realisation principles for traffic control. In *Symposium of the European Association for Research in Transportation (hEART)*, 4-6 September 2019, Budapest, Hungary, 2019.
- [Kulcsár and Varga(2017)] Balázs Kulcsár and Balázs Varga. Saefflow – safety and efficiency analysis of hct-traffic flow indicators. resreport, Chalmers University of Technology, 2017. URL <https://www.vinnova.se/globalassets/mikrosajter/ffi/dokument/slutrappporter-ffi/effektiva-och-uppkopplade-transporter-rappporter/2014-03933.pdf>.
- [Németh et al.(2014a)] Balázs Németh, Balázs Varga, and Péter Gáspár. Robust control design of an electro-hydraulic actuator. In *IEEE/ASME International Conference on Advanced Intelligent Mechatronics (AIM)*, pages 245–250, 8-11 July 2014, Besancon, France, 2014a. IEEE.
- [Németh et al.(2014b)] Balázs Németh, Balázs Varga, and Péter Gáspár. Design of a variable-geometry suspension system to enhance road stability. In *22nd Mediterranean Conference of Control and Automation (MED)*, pages 55–60, 16-19 June 2014, Palermo, Italy, 2014b. IEEE.
- [Németh et al.(2015)] Balázs Németh, Balázs Varga, and Péter Gáspár. Hierarchical design of an electro-hydraulic actuator based on robust lqv methods. *International Journal of Control*, 88(8):1429–1440, 2015.
- [Varga and Kulcsár(2016)] Balázs Varga and Balázs Kulcsár. Efficiency analysis of high capacity transport from traffic flow point of view. In *Swedish Transportation Research Conference*, 18-19 October 2016, Lund, Sweden, 2016.
- [Varga and Németh(2012)] Balázs Varga and Balázs Németh. Személygépjármű futómű modellezése újszerű felfüggesztés szabályozási rendszerek tervezéséhez. In *Innováció és Fenntartható Felszíni Közlekedés (IFFK)*, 29-31 August 2012, Budapest, Hungary, 2012 (In Hungarian).
- [Varga et al.(2013)] Balázs Varga, Balázs Németh, and Péter Gáspár. Control design of anti-roll bar actuator based on constrained lqv method. In *14th IEEE International*

Symposium on Computational Intelligence and Informatics (CINTI), pages 31–36, 19-21 November 2013, Budapest, Hungary, 2013. IEEE.

- [Varga et al.(2014)] Balázs Varga, Balázs Németh, and Péter Gáspár. Hierarchical design of electro-hydraulic actuator control for vehicle dynamic purposes. In *13th IEEE European Control Conference (ECC)*, pages 999–1004, 24-27 June 2014, Strasbourg, France, 2014. IEEE.
- [Varga et al.(2015)] Balázs Varga, Balázs Németh, and Péter Gáspár. Design of anti-roll bar systems based on hierarchical control. *Strojniški vestnik-Journal of Mechanical Engineering*, 61(6):374–382, 2015.
- [Varga et al.(2017)] Balázs Varga, Balázs Kulcsár, Leo Laine, Manjurul Islam, and Balázs Németh. Robust tracking controller design for active dolly steering. *Proceedings of the Institution of Mechanical Engineers, Part D: Journal of Automobile Engineering*, page 0954407017704779, 2017.
- [Varga et al.(2020)] Balázs Varga, Mátyás Szalai, Árpád Fehér, Szilárd Aradi, and Tamás Tettamanti. Mixed-reality automotive testing with sensoris. *Periodica Polytechnica Transportation Engineering*, 2020 (Accepted).